Università degli Studi di Milano – Bicocca
Dipartimento di Fisica "G. Occhialini"

PhD Program in Physics and Astronomy
XXXIII Cycle

Curriculum: Theoretical Physics

Power corrections in a transverse-momentum cut for colour-singlet production at NLO and NNLO in QCD

Marco Rocco

Matricola: 827259

Advisor: Prof. Carlo Oleari

Coordinator: Prof. Marta Calvi

Academic Year: 2019/2020

Declaration

This dissertation is a result of my own efforts. The work to which it refers is based on my PhD research projects:

1. L. Cieri, C. Oleari and M. Rocco, *Higher-order power corrections in a transverse-momentum cut for colour-singlet production at NLO*, Eur. Phys. J. **C79** (2019) 852 [1906.09044]

2. P. Nason, C. Oleari, M. Rocco and M. Zaro, *An interface between the* POWHEG BOX *and* MADGRAPH5_AMC@NLO, Eur. Phys. J. **C80** (2020) 985 [2008.06364]

3. C. Oleari and M. Rocco, *Power corrections in a transverse-momentum cut for vector-boson production at NNLO: the qg-initiated real-virtual contribution*, submitted to Eur. Phys. J. C, 2012.10538

I hereby declare that except where specific reference is made to the work of others, the contents of this dissertation are original and have not been submitted in whole or in part for consideration for any other degree or qualification in this, or any other university.

Marco Rocco

Milano, January 10th, 2021

Contents

Chapter 1

Introduction

In the last years, the quest for understanding the fundamental laws of nature has been progressively pushed to the highest level. A great amount of data has come from experiments at particle accelerators, where the fundamental interactions are under investigation with the highest degree of precision. In addition, the fast development of technology will provide an even greater collection of data in the next years. For example, at the Large Hadron Collider (LHC), many processes are already measured with an unprecedented level of precision, and the forthcoming high-luminosity program, along with the improvements in the analysis techniques, points towards a further level of accuracy.

On the theory side, precise perturbative predictions are demanded with an equal effort. An example of how theoretical calculations evolved in time can be illustrated by considering the so-called *Les Houches Wishlist*. This wishlist was born in 2004 when experimentalists started to identify processes which would have been useful to know at next-to-leading order (NLO) in QCD. Later, in 2005 in Les Houches, the cutting edge of the list corresponded to two-to-four processes at NLO [1]. In the following years, an NLO revolution took place, when automated tools calculating NLO corrections to high-multiplicity processes were developed. Thus, the list was not only ticked out, but more complex processes were successfully tackled. Later, the list has been updated with the request of next-to-next-to-leading-order (NNLO) calculations. Thanks to the development of different subtraction schemes for handling infrared divergences at NNLO, an NNLO revolution is taking place in the last few years.

Intense development is thus rapidly on-going, also in view of extensions to the next perturbative order, i.e. $\mathrm{N^3LO}$. New difficulties come both from the virtual contributions with the increasing number of loops and scales, and from the development of subtraction methods able to expose the divergent behaviour in the infrared limits. At NLO several schemes exist to subtract the infrared-divergent real radiation. The most widely used are the Frixione-Kunszt-Signer subtraction scheme [2] and the

Catani-Seymour dipole subtraction scheme [3].

At NNLO and beyond, the development of efficient and general methods takes up a vast area of the field, with a great progress witnessed in the last years. The schemes mostly fit into two categories: local methods based on subtraction, and slicing methods based on partitions of the phase space into infrared-sensitive regions, where the cancellation of divergences is intrinsically non-local, and hard regions. Slicing methods that have been successfully applied at NNLO are the transverse-momentum (q_{T}) subtraction method [4–7] and N-jettiness [8, 9].

Within the q_{T}-subtraction framework, the N^{n}LO differential cross section for the production of a colour singlet F can be schematically written as

$$\mathrm{d}\sigma^{F}_{\mathrm{N^nLO}} = \left[\mathrm{d}\sigma^{F+\mathrm{jets}}_{\mathrm{N^{n-1}LO}} - \mathrm{d}\sigma^{F\,\mathrm{CT}}_{\mathrm{N^nLO}}\right] + (\text{finite terms})\,, \tag{1.1}$$

where $\mathrm{d}\sigma^{F\,\mathrm{CT}}_{\mathrm{N^nLO}}$ is the non-local counterterm which cancels the divergences of $\mathrm{d}\sigma^{F+\mathrm{jets}}_{\mathrm{N^{n-1}LO}}$ in the zero-q_{T} limit. In addition, a resolution parameter, $q_{\mathrm{T}}^{\mathrm{cut}}$, is introduced in order to identify the phase-space region where the global subtraction of eq. (1.1) is used.

After the subtraction, the difference between the real contribution and the counterterm, which is derived from the truncation of a q_{T}-resummed result, consists of finite terms and power-suppressed terms. Although the latter formally vanish in the null-$q_{\mathrm{T}}^{\mathrm{cut}}$ limit, they give a non-zero numerical contribution for any finite choice of $q_{\mathrm{T}}^{\mathrm{cut}}$. Hence the non-local cancellations can be more successfully handled by computing power corrections in $q_{\mathrm{T}}^{\mathrm{cut}}$, and the numerical performance of the subtraction can be systematically improved.

The main part of the thesis, Chapter 2, is devoted to a study about the power corrections in a transverse-momentum cutoff affecting perturbative calculations at higher orders in the strong coupling constant. In particular, we take into account the production of colourless systems, which constitute the main focus of the q_{T}-subtraction method. At the same time, the calculation of power corrections can serve to deepen the theoretical structure on which our perturbative predictions stand, in order to make them firmer and clearer.

Along with the first study, we recall that higher-order calculations on their own do not comply with all the requirements coming from experimental collaborations. In order to make a sound comparison between experimental measurements and theoretical predictions, any fixed-order calculation should be matched to a parton-shower algorithm. Thus one fully simulates hadronic production processes by merging together a QCD component, the shower itself, and a model for hadron formation. The QCD component is typically given in the collinear approximation and, as a result, parton-shower generators are accurate only in the collinear regions, failing to predict hard, large-angle emissions.

In the past twenty years, a considerable effort was made in order to build NLO-improved parton-shower generators, that can benefit both from the inclusive accuracy of the NLO calculations and from the precision of the parton showers when being more exclusive. Methods like MC@NLO [10] and POWHEG [11, 12] allow to interface NLO calculations to parton-shower generators, such as PYTHIA [13] and HERWIG [14]. These techniques saw a considerable progress thanks to the appearance of computer frameworks that automatise some aspects of the calculation, such as the computation of virtual contributions, the implementation of a subtraction framework for the real corrections, and the interface to a parton shower. Examples are the interfaces of the POWHEG BOX [15] to MADGRAPH4 [16], allowing for the implementation of all tree-level ingredients required by a given NLO process, and to automatic generators of virtual processes such as GOSAM [17, 18] and OPENLOOPS [19]. One of the last product in this field is the MADGRAPH5_AMC@NLO framework [20], where all the aspects of an NLO calculation are automatised and where many beyond-the-Standard-Model processes are as well available.

The second part of the thesis, Chapter 3, is devoted to the development of an interface between MADGRAPH5_AMC@NLO and the POWHEG BOX framework [15], in order to match the flexibility of MADGRAPH5_AMC@NLO for the generation of matrix elements for Standard-Model processes and for several of its extensions, to all features of the POWHEG BOX framework. Among those, it is essential the possibility, via the POWHEG method, to generate events with positive weights, which makes it the method of choice when large samples of events are needed. The interface is now available and it is already used by the experimental collaborations at the LHC (ATLAS and CMS).

As a proof of concept, we provide here a phenomenological study for the production of a spin-0 Higgs-like boson, in association with up to two jets, with CP-violating couplings. We discuss a few distributions able to characterise the X_0 boson CP properties, and discuss a few results obtained using the POWHEG BOX reweighting feature. We also present a few distributions obtained with the MiNLO method, which allows the possibility of multijet merging without a merging scale.

Chapter 2

Power corrections for colour-singlet production

2.1 Introduction

Observables that can be theoretically predicted and experimentally measured with the same uncertainty of a few percent prove to be particularly fitting to a further investigation of the Standard Model (SM). Among them, processes involving the production of a high-invariant-mass colour singlet play a crucial role. For example, vector-boson Drell-Yan production and gluon-fusion Higgs production offer a wide choice of observables, such as the transverse momentum and the rapidity of the singlet, that have been measured with high accuracy in the last decades, given the large production rates and the clean experimental signatures, and represent an optimal setting for a deeper understanding of the underlying theory, given their formal simplicity.

Within this environment one is allowed to achieve notably accurate theoretical predictions, since QCD radiative corrections to total cross sections and differential distributions are known at least up to the next-to-next-to-leading order (NNLO) in the strong coupling α_{S}. The main point here is that, at this stage in the process of verifying the SM, there are two possible options to pursue.

- The first consists in going one step further in the perturbative computation, requiring both new techniques for the calculation of Feynman diagrams with more loop, legs or scales, and new subtraction methods, able to tame the infrared cancellation at higher orders – which is likely to ask for much more thinking with respect to the previous order in the perturbative series.

- The second, which we pursue in this thesis, relies on a deeper analysis about the methods that are used up to NNLO in QCD, in particular about those that are used to subtract infrared divergences. This second approach, while standing

within the present state of the art for higher-order calculations, allows for a broader understanding of many non-trivial features of QCD.

In this thesis, we will focus on the infrared behaviour of colour-singlet production, in order to deepen our knowledge about it.

As a matter of fact, the scale hierarchy that characterises a high-energy scattering process enhances the events at the boundary of the phase space, namely, the infrared region. When these kinematic configurations are populated, the convergence of the perturbative series in α_s is spoiled and an all-order technique has to be devised. In the last decades much effort has been made in order to correctly take into account such large contributions, which appear in the form of large logarithms of the ratio of two different scales. As of now, it is possible to resum these terms at all orders in the strong coupling and to recognize universal patterns that characterise them. However, we are only acquainted with the leading behaviour of these resummed contributions, while a knowledge of the subleading behaviour can both shed light on the deeper structure of QCD, and be of help when the resummation of large logarithms is used as a tool for subtracting infrared divergences at higher orders. In fact, this is the case for the so-called slicing methods, such as the transverse-momentum subtraction method [4–7] and the N-jettiness subtraction [8, 9], which shall take advantage of the knowledge of subleading contributions to the infrared behaviour of QCD observables.

In this thesis, we consider the production of a colourless system at next-to-leading order in the strong coupling α_s. We impose a transverse-momentum cutoff on the colourless final state and we compute the subleading corrections for the inclusive cross section in the cutoff, up to the fourth power. In particular, we present analytic results for both Drell–Yan vector boson and Higgs boson production in gluon fusion and we illustrate a process-independent procedure for the calculation of the all-order power corrections in the cutoff.

The outline of the present chapter is as follows. In Section 2.2 we give a theoretical overview about colour-singlet production at NLO in QCD, also recovering some useful results. In Section 2.3 we deepen the subject of subleading corrections to QCD observables, in view of either the outcome they carry along when dealing with the universal behaviour of cross sections and resummation structures, or the improvement they bring about to slicing subtraction methods. In Section 2.4 we outline the calculation we have done and in Section 2.4.4 we present and discuss our analytic results for Z and H production, along with a study of their numerical impact. In 2.5 we use the same procedure applied to Z + jet production at NLO in α_s. Finally, conclusions are drawn in Section 2.6.

2.2 Colour-singlet production

Since the start of the LHC programme, processes involving the production of high-invariant-mass colour singlets such as the W and Z bosons have played a prominent role, due to large production rates, clean experimental signatures and the possibility to use them as standard candles for detector calibration. In fact, this effort has led to a highly-precise determination of the W-boson mass and to accurate evaluations of parton distribution functions. Moreover, a great theoretical effort at computing QCD radiative corrections for those processes was already and successfully on-going well before the start of the LHC, and the interest even increased since the discovery of the rarer (and equally colourless) Higgs boson.

In this section, without the aim of being exhaustive, we recall some fundamental results in the field, as they turn out to be useful for the study that follows. In particular, since our analysis is devoted to the study of the infrared subleading behaviour of inclusive cross sections at NLO in α_{S}, here we restrict ourselves to Drell–Yan Z production and Higgs production in gluon fusion at that order in QCD.

For sake of generality, we start by considering a hadronic cross section for the production of a colourless system F, whose squared invariant mass amounts to Q^2, in association with a coloured and unspecified system X, at a hadron collider:

$$h_1 + h_2 \to F + X\,. \tag{2.2.1}$$

The definition of a set of standard variables is now in order. S is the hadronic squared center-of-mass energy, and the hadronic differential cross section for the process can be written as

$$\mathrm{d}\sigma = \sum_{a,b} \int_{\tau}^{1} \mathrm{d}x_1 \int_{\frac{\tau}{x_1}}^{1} \mathrm{d}x_2\, f_a(x_1)\, f_b(x_2)\, \mathrm{d}\hat{\sigma}_{ab}\,. \tag{2.2.2}$$

In the last expression

$$\tau = \frac{Q^2}{S}\,, \tag{2.2.3}$$

$f_{a/b}$ are the parton distribution functions for the partons a and b, which carry the energy fractions x_1 and x_2 from hadron h_1 and h_2 respectively, the dependence on the renormalisation and factorisation scales and on the other kinematic invariants of the process is implicitly assumed, and $\mathrm{d}\hat{\sigma}_{ab}$ is the partonic cross section for the subprocess

$$a(p_1) + b(p_2) \to F(q) + c(k)\,, \tag{2.2.4}$$

where a, b and c are quarks or gluons, in a combination compatible with the production process of the colourless system F. In parentheses, the four momenta of the particles are given.

In order to turn the expression of eq. (2.2.2) into the most suitable form for what comes next, we deviate from the main route for a few paragraphs in order to simplify

the partonic phase space appearing in the same equation. The standard Mandelstam invariants related to the partonic subprocess are given by

$$s = (p_1 + p_2)^2\,, \quad t = (p_1 - k)^2 = -2p_1 \cdot k, \quad u = (p_2 - k)^2 = -2p_2 \cdot k, \quad q^2 = Q^2\,, \tag{2.2.5}$$

and are accompanied by the definition of the threshold variable z

$$z = \frac{Q^2}{s}\,. \tag{2.2.6}$$

The phase-space volume with the appropriate flux factor is given by

$$\begin{aligned} \mathrm{d}\Phi_2 &= \frac{1}{2s}\frac{\mathrm{d}^3 q}{(2\pi)^3 2q^0}\frac{\mathrm{d}^3 k}{(2\pi)^3 2k^0}\,(2\pi)^4\delta^4(p_1 + p_2 - q - k) \\ &= \frac{1}{2s}\frac{1}{(2\pi)^2}\frac{\mathrm{d}^3 k}{2k^0}\,\delta\big((p_1 + p_2 - k)^2 - Q^2\big)\,. \end{aligned} \tag{2.2.7}$$

Since the colourless system recoils against the final coloured parton, their transverse momenta are equal. Calling θ the angle between p_1 and k, we can write

$$q_{\mathrm{T}} = k_T = k^0 \sin\theta\,, \tag{2.2.8}$$

$$t = -\sqrt{s}k^0(1 - \cos\theta)\,. \tag{2.2.9}$$

Inverting the system, we find the relations

$$k^0 = -\frac{sq_{\mathrm{T}}^2 + t^2}{2\sqrt{s}t}\,, \tag{2.2.10}$$

$$\cos\theta = \frac{sq_{\mathrm{T}}^2 - t^2}{sq_{\mathrm{T}}^2 + t^2}\,, \tag{2.2.11}$$

which lead to an expression of the phase-space volume in terms of q_{T} and t

$$\frac{1}{(2\pi)^2}\frac{\mathrm{d}^3 k}{2k^0} = \frac{1}{4\pi}k^0\mathrm{d}k^0\mathrm{d}\cos\theta = -\frac{1}{4\pi}\frac{sq_{\mathrm{T}}^2 + t^2}{2\sqrt{s}t}\frac{\sqrt{s}}{sq_{\mathrm{T}}^2 + t^2}\mathrm{d}q_{\mathrm{T}}^2\,\mathrm{d}t = -\frac{1}{8\pi}\frac{\mathrm{d}t}{t}\,\mathrm{d}q_{\mathrm{T}}^2\,. \tag{2.2.12}$$

On the other hand, using the identity

$$t\,u = 4\,p_1^0\,p_2^0\,(k^0)^2\,(1 - \cos\theta)\,(1 + \cos\theta) = s\,(k^0\sin\theta)^2 \equiv s\,q_{\mathrm{T}}^2\,, \tag{2.2.13}$$

we can write the argument of the δ function in eq. (2.2.7) as

$$\begin{aligned} (p_1 + p_2 - k)^2 - Q^2 &= s + t + u - Q^2 = s + t + \frac{sq_{\mathrm{T}}^2}{t} - Q^2 \\ &= \frac{1}{t}\left[t^2 + \left(s - Q^2\right)t + sq_{\mathrm{T}}^2\right] = \frac{1}{t}\,(t - t_+)\,(t - t_-)\,, \end{aligned} \tag{2.2.14}$$

where

$$t_\pm = \frac{1}{2}\left[Q^2 - s \pm \sqrt{(Q^2-s)^2 - 4\,s\,q_\mathrm{T}^2}\right]. \tag{2.2.15}$$

As a consequence, it is possible to write

$$\begin{aligned}\delta\left((p_1+p_2-k)^2 - Q^2\right)\frac{\mathrm{d}t}{t} &= \frac{t}{t^2 - t_+ t_-}\left[\delta\left(t-t_+\right) + \delta\left(t-t_-\right)\right]\mathrm{d}t \\ &= \frac{1}{\sqrt{(Q^2-s)^2 - 4\,s\,q_\mathrm{T}^2}}\left[\delta\left(t-t_+\right) + \delta\left(t-t_-\right)\right]\mathrm{d}t\,,\end{aligned} \tag{2.2.16}$$

and using eqs. (2.2.12) and (2.2.16), we can write eq. (2.2.7) as

$$\mathrm{d}\Phi_2 = \frac{1}{16\pi}\frac{1}{s}\frac{1}{\sqrt{(Q^2-s)^2 - 4\,s\,q_\mathrm{T}^2}}\left[\delta\left(t-t_+\right) + \delta\left(t-t_-\right)\right]\mathrm{d}t\,\mathrm{d}q_\mathrm{T}^2\,. \tag{2.2.17}$$

We then add a dummy integration over the z variable,

$$\mathrm{d}\Phi_2 = \frac{1}{16\pi}\frac{1}{s}\frac{1}{\sqrt{(Q^2-s)^2 - 4\,s\,q_\mathrm{T}^2}}\left[\delta\left(t-t_+\right) + \delta\left(t-t_-\right)\right]\delta\left(z - \frac{Q^2}{s}\right)\mathrm{d}t\,\mathrm{d}q_\mathrm{T}^2\,\mathrm{d}z\,, \tag{2.2.18}$$

that allows us to rewrite the phase-space volume as

$$\mathrm{d}\Phi_2 = \frac{1}{16\pi}\frac{z^2}{Q^4}\frac{1}{\sqrt{(1-z)^2 - 4z\,\dfrac{q_\mathrm{T}^2}{Q^2}}}\left[\delta(t-t_+) + \delta(t-t_-)\right]\delta\left(z - \frac{Q^2}{s}\right)\mathrm{d}t\,\mathrm{d}q_\mathrm{T}^2\,\mathrm{d}z\,, \tag{2.2.19}$$

where

$$t_\pm = \frac{Q^2}{2z}\left[z - 1 \pm \sqrt{(1-z)^2 - 4z\,\frac{q_\mathrm{T}^2}{Q^2}}\right]. \tag{2.2.20}$$

Now, we can write the partonic cross sections for a $2 \to 2$ process as

$$\mathrm{d}\hat{\sigma} = \left|\mathcal{M}(s,t,u)\right|^2 \mathrm{d}\Phi_2\,, \tag{2.2.21}$$

where $\mathcal{M}$ is the amplitude for the partonic process, that in general can be written as a function of the Mandelstam variables s, t and u. From eqs. (2.2.6) and (2.2.13) we

can express s and u as functions of z, q_{T} and t, and using eq. (2.2.19) we can write

$$\begin{aligned}
\mathrm{d}\hat{\sigma} &= \frac{1}{16\pi}\frac{z^2}{Q^4}\frac{1}{\sqrt{(1-z)^2-4z\,\dfrac{q_{\mathrm{T}}^2}{Q^2}}}\left[\delta(t-t_+)+\delta(t-t_-)\right] \\
&\qquad\qquad \times\,\delta\left(z-\frac{Q^2}{s}\right)\left|\mathcal{M}\left(z,t,q_{\mathrm{T}}\right)\right|^2\mathrm{d}t\,\mathrm{d}q_{\mathrm{T}}^2\,\mathrm{d}z \\
&= \frac{1}{16\pi}\frac{z^2}{Q^4\,\mathrm{d}z}\frac{1}{\sqrt{(1-z)^2-4z\,\dfrac{q_{\mathrm{T}}^2}{Q^2}}}\left[\left|\mathcal{M}\left(z,t_+,q_{\mathrm{T}}\right)\right|^2+\left|\mathcal{M}\left(z,t_-,q_{\mathrm{T}}\right)\right|^2\right] \\
&\qquad\qquad \times\,\delta\left(z-\frac{Q^2}{s}\right)\mathrm{d}q_{\mathrm{T}}^2\,\mathrm{d}z \\
&= \frac{d\hat{\sigma}_{ab}(q_{\mathrm{T}},z)}{dq_{\mathrm{T}}^2}\,\delta\left(z-\frac{Q^2}{s}\right)\mathrm{d}q_{\mathrm{T}}^2\,\mathrm{d}z\,,
\end{aligned} \tag{2.2.22}$$

where we have defined

$$\frac{d\hat{\sigma}_{ab}(q_{\mathrm{T}},z)}{dq_{\mathrm{T}}^2} \equiv \frac{1}{16\pi}\frac{z^2}{Q^4}\frac{1}{\sqrt{(1-z)^2-4z\,\dfrac{q_{\mathrm{T}}^2}{Q^2}}}\left[\left|\mathcal{M}\left(z,t_+,q_{\mathrm{T}}\right)\right|^2+\left|\mathcal{M}\left(z,t_-,q_{\mathrm{T}}\right)\right|^2\right]. \tag{2.2.23}$$

This is, besides the actual matrix elements, what one needs in order to compute the hadronic cross section of eq. (2.2.2). Using eqs. (2.2.22) and (2.2.23), we can write it as

$$\sigma = \sum_{a,b}\int_{\tau}^{1}\mathrm{d}x_1\int_{\frac{\tau}{x_1}}^{1}\mathrm{d}x_2\,f_a(x_1)\,f_b(x_2)\int\mathrm{d}q_{\mathrm{T}}^2\,\mathrm{d}z\,\frac{d\hat{\sigma}_{ab}(q_{\mathrm{T}},z)}{dq_{\mathrm{T}}^2}\,\delta\left(z-\frac{Q^2}{s}\right), \tag{2.2.24}$$

where s is the partonic center-of-mass energy, equal to

$$s = S\,x_1\,x_2\,. \tag{2.2.25}$$

We have also made explicit the dependence on z, the ratio between the squared invariant mass of the system F and the partonic center-of-mass energy, and on q_{T}, the transverse momentum of the system F with respect to the hadronic beams. Using eqs. (2.2.25) and (2.2.3) we can write

$$\sigma = \sum_{a,b}\int_{0}^{1}\mathrm{d}z\,\delta\left(z-\frac{\tau}{x_1x_2}\right)\int_{\tau}^{1}\mathrm{d}x_1\int_{\frac{\tau}{x_1}}^{1}\mathrm{d}x_2\,f_a(x_1)\,f_b(x_2)\int\mathrm{d}q_{\mathrm{T}}^2\,\frac{d\hat{\sigma}_{ab}(q_{\mathrm{T}},z)}{dq_{\mathrm{T}}^2}\,, \tag{2.2.26}$$

and by using the δ function to integrate over x_2, we obtain

$$\sigma = \sum_{a,b}\tau\int_{\tau}^{1}\frac{\mathrm{d}z}{z}\int_{\frac{\tau}{z}}^{1}\frac{\mathrm{d}x_1}{x_1}\,f_a(x_1)\,f_b\left(\frac{\tau}{z\,x_1}\right)\frac{1}{z}\int\mathrm{d}q_{\mathrm{T}}^2\,\frac{d\hat{\sigma}_{ab}(q_{\mathrm{T}},z)}{dq_{\mathrm{T}}^2}\,. \tag{2.2.27}$$

We then introduce the parton luminosity $\mathcal{L}_{ab}(y)$ defined by

$$\mathcal{L}_{ab}(y) \equiv \int_y^1 \frac{\mathrm{d}x}{x}\, f_a(x)\, f_b\Big(\frac{y}{x}\Big)\,, \tag{2.2.28}$$

so that we can finally write

$$\sigma = \sum_{a,b} \tau \int_\tau^1 \frac{\mathrm{d}z}{z}\, \mathcal{L}_{ab}\Big(\frac{\tau}{z}\Big)\, \frac{1}{z} \int \mathrm{d}q_{\mathrm{T}}^2\, \frac{d\hat{\sigma}_{ab}(q_{\mathrm{T}}, z)}{dq_{\mathrm{T}}^2}\,. \tag{2.2.29}$$

At this stage, we proceed by analysing in detail the partonic subprocesses that we are interested in. The partonic differential cross sections are computable in perturbative QCD as power series in α_{S}

$$\frac{d\hat{\sigma}_{ab}(q_{\mathrm{T}}, z)}{dq_{\mathrm{T}}^2} = \frac{d\hat{\sigma}^{(0)}(q_{\mathrm{T}}, z)}{dq_{\mathrm{T}}^2} + \frac{\alpha_{\mathrm{S}}}{2\pi}\, \frac{d\hat{\sigma}^{(1)}_{ab}(q_{\mathrm{T}}, z)}{dq_{\mathrm{T}}^2} + \dots \tag{2.2.30}$$

The Born contribution $d\hat{\sigma}^{(0)}(q_{\mathrm{T}}, z)/dq_{\mathrm{T}}^2$ and the virtual contributions to $d\hat{\sigma}^{(1)}_{ab}(q_{\mathrm{T}}, z)/dq_{\mathrm{T}}^2$ are proportional to $\delta(q_{\mathrm{T}})$. Applying eq. (2.2.23), with a little abuse of notation,[1] we can write at once the partonic differential cross sections. For what concerns Z production, there are two channels contributing to the total cross section, a qg- and a $q\bar{q}$-initiated channel, respectively

$$q(\bar{q}) + g \;\to\; Z + q(\bar{q})\,, \tag{2.2.31}$$

$$q + \bar{q} \;\to\; Z + g\,. \tag{2.2.32}$$

For what concerns Higgs production via gluon fusion, in the infinite-top-mass limit, there are three channels contributing to the total cross section, a qg-, a gg- and a $q\bar{q}$-initiated channel, respectively

$$q(\bar{q}) + g \;\to\; H + q(\bar{q})\,, \tag{2.2.33}$$

$$g + g \;\to\; H + g\,, \tag{2.2.34}$$

$$q + \bar{q} \;\to\; H + g\,. \tag{2.2.35}$$

2.2.1 Drell-Yan Z production

In this section we deal with the computation of the real emission amplitude for the neutral-current Drell–Yan process. We start from the qg-initiated channel,

$$q(p_1) + g(k) \;\to\; Z(q) + q(p_2)\,, \tag{2.2.36}$$

where the four-momenta associated to the particles are shown between parentheses and the same-flavour quarks q may be substitued by same-flavour anti-quarks $\bar{q}$. The

[1] In the rest of the thesis we only deal with the real corrections to Z and H production. We then use $d\hat{\sigma}^{(1)}_{ab}(q_{\mathrm{T}}, z)/dq_{\mathrm{T}}^2$ to indicate them.

matrix element is computed by considering two diagrams and their interference – we denote with the subscript s the s-channel, with t the t-channel and with $s|t$ the interference. We are allowed to work in a number of space-time dimensions $d = 4$ for reasons that will be clear in Section 2.3. We quote here the intermediate results for the three contributions to the squared matrix element $|\mathcal{M}_{qg}|^2(s,t)$, summed over polarisations and colors

$$\begin{aligned}
\sum_{\text{pol's,col's}} |\mathcal{M}_s|^2 &= \frac{g^2\, g_{\text{S}}^2}{c_w^2}\, T_{\text{R}} \left(N_{\text{c}}^2 - 1\right) \frac{1}{s^2} \\
&\quad \times \text{Tr}\left[\gamma_\mu \left(g_v - g_a\gamma_5\right) \left(\not{p}_1 + \not{k}\right) \gamma^\alpha \not{p}_1 \, \gamma_\alpha \left(\not{p}_1 + \not{k}\right) \gamma^\mu \left(g_v - g_a\gamma_5\right) \not{p}_2\right] \\
&= -32\pi \, \frac{g^2 \left(g_v^2 + g_a^2\right)}{c_w^2}\, T_{\text{R}} \left(N_{\text{c}}^2 - 1\right) \alpha_{\text{S}} \, \frac{t}{s}\,, \qquad (2.2.37) \\
\sum_{\text{pol's, col's}} |\mathcal{M}_t|^2 &= \sum_{\text{pol's, col's}} |\mathcal{M}_s|^2 \, \{s \leftrightarrow t\}\,, \qquad (2.2.38) \\
\sum_{\text{pol's, col's}} \left|\mathcal{M}_{s|t}\right|^2 &= \frac{g^2\, g_{\text{S}}^2}{c_w^2}\, T_{\text{R}} \left(N_{\text{c}}^2 - 1\right) \frac{1}{st} \\
&\quad \times \text{Tr}\left[\gamma_\mu \left(g_v - g_a\gamma_5\right) \not{p}_2 \, \gamma^\alpha \left(\not{p}_2 - \not{k}\right) \gamma^\mu \left(g_v - g_a\gamma_5\right) \not{p}_1 \, \gamma_\alpha \left(\not{p}_1 + \not{k}\right)\right] \\
&= -16\pi \, \frac{g^2 \left(g_v^2 + g_a^2\right)}{c_w^2}\, T_{\text{R}} \left(N_{\text{c}}^2 - 1\right) \alpha_{\text{S}} \frac{2u\, Q^2}{st}\,, \qquad (2.2.39)
\end{aligned}$$

where g, g_v and g_a are the weak, the vector and the axial coupling, respectively, c_w is the cosine of the weak angle, g_{S} is the strong coupling, N_{c} is the number of colours and $T_{\text{R}} = 1/2$. The squared amplitude averaged over the initial colour and polarisation $(s_g,\, s_q)$ states yields

$$\begin{aligned}
|\mathcal{M}_{qg}|^2(s,t) &\equiv \overline{\sum}_{\text{pol's, col's}} |\mathcal{M}_s|^2 + \overline{\sum}_{\text{pol's, col's}} |\mathcal{M}_t|^2 + 2\text{Re}\, \overline{\sum}_{\text{pol's, col's}} \left|\mathcal{M}_{s|t}\right|^2 \\
&= -\frac{32\pi}{s_q\, s_g} \, \frac{1}{N_{\text{c}}\left(N_{\text{c}}^2 - 1\right)} \frac{g^2 \left(g_v^2 + g_a^2\right)}{c_w^2}\, T_{\text{R}} \left(N_{\text{c}}^2 - 1\right) \alpha_{\text{S}} \left(\frac{t}{s} + \frac{s}{t} + \frac{2u\, Q^2}{st}\right). \qquad (2.2.40)
\end{aligned}$$

Applying eq. (2.2.23), we can write the NLO partonic differential cross section for the Z-production qg-initiated channel as

$$\frac{\mathrm{d}\hat{\sigma}_{qg}^{(1)}(q_{\text{T}}, z)}{\mathrm{d}q_{\text{T}}^2} = \sigma_{qq}^{(0)}\, T_{\text{R}}\, z \, \frac{z\,(1+3z)\,\dfrac{q_{\text{T}}^2}{Q^2} + (1-z)\, p_{qg}(z)}{\sqrt{(1-z)^2 - 4z\,\dfrac{q_{\text{T}}^2}{Q^2}}} \, \frac{1}{q_{\text{T}}^2}\,, \qquad (2.2.41)$$

where

$$\sigma_{qq}^{(0)} = \frac{\pi}{N_{\text{c}}} \, \frac{g^2 \left(g_v^2 + g_a^2\right)}{c_w^2} \frac{1}{Q^2} \qquad (2.2.42)$$

is the Born-level cross section for the process $q\bar{q} \to Z$. The same result holds for the production of a W boson, if the correct quark flavours and the relevant Cabibbo–Kobayashi–Maskawa matrix element are taken into account. The expression of the Altarelli–Parisi splitting function $p_{qg}(z)$ is given in eq. (F.2).

As we turn to the $q\bar{q}$-initiated channel,

$$q(p_1) + \bar{q}(p_2) \;\to\; g(k) + Z(q)\,, \tag{2.2.43}$$

we notice that the corresponding matrix element can be obtained by crossing the four-momenta, starting from the qg-initiated result, with the exchange

$$|\mathcal{M}_{q\bar{q}}|^2(s,t) = -|\mathcal{M}_{qg}|^2(u,t)\,. \tag{2.2.44}$$

The squared amplitude averaged over the initial colour and polarisation states yields

$$|\mathcal{M}_{q\bar{q}}|^2(s,t) = \frac{32\pi}{s_q\, s_q}\,\frac{1}{N_{\mathrm{c}}^2}\,\frac{g^2\,(g_v^2+g_a^2)}{c_w^2}\,T_{\mathrm{R}}\left(N_{\mathrm{c}}^2-1\right)\alpha_{\mathrm{S}}\left(\frac{t}{u}+\frac{u}{t}+\frac{2s\,Q^2}{ut}\right), \tag{2.2.45}$$

and applying eq. (2.2.23), we can write the NLO partonic differential cross section for the Z-production $q\bar{q}$-initiated channel as

$$\frac{\mathrm{d}\hat{\sigma}^{(1)}_{q\bar{q}}(q_{\mathrm{T}},z)}{\mathrm{d}q_{\mathrm{T}}^2} = \sigma^{(0)}_{qq}\,C_{\mathrm{F}}\,z\,\frac{-4z\,\dfrac{q_{\mathrm{T}}^2}{Q^2}+2\,(1-z)\,\hat{p}_{qq}(z)}{\sqrt{(1-z)^2-4z\,\dfrac{q_{\mathrm{T}}^2}{Q^2}}}\,\frac{1}{q_{\mathrm{T}}^2}\,, \tag{2.2.46}$$

where $\sigma^{(0)}_{qq}$ is defined in eq. (2.2.42), $C_{\mathrm{F}} = \left(N_{\mathrm{c}}^2-1\right)/(2N_{\mathrm{c}}) = 4/3$ and the expression of the Altarelli–Parisi splitting function $\hat{p}_{qq}(z)$ is given in eq. (F.5).

2.2.2 Higgs production in gluon fusion

In this section we deal with the computation of the real emission amplitude for Higgs boson production via gluon fusion. The lowest-order amplitude for this process arises from a triangle diagram. The amplitude is sensitive to all quarks which can couple to the gluon and to the Higgs boson via a Yukawa interaction: thus it depends on the heaviest quark mass, namely on the top-quark mass M_t. The Born-level cross section for the process $gg \to H$ has been available in the literature from the late Seventies – see e.g. ref. [21] for a review – and it is usually written as

$$\sigma^{(0)}_{gg} = \frac{\alpha_{\mathrm{S}}^2}{\pi}\,\frac{M_H^2}{256v^2}\,|\mathcal{A}|^2\,\delta(s-M_H^2)\,, \tag{2.2.47}$$

where

$$|\mathcal{A}|^2 = \left|\sum_q \tau_q\left[1+(1-\tau_q)f(\tau_q)\right]\right|^2 \tag{2.2.48}$$

and M_H is the Higgs boson mass. In eq. (2.2.48) the sum runs over the quark flavour q with mass m_q, v is the Higgs vacuum expectation value, $\tau_q = 4m_q^2/M_H^2$ and

$$f(\tau_q) = \begin{cases} \arcsin^2\left(\sqrt{\dfrac{1}{\tau_q}}\right) & \text{if } \tau_q \geqslant 1 \\ -\dfrac{1}{4}\left(\log\dfrac{\eta_+}{\eta_-} - i\pi\right)^2 & \text{if } \tau_q < 1\,, \end{cases} \tag{2.2.49}$$

where

$$\eta_\pm = 1 \pm \sqrt{1-\tau_q}\,. \tag{2.2.50}$$

In the limit in which the quark mass is infinitely large, namely $\tau_q \to \infty$, $\mathcal{A} \to 2/3$, we have

$$\sigma_{gg}^{(0),\infty} = \frac{\alpha_{\rm S}^2}{\pi}\frac{M_H^2}{576v^2} \equiv \frac{\alpha_{\rm S}^2}{72\pi}\frac{M_H^2}{(N_{\rm c}^2-1)\,v^2}\,\delta(s-M_H^2)\,. \tag{2.2.51}$$

For sake of simplicity, in the formulae that follow we re-define the total Born cross-section as

$$\sigma_{gg}^{(0)} \equiv \frac{\alpha_{\rm S}^2}{72\pi}\frac{1}{(N_{\rm c}^2-1)\,v^2}\,. \tag{2.2.52}$$

Thus, in the infinite-top-mass limit, the $\mathcal{O}(\alpha_{\rm S}^3)$ cross section for Higgs production in gluon fusion can be obtained from the effective Lagrangian (see ref. [21] for more details)

$$\mathcal{L}_{\rm eff} = -\frac{1}{4}\left(1 - \frac{\alpha_{\rm S}}{3\pi v}\,H\right) G_{\mu\nu}G^{\mu\nu} \tag{2.2.53}$$

where H is the scalar Higgs field and $G_{\mu\nu}$ is the field strength tensor associated to the gluons. From eq. (2.2.53) it is straightforward to obtain eq. (2.2.52), and now the effective Lagrangian is the starting point in order to compute the differential cross sections associated to the three relevant channels at NLO in $\alpha_{\rm S}$.

We start with the qg-initiated one,

$$g(k) + q(p_1) \;\to\; H(q) + q(p_2)\,. \tag{2.2.54}$$

This contribution origins from a t-channel diagram, whose squared amplitude, averaged over polarisation states and colours, yields

$$|\mathcal{M}_{gq}|^2\,(s,t) = -\frac{1}{s_q\,s_g}\,\frac{C_{\rm F}\,N_{\rm c}}{N_{\rm c}\,(N_{\rm c}^2-1)}\,\frac{4}{9}\,\frac{\alpha_{\rm S}^3}{\pi v^2}\,\frac{1}{t}\left(u^2+s^2\right)\,. \tag{2.2.55}$$

Applying eq. (2.2.23), we can write the NLO partonic differential cross section for the H-production qg-initiated channel as

$$\frac{{\rm d}\hat{\sigma}_{gq}^{(1)}(q_{\rm T},z)}{{\rm d}q_{\rm T}^2} = \sigma_{gg}^{(0)}\,C_{\rm F}\,z\,\frac{-3\,(1-z)\,\dfrac{q_{\rm T}^2}{Q^2} + (1-z)\,p_{gq}(z)}{\sqrt{(1-z)^2 - 4z\,\dfrac{q_{\rm T}^2}{Q^2}}}\,\frac{1}{q_{\rm T}^2}\,, \tag{2.2.56}$$

where $\sigma_{gg}^{(0)}$ is defined in eq. (2.2.52) and the expression of the Altarelli–Parisi splitting function $p_{gq}(z)$ is given in eq. (F.3).

The contribution from the gg-initiated channel,

$$g(k_1) + g(k_2) \;\to\; H(q) + g(k)\,, \tag{2.2.57}$$

consists of a sum of six diagrams, connected one to another via momentum permutations. The squared amplitude, averaged over the initial polarisation and colour states, yields

$$|\mathcal{M}_{gg}|^2 = \frac{1}{s_g^2}\,\frac{C_{\rm A}\,(N_{\rm c}^2-1)}{(N_{\rm c}^2-1)^2}\,\frac{4}{9}\,\frac{\alpha_{\rm S}^3}{\pi v^2}\,\frac{Q^8+s^4+t^4+u^4}{stu}\,. \tag{2.2.58}$$

Applying eq. (2.2.23), we can write the NLO partonic differential cross section for the H-production gg-initiated channel as

$$\frac{{\rm d}\hat{\sigma}_{gg}^{(1)}(q_{\rm T},z)}{{\rm d}q_{\rm T}^2} = \sigma_{gg}^{(0)}\,C_{\rm A}\,z\,\frac{4z\left(\dfrac{q_{\rm T}^2}{Q^2}\right)^2 - 8\,(1-z)^2\,\dfrac{q_{\rm T}^2}{Q^2} + 2\,(1-z)\,\hat{p}_{gg}(z)}{\sqrt{(1-z)^2 - 4z\,\dfrac{q_{\rm T}^2}{Q^2}}}\,\frac{1}{q_{\rm T}^2}\,, \tag{2.2.59}$$

where $\sigma_{gg}^{(0)}$ is defined in eq. (2.2.52), $C_{\rm A}=3$ and the expression of the Altarelli–Parisi splitting function $\hat{p}_{gg}(z)$ is given in eq. (F.6).

The third channel,

$$q(p_1) + \bar{q}(p_2) \;\to\; g(k) + H(q)\,, \tag{2.2.60}$$

origins from an s-diagram, whose squared amplitude, averaged over helicities and colours, is obtained from the diagram contributing to the qg-initiated channel, applying the crossing $s \leftrightarrow t$ with an overall minus sign:

$$|\mathcal{M}_{qqH}|^2 = \frac{1}{s_q\,s_{\bar{q}}}\,\frac{C_{\rm F}\,N_{\rm c}}{N_{\rm c}^2}\,\frac{4}{9}\,\frac{\alpha_{\rm S}^3}{\pi v^2}\,\frac{1}{s}\left(u^2+t^2\right)\,. \tag{2.2.61}$$

Applying eq. (2.2.23), we can write the NLO partonic differential cross section for the H-production $q\bar{q}$ channel as

$$\frac{{\rm d}\hat{\sigma}_{q\bar{q}H}^{(1)}(q_{\rm T},z)}{{\rm d}q_{\rm T}^2} = \sigma_{gg}^{(0)}\,C_{\rm F}^2\,z\,\frac{-8z\left(\dfrac{q_{\rm T}^2}{Q^2}\right)^2 + 4\,(1-z)^2\,\dfrac{q_{\rm T}^2}{Q^2}}{\sqrt{(1-z)^2 - 4z\,\dfrac{q_{\rm T}^2}{Q^2}}}\,\frac{1}{q_{\rm T}^2}\,, \tag{2.2.62}$$

where $\sigma_{gg}^{(0)}$ is defined in eq. (2.2.52). It is clear at this stage that the cross section in eq. (2.2.62), at variance with the corresponding quantities for the other production

channels, is not singular in the infrared limit, namely in the limit $q_{\rm T} \to 0$. Hence it does not require an infrared subtraction, nor it is affected by transverse-momentum subleading power corrections.

In table 2.2.2 we collect the results for the NLO partonic differential cross sections, both for Z and H production, whereas the corresponding Born-level cross section, $\sigma^{(0)}_{q\bar{q}}$ and $\sigma^{(0)}_{gg}$, are defined in eq. (2.2.42) and eq. (2.2.52), respectively. The expressions of the Altarelli–Parisi splitting functions $\hat{p}_{ab}(z)$ and $p_{ab}(z)$ are given in Appendix F and

$$\mathcal{G}\left(q_{\rm T}^2\right) \equiv q_{\rm T}^2 \sqrt{(1-z)^2 - 4z\,\frac{q_{\rm T}^2}{Q^2}}\,. \tag{2.2.63}$$

a	b	F	$\dfrac{\mathrm{d}\hat{\sigma}^{(1)}_{ab\to F}(q_{\rm T}, z)}{\mathrm{d}q_{\rm T}^2}$	eq.
q	g	Z	$\sigma^{(0)}_{qq}\, T_{\rm R}\, \dfrac{z}{\mathcal{G}\left(q_{\rm T}^2\right)} \left[z\,(1+3z)\,\dfrac{q_{\rm T}^2}{Q^2} + (1-z)\,p_{qg}(z) \right]$	(2.2.41)
q	$\bar{q}$	Z	$\sigma^{(0)}_{qq}\, C_{\rm F}\, \dfrac{z}{\mathcal{G}\left(q_{\rm T}^2\right)} \left[-4z\,\dfrac{q_{\rm T}^2}{Q^2} + 2\,(1-z)\,\hat{p}_{qq}(z) \right]$	(2.2.46)
g	q	H	$\sigma^{(0)}_{gg}\, C_{\rm F}\, \dfrac{z}{\mathcal{G}\left(q_{\rm T}^2\right)} \left[-3\,(1-z)\,\dfrac{q_{\rm T}^2}{Q^2} + (1-z)\,p_{gq}(z) \right]$	(2.2.56)
g	g	H	$\sigma^{(0)}_{gg}\, C_{\rm A}\, \dfrac{z}{\mathcal{G}\left(q_{\rm T}^2\right)} \left[4z \left(\dfrac{q_{\rm T}^2}{Q^2}\right)^2 - 8\,(1-z)^2\,\dfrac{q_{\rm T}^2}{Q^2} + 2\,(1-z)\,\hat{p}_{gg}(z) \right]$	(2.2.59)
q	$\bar{q}$	H	$\sigma^{(0)}_{gg}\, C_{\rm F}^2\, \dfrac{z}{\mathcal{G}\left(q_{\rm T}^2\right)} \left[-8z \left(\dfrac{q_{\rm T}^2}{Q^2}\right)^2 + 4\,(1-z)^2\,\dfrac{q_{\rm T}^2}{Q^2} \right]$	(2.2.62)

Table 2.1. NLO partonic differential cross sections for Drell–Yan Z production and H production in gluon fusion. The function $\mathcal{G}\left(q_{\rm T}^2\right)$ is defined in eq. (2.2.63).

We notice that the terms proportional to the Altarelli–Parisi splitting functions in eqs. (2.2.41), (2.2.46), (2.2.56) and (2.2.59) embody in a single expression the whole infrared behaviour of the amplitudes, i.e. their soft and collinear limits. The structure of these terms was derived in a completely general form, from the universal behaviour of the scattering amplitudes in those limits, in ref. [22].

2.3 Subleading power corrections

The current precision-physics program at the LHC requires SM theoretical predictions at the highest accuracy: thus, the calculation of perturbative QCD corrections plays a dominant role in this context. Until a few years ago, the standard for such calculations was NLO accuracy. In recent years, a continuously-growing number of NNLO results for many important processes has appeared in the literature, giving birth to the so called "NNLO revolution". For several "standard candles" processes, the first steps towards the calculation of differential cross sections at N^{3}LO have also been taken – see e.g. refs. [23–30].

2.3.1 Subtraction methods

The computation of higher-order terms in the perturbative series becomes more involved due to the technical difficulties arising in the evaluation of virtual contributions and to the increasing complexity of the infrared (IR) structure of the real contributions. In order to expose the cancellation of the IR divergences between real and virtual contributions, the knowledge of the behaviour of the scattering amplitudes at the boundaries of the phase space is then a crucial ingredient and it is indeed what is used by the subtraction methods in order to work. These methods can be roughly divided into local and slicing. Among the first, the most extensively used at NLO were proposed in refs. [2, 3]. As far as the NNLO subtraction methods are concerned, the past few years have witnessed a great activity in their development: the transverse-momentum ($q_{\rm T}$) subtraction method [4–7], the N-jettiness subtraction [8, 9], the projection-to-Born [31], the residue subtraction [32, 33] and the antenna subtraction method [34–36] have all been successfully applied to LHC phenomenology. The first application of the $q_{\rm T}$-subtraction method to differential cross sections at N^{3}LO was recently proposed in ref. [23], in the calculation of the rapidity distribution of the Higgs boson.

While a local subtraction is independent of any regularising parameter, in a slicing method a resolution parameter, $\lambda_{\rm cut}$, is introduced in order to avoid the issue of cancelling infrared divergences between virtual and real contributions by separating the integration into two regions. For example, in order to compute a QCD NLO total cross section, we observe that

$$\sigma^{\rm NLO} = \int_0^{\lambda_{\rm cut}} {\rm d}\lambda \, \frac{{\rm d}\sigma^{\rm NLO}}{{\rm d}\lambda} + \int_{\lambda_{\rm cut}}^{\lambda_{\rm max}} {\rm d}\lambda \, \frac{{\rm d}\sigma^{\rm NLO}}{{\rm d}\lambda} \, . \tag{2.3.1}$$

In eq. (2.3.1) the integration below $\lambda_{\rm cut}$ is sensitive to infrared physics, namely, it can be obtained by taking the limit for the observable λ going to zero. For example, the integrand is given by the Born contribution multiplied by the Altarelli–Parisi kernels if λ is the emission angle of the radiation, or by the Born contribution multiplied by the eikonal factor if λ is the energy of the emitted radiation. If λ is the transverse

momentum of the radiation, the integration below the cutoff is typically obtained from the expansion of a resummed formula. Otherwise, a Monte-Carlo integration can be safely used above λ_{cut} since there are no singularities in that region. In fact, for colour-singlet production, a non-zero transverse momentum of the singlet implies that a resolved radiation is recoiling against the heavy boson and this allows for a numerical integration in $d = 4$ dimensions.

2.3.2 The q_{T}-subtraction method

An example of this procedure comes from the q_{T}-subtraction method, where a transverse momentum cutoff is used as the resolution parameter: $\lambda = q_{\text{T}}^2$. More in detail, the integral in the below-cutoff region, for small values of the cutoff, behaves as

$$\int_0^{(q_{\text{T}}^{\text{cut}})^2} \mathrm{d}q_{\text{T}}^2 \, \frac{\mathrm{d}\sigma^{\text{NLO}}}{\mathrm{d}q_{\text{T}}^2} \quad \xrightarrow{(q_{\text{T}}^{\text{cut}})^2 \to 0} \quad \sum_{r=0}^{\infty} \int_0^{(q_{\text{T}}^{\text{cut}})^2} \mathrm{d}q_{\text{T}}^2 \, \frac{\mathrm{d}\sigma^{\text{NLO}(r)}}{\mathrm{d}q_{\text{T}}^2} \tag{2.3.2}$$

where

$$\frac{\mathrm{d}\sigma^{\text{NLO}(0)}}{\mathrm{d}q_{\text{T}}^2} = \frac{\alpha_{\text{S}}}{2\pi} \left[\mathcal{C}^{(1,-1,0)} \, \delta\big(q_{\text{T}}^2\big) + \mathcal{C}^{(1,0,0)} \, \frac{1}{q_{\text{T}}^2} + \mathcal{C}^{(1,1,0)} \, \frac{\log q_{\text{T}}^2}{q_{\text{T}}^2} \right] \tag{2.3.3}$$

$$\frac{\mathrm{d}\sigma^{\text{NLO}(r>0)}}{\mathrm{d}q_{\text{T}}^2} = \frac{\alpha_{\text{S}}}{2\pi} \left[\mathcal{C}^{(1,0,r)} + \mathcal{C}^{(1,1,r)} \, \big(q_{\text{T}}^2\big)^{r-1} \, \log q_{\text{T}}^2 \right] . \tag{2.3.4}$$

The first figure in the superscript of the coefficients $\mathcal{C}^{(n,m,r)}$ stands for the perturbative order in α_{S}. In this case we are at NLO in QCD, namely $n = 1$. The second figure refers to the logarithmic accuracy, which starts from zero and counts, for the n-th order in α_{S}, up to $2n-1$ powers (the δ-term in eq. (2.3.3) corresponds to the virtual contribution once the divergences are subtracted according to the scheme of choice). The third figure denotes the expansion in powers of the event-shape variable chosen as resolution parameter.

The same expansion can be straightforwardly generalised to higher orders in α_{S} and the knowledge of the coefficients $c^{(n,m,0)}$, with $0 \leqslant m \leqslant 3$, allows us to build the global counterterms of the q_{T}-subtraction method at N^{n}LO in QCD. Such coefficients, see eq. (2.3.3), correspond to the singular terms and are known from resummation techniques or effective field theories [37–47]. In both cases one exploits the universal behaviour of scattering amplitudes at the boundaries of the phase space, namely in soft-collinear regions. Otherwise, the terms in eq. (2.3.4) are power corrections that vanish in the small-cutoff limit and that are, in general, process dependent as much as the finite virtual delta-term in eq. (2.3.3). Thus, after the subtraction procedure, a residual dependence on the cutoff can remain as power corrections. While these terms formally vanish in the null-cutoff limit, they give a non-zero numerical contribution for any finite choice of the cutoff.

Until recently, since only the term in eq. (2.3.3), i.e. the *leading power*, was under control, the solution consisted in stopping the expansion of eq. (2.3.2) at order zero

and taking an extremely small cutoff in order to minimize the residual error induced by the neglected *subleading powers* of eq. (2.3.4). As a result, the separation of the phase space introduced by the slicing method introduces instabilities in the numerical evaluation of cross sections and differential distributions [48–51] – some care has then to be taken in order to obtain stable and reliable results.

From a theoretical point of view, then, the knowledge of the power corrections greatly increases our understanding of the perturbative behaviour of the QCD cross sections, since more non-trivial (universal and non-universal) terms appear. The origin of these terms can be traced back both to the scattering amplitudes, evaluated at phase-space boundaries, and to the phase space itself. Thus, several papers have tackled the study of power corrections in the soft and collinear limits [52–54], while studies in the general framework of fixed-order and threshold-resummed computations have been also performed [55–63].

From a practical point of view, the knowledge of the subleading power corrections makes the numerical implementation of a subtraction method more robust, since the power terms weaken the dependence of the final result on the arbitrary cutoff. This is not only valid when the subtraction method is applied to NLO computations, but it is numerically more relevant when applied to higher-order calculation, as pointed out, for example, in the evaluation of NNLO cross sections in refs. [50, 51].

Power corrections at NLO have been extensively studied in refs. [64–74] in the context of the N-jettiness subtraction method, and in refs. [75–80] within SCET-based subtraction methods. Power corrections at NLO for the transverse momentum of a colour singlet have been derived for the first time at differential level in ref. [81] within the SCET framework. In ref. [82], we presented a method to compute the transverse-momentum power corrections at all orders, for the inclusive production of a colourless final-state system, at NLO in QCD. Recently, the leading power corrections for the electroweak NLO corrections to the inclusive cross section for the production of a massive lepton pair through the Drell–Yan mechanism have been computed in ref. [83].

N-jettiness power corrections at NNLO have been considered in refs. [64, 67]. In particular, analytic results are obtained for the dominant $\alpha_{\rm s}\,\tau\log(\tau)$ and $\alpha_{\rm s}^2\,\tau\log^3(\tau)$ subleading terms, where τ is the 0-jettiness, for $q\bar{q}$-initiated Drell–Yan production and for gg-, gq- and $q\bar{q}$-initiated Higgs boson production, along with a numerical fit for the subdominant terms.

In addition, a numerical extraction of power corrections in the context of NNLL'+ NNLO calculations was done in N-jettiness [47], and a general discussion in the context of the fixed-order implementation of the N-jettiness subtraction can be found in ref. [9].

In ref. [84] we tackled instead the first step in order to compute the transverse-momentum power corrections, up to the second power, of the NNLO cumulative cross section for vector-boson production. In fact, together with the real-virtual qg-

initiated channel that we consider therein, also the qq-initiated channel contributes to the real-virtual terms, together with all the double-real radiation contributions. These contributions will be considered in future works.

2.4 Subleading power corrections for Z and H production

In this section we outline the calculation we have done in order to obtain the subleading power corrections to an inclusive cross section at NLO in $\alpha_{\rm S}$. We present analytic results for both Drell–Yan Z production and Higgs boson production in gluon fusion and we illustrate a process-independent procedure for the calculation of the all-order power corrections in a transverse momentum cutoff.

In the small-$q_{\rm T}$ region, i.e. $q_{\rm T} \ll Q$, the real contribution to the perturbative cross sections of eqs. (2.2.41)–(2.2.59) contains well-known logarithmically-enhanced terms that are singular in the $q_{\rm T} \to 0$ limit [37–46]. In the context of inclusive NLO fixed-order calculations, the logarithmic terms are cancelled when using the subtraction prescriptions. For more exclusive quantities, such as the transverse-momentum distribution of the colourless system, the same logarithmic terms need to be resummed at all orders in the strong coupling constant to produce reliable results. Although our studies are of value in the context of the transverse-momentum resummation, here we limit ourselves to the case of inclusive fixed-order predictions at NLO, leaving the resummation program to future investigations. In the following we compute power-correction terms to the cross section that, although vanishing in the small-$q_{\rm T}$ limit, may give a sizable numerical contribution when using a slicing subtraction method.

To explicitly present the perturbative structure of these terms at small $q_{\rm T}$, it is customary in the literature [22, 68] to compute the following cumulative partonic cross section, integrating the differential cross section in the range $0 \leq q_{\rm T} \leq q_{\rm T}^{\rm cut}$,

$$\hat{\sigma}_{ab}^{<}(z) \equiv \int_0^{\left(q_{\rm T}^{\rm cut}\right)^2} {\rm d}q_{\rm T}^2 \, \frac{{\rm d}\hat{\sigma}_{ab}(q_{\rm T}, z)}{{\rm d}q_{\rm T}^2}. \tag{2.4.1}$$

The cross section in eq. (2.4.1) receives contributions from the Born and the virtual terms, both proportional to $\delta(q_{\rm T})$, and from the part of the real amplitude that describes the production of the F system with transverse momentum less than $q_{\rm T}^{\rm cut}$. The virtual and real contributions are separately divergent and are typically regularised in dimensional regularisation. Since the total partonic cross section is finite and analytically known for the processes under study, following what was done in refs. [85, 86][2], we compute the above integral as

$$\hat{\sigma}_{ab}^{<}(z) = \hat{\sigma}_{ab}^{\rm tot}(z) - \hat{\sigma}_{ab}^{>}(z)\,, \tag{2.4.2}$$

[2]The same technique was used in order to compute the soft constant of the $q_{\rm T}$-subtraction hard function and the second-order collinear coefficient functions for transverse-momentum resummation.

with

$$\hat{\sigma}_{ab}^{\rm tot}(z) = \int_0^{\left(q_{\rm T}^{\rm max}\right)^2} {\rm d}q_{\rm T}^2 \, \frac{{\rm d}\hat{\sigma}_{ab}(q_{\rm T}, z)}{{\rm d}q_{\rm T}^2} \,, \tag{2.4.3}$$

$$\hat{\sigma}_{ab}^{>}(z) = \int_{\left(q_{\rm T}^{\rm cut}\right)^2}^{\left(q_{\rm T}^{\rm max}\right)^2} {\rm d}q_{\rm T}^2 \, \frac{{\rm d}\hat{\sigma}_{ab}(q_{\rm T}, z)}{{\rm d}q_{\rm T}^2} \,, \tag{2.4.4}$$

where $q_{\rm T}^{\rm max}$ is the maximum transverse momentum allowed by the kinematics, $\hat{\sigma}_{ab}^{\rm tot}(z)$ is the total partonic cross section and $\hat{\sigma}_{ab}^{>}(z)$ is the partonic cross section integrated above $q_{\rm T}^{\rm cut}$. The advantage of using eq. (2.4.2) is that the partonic cross section integrated in the range $0 \leq q_{\rm T} \leq q_{\rm T}^{\rm cut}$ is obtained as difference of the total cross section (formally free from any dependence on $q_{\rm T}^{\rm cut}$) and the partonic cross section integrated in the range above $q_{\rm T}^{\rm cut}$ of eq. (2.4.4). Since $q_{\rm T} > q_{\rm T}^{\rm cut} > 0$, the last integration can be performed in four space-time dimensions, with no further use of dimensional regularisation. This explains why in section 2.2 we work in $d = 4$ dimensions.

In refs. [85, 86] the computation of the cumulative cross section was performed in the limit $q_{\rm T}^{\rm cut} \ll Q$, neglecting terms of $\mathcal{O}((q_{\rm T}^{\rm cut})^2)$ on the right-hand side of eq. (2.4.2). Here, we compute these terms up to $\mathcal{O}((q_{\rm T}^{\rm cut})^4)$ included.

2.4.1 $q_{\rm T}$-integrated partonic cross sections

In the following we present the results for the partonic cross section in eq. (2.4.4), integrated in $q_{\rm T}$, from an arbitrary value $q_{\rm T}^{\rm cut}$ up to the maximum transverse momentum $q_{\rm T}^{\rm max}$ allowed by the kinematics of the event, given by

$$\left(q_{\rm T}^{\rm max}\right)^2 = Q^2 \, \frac{(1-z)^2}{4\,z} \,, \tag{2.4.5}$$

at a fixed value of z. The integrations are straightforward and do not need any dedicated comment beyond the results, that we report here along with the only three master integrals needed in order to accomplish the integration. Before showing them, in order to lighten up the notation, we introduce the dimensionless quantity[3]

$$a \equiv \frac{\left(q_{\rm T}^{\rm cut}\right)^2}{Q^2} \,, \tag{2.4.6}$$

that will be our expansion parameter in the rest of the study, and we define

$$\pi_{\rm T}^2 \equiv \frac{4az}{(1-z)^2} \,, \tag{2.4.7}$$

that will allow us to write the upcoming differential cross sections in a more compact form. In Appendix B we recall the minimal set of integrals needed in order to compute the following $q_{\rm T}$-integrated cross sections.

[3] In the literature, the parameter a is also referred to as $r_{\rm cut}^2$ (see e.g. [50]).

Z production

- $q(\bar{q}) + g \to Z + q(\bar{q})$

$$
\begin{aligned}
\hat{\sigma}_{qg}^{>(1)}(z) &= \int_{\left(q_{\mathrm{T}}^{\mathrm{cut}}\right)^2}^{\left(q_{\mathrm{T}}^{\mathrm{max}}\right)^2} \mathrm{d}q_{\mathrm{T}}^2 \, \frac{\mathrm{d}\hat{\sigma}_{qg}^{(1)}(q_{\mathrm{T}}, z)}{\mathrm{d}q_{\mathrm{T}}^2} \\
&= \sigma_{qq}^{(0)} \, T_{\mathrm{R}} \, z \left\{ \frac{1}{2}(1+3z)(1-z) \sqrt{1 - \frac{4az}{(1-z)^2}} \right. \\
&\qquad \left. + p_{qg}(z) \left[-\log \frac{az}{(1-z)^2} + 2 \log \frac{1}{2} \left(\sqrt{1 - \frac{4az}{(1-z)^2}} + 1 \right) \right] \right\} \\
&= \sigma_{qq}^{(0)} \, T_{\mathrm{R}} \, z \left\{ \frac{1}{2}(1+3z)(1-z) \sqrt{1-\pi_{\mathrm{T}}^2} \right. \\
&\qquad \left. + p_{qg}(z) \log \frac{1 + \sqrt{1-\pi_{\mathrm{T}}^2}}{1 - \sqrt{1-\pi_{\mathrm{T}}^2}} \right\},
\end{aligned}
\tag{2.4.8}
$$

- $q + \bar{q} \to Z + g$

$$
\begin{aligned}
\hat{\sigma}_{q\bar{q}}^{>(1)}(z) &= \int_{\left(q_{\mathrm{T}}^{\mathrm{cut}}\right)^2}^{\left(q_{\mathrm{T}}^{\mathrm{max}}\right)^2} \mathrm{d}q_{\mathrm{T}}^2 \frac{\mathrm{d}\hat{\sigma}_{q\bar{q}}^{(1)}(q_{\mathrm{T}}, z)}{\mathrm{d}q_{\mathrm{T}}^2} \\
&= \sigma_{qq}^{(0)} \, C_{\mathrm{F}} \, z \left\{ -2\,(1-z) \sqrt{1 - \frac{4az}{(1-z)^2}} \right. \\
&\qquad \left. + 2\,\hat{p}_{qq}(z) \left[-\log \frac{az}{(1-z)^2} + 2 \log \frac{1}{2} \left(\sqrt{1 - \frac{4az}{(1-z)^2}} + 1 \right) \right] \right\} \\
&= \sigma_{qq}^{(0)} \, C_{\mathrm{F}} \, z \left\{ -2\,(1-z) \sqrt{1-\pi_{\mathrm{T}}^2} \right. \\
&\qquad \left. + 2\,\hat{p}_{qq}(z) \log \frac{1 + \sqrt{1-\pi_{\mathrm{T}}^2}}{1 - \sqrt{1-\pi_{\mathrm{T}}^2}} \right\}.
\end{aligned}
\tag{2.4.9}
$$

H production

- $g + q(\bar{q}) \to H + q(\bar{q})$

$$\begin{aligned}
\hat{\sigma}_{gq}^{>(1)}(z) &= \int_{\left(q_{\mathrm{T}}^{\mathrm{cut}}\right)^2}^{\left(q_{\mathrm{T}}^{\mathrm{max}}\right)^2} \mathrm{d}q_{\mathrm{T}}^2 \frac{\mathrm{d}\hat{\sigma}_{gq}^{(1)}(q_{\mathrm{T}}, z)}{\mathrm{d}q_{\mathrm{T}}^2} \\
&= \sigma_{gg}^{(0)} C_{\mathrm{F}}\, z \left\{ -\frac{3(1-z)^2}{2z} \sqrt{1 - \frac{4az}{(1-z)^2}} \right. \\
&\qquad \left. + p_{gq}(z) \left[-\log \frac{az}{(1-z)^2} + 2 \log \frac{1}{2} \left(\sqrt{1 - \frac{4az}{(1-z)^2}} + 1 \right) \right] \right\} \\
&= \sigma_{gg}^{(0)} C_{\mathrm{F}}\, z \left\{ -\frac{3(1-z)^2}{2z} \sqrt{1 - \pi_{\mathrm{T}}^2} \right. \\
&\qquad \left. + p_{gq}(z) \log \frac{1 + \sqrt{1 - \pi_{\mathrm{T}}^2}}{1 - \sqrt{1 - \pi_{\mathrm{T}}^2}} \right\},
\end{aligned} \tag{2.4.10}$$

- $g + g \to H + g$

$$\begin{aligned}
\hat{\sigma}_{gg}^{>(1)}(z) &= \int_{\left(q_{\mathrm{T}}^{\mathrm{cut}}\right)^2}^{\left(q_{\mathrm{T}}^{\mathrm{max}}\right)^2} \mathrm{d}q_{\mathrm{T}}^2 \frac{\mathrm{d}\hat{\sigma}_{gg}^{(1)}(q_{\mathrm{T}}, z)}{\mathrm{d}q_{\mathrm{T}}^2} \\
&= \sigma_{gg}^{(0)} C_{\mathrm{A}}\, z \left\{ -\frac{4(1-z)^3}{z} \sqrt{1 - \frac{4az}{(1-z)^2}} \right. \\
&\qquad + 4\, z \left[\frac{1-z}{2z} \frac{(1-z)^2}{6z} \sqrt{1 - \frac{4az}{(1-z)^2}} \left(1 + \frac{2az}{(1-z)^2} \right) \right] \\
&\qquad \left. + 2\, \hat{p}_{gg}(z) \left[-\log \frac{az}{(1-z)^2} + 2 \log \frac{1}{2} \left(\sqrt{1 - \frac{4az}{(1-z)^2}} + 1 \right) \right] \right\} \\
&= \sigma_{gg}^{(0)} C_{\mathrm{A}}\, z \left\{ -\frac{11}{3} \frac{(1-z)^3}{z} \left(1 - \frac{\pi_{\mathrm{T}}^2}{22} \right) \sqrt{1 - \pi_{\mathrm{T}}^2} \right. \\
&\qquad \left. + 2\, \hat{p}_{gg}(z) \log \frac{1 + \sqrt{1 - \pi_{\mathrm{T}}^2}}{1 - \sqrt{1 - \pi_{\mathrm{T}}^2}} \right\}.
\end{aligned} \tag{2.4.11}$$

As anticipated in section 2.2, we do not consider the process $q\bar{q} \to Hg$ since it is not singular in the limit $q_{\mathrm{T}} \to 0$ and the corresponding analytic/numeric integration in the transverse momentum can be performed setting explicitly $q_{\mathrm{T}}^{\mathrm{cut}} = 0$.

A couple of further comments about the above expressions are also in order. In first place, the part of the cross sections proportional to the Altarelli–Parisi splitting

functions in eqs. (2.4.8)–(2.4.11) has a universal origin, due to the factorisation of the collinear singularities on the underlying Born. The rest of the above cross sections is, in general, not universal. In addition, for Higgs boson production, the NLO cumulative cross sections that we have computed coincide exactly with the jet-vetoed cross sections $\sigma^{\rm veto}(p_{\rm T}^{\rm veto})$ of ref. [87], provided we identify $q_{\rm T}^{\rm cut} = p_{\rm T}^{\rm veto}$.

2.4.2 Extending the integration in z

According to eq. (2.2.29), in order to compute the hadronic cross section we need to integrate the partonic cross sections convoluted with the corresponding luminosities. In the calculation of the total cross sections, the upper limit in the z integration is unrestricted and is equal to 1. When a cut on the transverse momentum $q_{\rm T}$ is applied, the reality of eqs. (2.4.8)–(2.4.11) imposes the non negativity of the argument of the square roots, i.e.

$$1 - \pi_{\rm T}^2 \geq 0\,, \tag{2.4.12}$$

that in turn gives

$$z \leq z^{\rm max} \equiv 1 - f(a)\,, \qquad\qquad f(a) \equiv 2\sqrt{a}\left(\sqrt{1+a} - \sqrt{a}\right). \tag{2.4.13}$$

Since our aim is to make contact with the transverse-momentum subtraction formulae, that describe the behaviour of the cross sections in the soft and collinear limits, we need to extend the integration range of the z variable up to 1, i.e. the upper integration limit of z in a Born-like kinematics. In fact, only in the $z \to 1$ limit we recover the logarithmic structure from the soft region of the emission. In order to obtain explicitly all the logarithmic-enhanced terms in the small-$q_{\rm T}^{\rm cut}$ limit, we have then to expand our results in powers of a. Since both the integrand and the upper limit of the integral depend on a, the naïve approach of expanding only the integrand does not work, due to the appearance of divergent terms in the $z \to 1$ limit, that have to be handled with the introduction of plus distributions.

Using the notation of ref. [85], we first introduce the function $\hat{R}_{ab}(z)$, defined by

$$\sigma_{ab}^{<} = \tau \int_{\tau}^{1-f(a)} \frac{{\rm d}z}{z}\, \mathcal{L}_{ab}\left(\frac{\tau}{z}\right) \frac{1}{z}\, \hat{\sigma}_{ab}^{<}(z) \equiv \tau \int_{\tau}^{1} \frac{{\rm d}z}{z}\, \mathcal{L}_{ab}\left(\frac{\tau}{z}\right) \hat{\sigma}^{(0)} \hat{R}_{ab}(z)\,, \tag{2.4.14}$$

where the upper integration limit in z in the last integral is exactly 1 and $\hat{\sigma}^{(0)}$ is the partonic Born-level cross section for the production of the colourless system F. The function $\hat{R}_{ab}(z)$ can be written as a perturbative expansion in $\alpha_{\rm S}$

$$\hat{R}_{ab}(z) = \delta_{\rm B}\, \delta(1-z) + \sum_{n=1}^{\infty} \left(\frac{\alpha_{\rm S}}{2\pi}\right)^n \hat{R}_{ab}^{(n)}(z)\,, \tag{2.4.15}$$

where the $\delta(1-z)$ term is the Born-level contribution, and $\delta_{\rm B} = 1$ when partons a and b are such that $a + b \to F$ is a possible Born-like process, otherwise its value is 0.

The coefficient functions $\hat{R}_{ab}^{(n)}(z)$ can be computed as power series in a. It is in fact well known in the literature [85] that the NLO coefficient $\hat{R}_{ab}^{(1)}(z)$ has the following form[4]

$$\hat{R}_{ab}^{(1)}(z) = \log^2(a)\,\hat{R}_{ab}^{(1,2,0)}(z) + \log(a)\,\hat{R}_{ab}^{(1,1,0)}(z) + \hat{R}_{ab}^{(1,0,0)}(z) + \mathcal{O}\left(a^{\frac{1}{2}}\log a\right), \quad (2.4.16)$$

and the aim of this study is to compute the first unknown terms in eq. (2.4.16) that were neglected in refs. [85] and [86], namely $R_{ab}^{(1,m,r)}(z)$, for r up to 4 and for any m.

In a way similar to what was done in eq. (2.4.14) for $\hat{R}_{ab}(z)$, we introduce the function $\hat{G}_{ab}(z)$ defined by

$$\sigma_{ab}^{>} = \tau \int_{\tau}^{1-f(a)} \frac{\mathrm{d}z}{z}\,\mathcal{L}_{ab}\left(\frac{\tau}{z}\right)\frac{1}{z}\,\hat{\sigma}_{ab}^{>}(z) \equiv \tau \int_{\tau}^{1} \frac{\mathrm{d}z}{z}\,\mathcal{L}_{ab}\left(\frac{\tau}{z}\right)\hat{\sigma}^{(0)}\,\hat{G}_{ab}(z)\,. \quad (2.4.17)$$

Since

$$\sigma_{ab}^{<} + \sigma_{ab}^{>} = \tau \int_{\tau}^{1} \frac{\mathrm{d}z}{z}\,\mathcal{L}_{ab}\left(\frac{\tau}{z}\right)\hat{\sigma}_{ab}^{\mathrm{tot}}(z) \equiv \sigma_{ab}^{\mathrm{tot}}\,, \quad (2.4.18)$$

and $\sigma_{ab}^{\mathrm{tot}}$ is independent of a, the coefficients of the terms that vanish in the small-q_{T} limit in the series expansion in a of $\hat{R}_{ab}(z)$ and $\hat{G}_{ab}(z)$ are equal but with opposite sign, at any order in α_{S}. We recall that $\hat{R}_{ab}(z)$ contains terms of the form $\delta(1-z)$, coming from the Born and the virtual contributions, that are independent of a and are obviously absent in $\hat{G}_{ab}(z)$.

In the rest of the study we compute the first terms of the expansion in a of $\hat{G}_{ab}^{(1)}(z)$, that will be obtained from the following identity

$$\sigma_{ab}^{>(1)} = \tau \int_{\tau}^{1-f(a)} \frac{\mathrm{d}z}{z}\,\mathcal{L}_{ab}\left(\frac{\tau}{z}\right)\frac{1}{z}\,\hat{\sigma}_{ab}^{>(1)}(z) = \tau \int_{\tau}^{1} \frac{\mathrm{d}z}{z}\,\mathcal{L}_{ab}\left(\frac{\tau}{z}\right)\hat{\sigma}^{(0)}\,\hat{G}_{ab}^{(1)}(z)\,. \quad (2.4.19)$$

We have elaborated a process-independent formula to transform an integral of the form of the first one in eq. (2.4.19) into the form of the second one, producing the series expansion of $\hat{G}_{ab}^{(1)}(z)$ in a. The application of our formula reorganizes the divergent terms in the $z \to 1$ limit into terms that are integrable up to $z = 1$ and logarithmic terms in a. Since this is a very technical procedure, we quote in the following section the general method, whereas all the practical details are collected in Appendix C, and we refer the interested reader to that appendix for the application of the method to the four channels under investigation.

[4] The notation for the expansion of $R_{ab}^{(1)}(z)$ follows from the number of powers of α_{S}, $\log(a)$ and $a^{\frac{1}{2}}$, i.e.

$$\hat{R}_{ab}^{(1)}(z) = \sum_{m,r} \log^m(a)\,a^{\frac{r}{2}}\,\hat{R}_{ab}^{(1,m,r)}(z)\,.$$

In refs. [5, 85], the leading-logarithmic $R_{ab}^{(1,2,0)}(z)$ and next-to-leading-logarithmic $R_{ab}^{(1,1,0)}(z)$ coefficient functions are directly associated to $\Sigma_{c\bar{c}\leftarrow ab}^{F(1;2)}(z)$ and $\Sigma_{c\bar{c}\leftarrow ab}^{F(1;1)}(z)$, respectively. The hard-virtual coefficient function $\mathcal{H}_{c\bar{c}\leftarrow ab}^{F(1)}$ corresponds to $R_{ab}^{(1,0,0)}(z)$.

2.4.3 Process-independent procedure for extending the z integration

In this section we describe the procedure followed to extend the integration range of the z variable up to 1, as displayed in eq. (2.4.19), performing an expansion in a. We consider an integral of the following form

$$I = \int_{\tau}^{1-f(a)} \mathrm{d}z \; l(z)\, g(z)\,, \tag{2.4.20}$$

with $g(z)$ not defined for $z > 1 - f(a)$, $l(z)$ well behaved for $\tau \leq z \leq 1$ and $l(z) = 0$ for $z < \tau$. We also assume that $l(z)$ is $\mathcal{C}^\infty$, so that we can derive it as many times as necessary. We then suppose that $g(z)$ can be written as an expansion in (negative) powers of $(1 - z)$

$$g(z) = g_0(z,a) + \frac{g_1(z,a)}{1-z} + \frac{g_2(z,a)}{(1-z)^2} + \ldots = \sum_{n=0}^{\infty} \frac{g_n(z,a)}{(1-z)^n}\,, \tag{2.4.21}$$

where, in $z = 1$, the $g_i(z,a)$ are not singular or have an integrable singularity. If not identically zero everywhere, the $g_i(z,a)$ are different from 0 for $z = 1$ and $i \geq 1$, and, in general, the $g_i(z,a)$ functions contain growing powers of a as i increases.

The point we would like to make here is that the right-hand side of eq. (2.4.21) is convergent only for $z \leq 1 - f(a)$, and it converges to $g(z)$. For $z > 1 - f(a)$ the series does not converge to $g(z)$, otherwise $g(z)$ would be defined in this region too.

We also assume that we can exchange the order of integration and summation of the series, and we write eq. (2.4.20) as

$$I = \sum_{n=0}^{\infty} I_n\,, \tag{2.4.22}$$

where

$$I_n \equiv \int_{\tau}^{1-f(a)} \mathrm{d}z\, l(z)\, \frac{g_n(z,a)}{(1-z)^n} = \int_{0}^{1-f(a)} \mathrm{d}z\, l(z)\, \frac{g_n(z,a)}{(1-z)^n}\,, \tag{2.4.23}$$

where we have extended the z-integration down to 0, since $l(z) = 0$ for $z < \tau$. Each term of the series can now be manipulated as shown in the following.

I_0

$$\begin{aligned} I_0 &= \int_{0}^{1-f(a)} \mathrm{d}z\, l(z)\, g_0(z,a) \\ &= \int_{0}^{1} \mathrm{d}z\, l(z)\, g_0(z,a) - \int_{1-f(a)}^{1} \mathrm{d}z\, l(z)\, g_0(z,a) \end{aligned} \tag{2.4.24}$$

is finite and poses no problems.

I_1

$$\begin{aligned} I_1 \;=\; &+\int_0^{1-f(a)} \mathrm{d}z \big[l(z)-l(1)\big]\,\frac{g_1(z,a)}{1-z} + \int_0^{1-f(a)} \mathrm{d}z\, l(1)\,\frac{g_1(z,a)}{1-z} \\ =\; &+\int_0^{1} \mathrm{d}z \big[l(z)-l(1)\big]\,\frac{g_1(z,a)}{1-z} - \int_{1-f(a)}^{1} \mathrm{d}z \big[l(z)-l(1)\big]\,\frac{g_1(z,a)}{1-z} \\ &+\int_0^{1-f(a)} \mathrm{d}z\, l(1)\,\frac{g_1(z,a)}{1-z}\,, \end{aligned} \tag{2.4.25}$$

where we have added and subtracted the first term of the Taylor expansion of $l(z)$ around the point $z=1$, and performed straightforward manipulations of the integration limits. The first and second integrands in the above equation are well behaved when $z \to 1$, since the numerator goes to zero at least as fast as $(1-z)$, cancelling the divergence of the denominator.

I_2

In a similar way, we can manipulate I_2 to have

$$\begin{aligned} I_2 \;=\; &+\int_0^{1} \mathrm{d}z \big[l(z)-l(1)-(z-1)\,l^{(1)}(1)\big]\,\frac{g_2(z,a)}{(1-z)^2} \\ &-\int_{1-f(a)}^{1} \mathrm{d}z \big[l(z)-l(1)-l^{(1)}(1)\,(z-1)\big]\,\frac{g_2(z,a)}{(1-z)^2} \\ &+\int_0^{1-f(a)} \mathrm{d}z \big[l(1)+l^{(1)}(1)\,(z-1)\big]\,\frac{g_2(z,a)}{(1-z)^2}\,, \end{aligned} \tag{2.4.26}$$

where we have added and subtracted the first two terms of the Taylor expansion of $l(z)$ around $z=1$. Again the first two integrands are finite when $z \to 1$, since the numerator is $\mathcal{O}((1-z)^2)$.

Final expression

The same procedure can be applied to all the integrals I_n and leads to the final result

$$I = \tilde{I}_1 + \tilde{I}_2 + \tilde{I}_3\,, \tag{2.4.27}$$

where

$$\begin{aligned}\tilde{I}_1 = &+\int_0^1 \mathrm{d}z\, l(z)\, g_0(z,a)\\ &+\int_0^1 \mathrm{d}z\, \big[l(z)-l(1)\big]\,\frac{g_1(z,a)}{1-z}\\ &+\int_0^1 \mathrm{d}z\, \Big[l(z)-l(1)-l^{(1)}(1)\,(z-1)\Big]\,\frac{g_2(z,a)}{(1-z)^2}+\dots\end{aligned} \tag{2.4.28}$$

$$\begin{aligned}\tilde{I}_2 = &+\int_0^{1-f(a)} \mathrm{d}z\, l(1)\big[g(z)-g_0(z,a)\big]\\ &+\int_0^{1-f(a)} \mathrm{d}z\, l^{(1)}(1)\,(z-1)\left[g(z)-g_0(z,a)-\frac{g_1(z,a)}{1-z}\right]\\ &+\int_0^{1-f(a)} \mathrm{d}z\, \frac{1}{2!}\,l^{(2)}(1)\,(z-1)^2\left[g(z)-g_0(z,a)-\frac{g_1(z,a)}{1-z}-\frac{g_2(z,a)}{(1-z)^2}\right]+\dots\end{aligned} \tag{2.4.29}$$

$$\begin{aligned}\tilde{I}_3 = &-\int_{1-f(a)}^1 \mathrm{d}z\, l(z)\, g_0(z,a)\\ &-\int_{1-f(a)}^1 \mathrm{d}z\big[l(z)-l(1)\big]\,\frac{g_1(z,a)}{1-z}\\ &-\int_{1-f(a)}^1 \mathrm{d}z\, \Big[l(z)-l(1)-l^{(1)}(1)\,(z-1)\Big]\,\frac{g_2(z,a)}{(1-z)^2}+\dots\end{aligned} \tag{2.4.30}$$

Notice that in $\tilde{I}_2$ the sum of the terms of the series add up to give back $g(z)$, since the upper integration limit is $1-f(a)$, so that we are within the region of convergence of the series. The integrals in $\tilde{I}_2$ have to be evaluated exactly analytically, and this is the harsh part of the calculation.

The integrals in $\tilde{I}_3$ can instead be computed by performing an expansion in a, and this part of the calculation poses no problems. Examples for the resolution of these integrals are given in Appendix C.

Finally, by using of the plus distributions defined in Appendix G, we can write $\tilde{I}_1$ in a more compact form

$$\tilde{I}_1 = \int_0^1 \mathrm{d}z\, l(z)\, g_0(z,a) + \int_0^1 \mathrm{d}z\, l(z)\left[\frac{g_1(z,a)}{1-z}\right]_+ + \int_0^1 \mathrm{d}z\, l(z)\left[\frac{g_2(z,a)}{(1-z)^2}\right]_{2+}+\dots \tag{2.4.31}$$

This completes our process-independent procedure for the manipulation of the integral in eq. (2.4.20).

2.4.4 Results

In this section we summarise our findings. In particular, we present the analytic results for the $\hat{G}^{(1)}_{ab}(z)$ functions we have computed. In the calculation of these functions,

we kept trace of all the terms originating from the manipulation of the contributions proportional to the Altarelli–Parisi splitting functions, in the partonic cross sections of eqs. (2.2.41)–(2.2.59). These terms constitute what we call the "universal part" of our results, as detailed in secs. 2.2 and 2.4.1. We will indicate these terms with the superscript "U", while the remaining terms will have a superscript "R". We stress here that the distinction between universal and non-universal part is purely formal, and it does not have a physical implication. The reason of this separation is to have hints on the general structure of the $q_{\mathrm{T}}^{\mathrm{cut}}$ dependence of inclusive cross sections for the production of arbitrary colorless systems. We comment on the results that we have obtained in the subsequent paragraphs.

In the last part of this section we study the numerical significance of the power-correction terms we have computed, discussing first their impact on the different production channels for Drell–Yan Z boson and Higgs boson production in gluon fusion. Then we present their overall effect, normalising the results with respect to the total NLO cross section, in order to have a better grasp on the size of these contributions.

Results for the $\hat{G}_{ab}^{(1)}(z)$ functions

We indicate with $\hat{g}_{ab}^{\mathrm{U}(1)}(z)$ the universal part of the $\hat{G}_{ab}^{(1)}(z)$ functions, and with $\hat{g}_{ab}^{\mathrm{R}(1)}(z)$ the remaining part, stripped off of a common colour factor. Our expressions for $\hat{G}_{ab}^{(1)}(z)$ contain derivatives of the Dirac δ function, $\delta^{(n)}(z)$, up to $n = 5$, and plus distributions up to order 5. We report here the definition of a plus distribution of order n

$$\int_0^1 \mathrm{d}z\, l(z)\, [g(z)]_{n+} \equiv \int_0^1 \mathrm{d}z \left\{ l(z) - \sum_{i=0}^{n-1} \frac{1}{i!}\, l^{(i)}(1)\, (z-1)^i \right\} g(z)\,, \tag{2.4.32}$$

where $g(z)$ has a pole of order n for $z = 1$, and $l(z)$ is a continuous function in $z = 1$, together with all its derivatives up to order $(n-1)$. For completeness, we collect in Appendix G more details on the plus distributions, and the identities we have used to simplify our results.

Z production

- $q(\bar{q}) + g \to Z + q(\bar{q})$

$$\hat{G}_{qg}^{(1)}(z) = T_{\mathrm{R}}\, \hat{g}_{qg}^{(1)}(z)\,, \qquad \hat{g}_{qg}^{(1)}(z) = \hat{g}_{qg}^{\mathrm{U}(1)}(z) + \hat{g}_{qg}^{\mathrm{R}(1)}(z)\,, \tag{2.4.33}$$

  where

$$
\begin{aligned}
\hat{g}_{qg}^{\mathrm{U}(1)}(z) = & -p_{qg}(z)\log(a) - p_{qg}(z)\,\log\frac{z}{(1-z)^2} \\
& + \left\{\delta^{(1)}(1-z) - 3\,\delta(1-z)\right\} a\log(a) \\
& + \left\{\delta(1-z) - 2\,z\,p_{qg}(z)\left[\frac{1}{(1-z)^2}\right]_{2+}\right\} a \\
& + \left\{-9\,\delta(1-z) + \frac{21}{2}\,\delta^{(1)}(1-z)\right. \\
& \qquad \left. - 3\,\delta^{(2)}(1-z) + \frac{1}{4}\,\delta^{(3)}(1-z)\right\} a^2\log(a) \\
& + \left\{+2\,\delta(1-z) + \frac{7}{4}\,\delta^{(1)}(1-z) - \frac{5}{4}\,\delta^{(2)}(1-z) + \frac{1}{6}\,\delta^{(3)}(1-z)\right. \\
& \qquad \left. -3\,z^2 p_{qg}(z)\left[\frac{1}{(1-z)^4}\right]_{4+}\right\} a^2 \\
& + \mathcal{O}\Big(a^{\frac{5}{2}}\log(a)\Big)\,,
\end{aligned}
\tag{2.4.34}
$$

$$
\begin{aligned}
\hat{g}_{qg}^{\mathrm{R}(1)}(z) = & \frac{1}{2}\,(1+3z)(1-z) - z(1+3z)\left[\frac{1}{1-z}\right]_{+} a \\
& - z^2(1+3z)\left[\frac{1}{(1-z)^3}\right]_{3+} a^2 \\
& + 2\,\delta(1-z)\,a\log(a) - 2\,\delta(1-z)\,a \\
& + \left\{5\,\delta(1-z) - \frac{11}{2}\,\delta^{(1)}(1-z) + \delta^{(2)}(1-z)\right\} a^2\log(a) \\
& + \left\{-2\,\delta(1-z) - \frac{3}{4}\,\delta^{(1)}(1-z) + \frac{1}{2}\,\delta^{(2)}(1-z)\right\} a^2 \\
& + \mathcal{O}\Big(a^{\frac{5}{2}}\log(a)\Big)\,,
\end{aligned}
\tag{2.4.35}
$$

and

$$
p_{qg}(z) = 2z^2 - 2z + 1\,. \tag{2.4.36}
$$

- $q + \bar{q} \to Z + g$

$$
\hat{G}_{q\bar{q}}^{(1)}(z) = C_{\mathrm{F}}\,\hat{g}_{q\bar{q}}^{(1)}(z)\,, \qquad\qquad \hat{g}_{q\bar{q}}^{(1)}(z) = \hat{g}_{q\bar{q}}^{\mathrm{U}(1)}(z) + \hat{g}_{q\bar{q}}^{\mathrm{R}(1)}(z)\,, \tag{2.4.37}
$$

where

$$\begin{aligned}
\hat{g}_{q\bar{q}}^{\mathrm{U}(1)}(z) = {} & \delta(1-z)\log^2(a) - 2\,p_{qq}(z)\log(a) \\
& - \frac{\pi^2}{3}\delta(1-z) - 2\,\hat{p}_{qq}(z)\log(z) + 4\,(1-z)\,\hat{p}_{qq}(z)\left[\frac{\log(1-z)}{1-z}\right]_+ \\
& + \left\{6\,\delta(1-z) - 8\,\delta^{(1)}(1-z) + 2\,\delta^{(2)}(1-z)\right\} a\log(a) \\
& + \left\{-6\,\delta(1-z) + 4\,\delta^{(1)}(1-z) - 4\,z\,(1-z)\,\hat{p}_{qq}(z)\left[\frac{1}{(1-z)^3}\right]_{3+}\right\} a \\
& + \left\{3\,\delta(1-z) - 12\,\delta^{(1)}(1-z) + \frac{21}{2}\,\delta^{(2)}(1-z) - 3\,\delta^{(3)}(1-z)\right. \\
& \qquad \left. + \frac{1}{4}\,\delta^{(4)}(1-z)\right\} a^2\log(a) \\
& + \left\{-4\,\delta(1-z) + 6\,\delta^{(1)}(1-z) - \frac{1}{2}\,\delta^{(2)}(1-z) - \delta^{(3)}(1-z)\right. \\
& \qquad \left. + \frac{1}{6}\,\delta^{(4)}(1-z) - 6z^2(1-z)\,\hat{p}_{qq}(z)\left[\frac{1}{(1-z)^5}\right]_{5+}\right\} a^2 \\
& + \mathcal{O}\Big(a^{\frac{5}{2}}\log(a)\Big)\,,
\end{aligned} \tag{2.4.38}$$

$$\begin{aligned}
\hat{g}_{q\bar{q}}^{\mathrm{R}(1)}(z) = {} & -2\,(1-z) + 4\,z\left[\frac{1}{1-z}\right]_+ a + 4\,z^2\left[\frac{1}{(1-z)^3}\right]_{3+} a^2 \\
& - 2\,\delta(1-z)\,a\log(a) + 2\,\delta(1-z)\,a \\
& + \left\{-2\,\delta(1-z) + 4\,\delta^{(1)}(1-z) - \delta^{(2)}(1-z)\right\} a^2\log(a) \\
& + \left\{2\,\delta(1-z) - \frac{1}{2}\,\delta^{(2)}(1-z)\right\} a^2 + \mathcal{O}\Big(a^{\frac{5}{2}}\log(a)\Big)\,,
\end{aligned} \tag{2.4.39}$$

and

$$\hat{p}_{qq}(z) = \frac{1+z^2}{1-z}\,, \qquad\qquad p_{qq}(z) = \frac{1+z^2}{(1-z)_+}\,. \tag{2.4.40}$$

In eq. (2.4.38) we have written the $(1+z^2)$ terms coming from the numerator of the $\hat{p}_{qq}(z)$ splitting function as

$$1 + z^2 = (1-z)\,\hat{p}_{qq}(z)\,, \tag{2.4.41}$$

in order to keep track of the universal origin of those terms.

H production

- $g + q(\bar{q}) \to H + q(\bar{q})$

$$\hat{G}_{gq}^{(1)}(z) = C_{\mathrm{F}}\,\hat{g}_{gq}^{(1)}(z)\,, \qquad\qquad \hat{g}_{gq}^{(1)}(z) = \hat{g}_{gq}^{\mathrm{U}(1)}(z) + \hat{g}_{gq}^{\mathrm{R}(1)}(z)\,, \tag{2.4.42}$$

where

$$\begin{aligned}\hat{g}_{gq}^{\mathrm{U}(1)}(z) = & -p_{gq}(z)\log(a) - p_{gq}(z)\log\frac{z}{(1-z)^2} \\ & + \delta^{(1)}(1-z)\,a\log(a) + \left\{\delta(1-z) - 2\,z\,p_{gq}(z)\left[\frac{1}{(1-z)^2}\right]_{2+}\right\} a \\ & + \left\{-\frac{3}{2}\,\delta(1-z) + \frac{3}{2}\,\delta^{(1)}(1-z)\right. \\ & \qquad \left. - \frac{3}{4}\,\delta^{(2)}(1-z) + \frac{1}{4}\,\delta^{(3)}(1-z)\right\} a^2\log(a) \\ & + \left\{\frac{1}{4}\,\delta(1-z) + \frac{1}{4}\,\delta^{(1)}(1-z) + \frac{1}{4}\,\delta^{(2)}(1-z) + \frac{1}{6}\,\delta^{(3)}(1-z)\right. \\ & \qquad \left. - 3\,z^2\,p_{gq}(z)\left[\frac{1}{(1-z)^4}\right]_{4+}\right\} a^2 + \mathcal{O}\Big(a^{\frac{5}{2}}\log(a)\Big)\,, \end{aligned} \tag{2.4.43}$$

$$\begin{aligned}\hat{g}_{gq}^{\mathrm{R}(1)}(z) = & -\frac{3}{2z}(1-z)^2 + 3\,a + 3\,z\left[\frac{1}{(1-z)^2}\right]_{2+} a^2 \\ & + \frac{3}{2}\left\{\delta(1-z) - \delta^{(1)}(1-z)\right\} a^2\log(a) \\ & - \frac{3}{4}\left\{\delta(1-z) + \delta^{(1)}(1-z)\right\} a^2 + \mathcal{O}\Big(a^{\frac{5}{2}}\log(a)\Big)\,, \end{aligned} \tag{2.4.44}$$

and

$$p_{gq}(z) = \frac{z^2 - 2z + 2}{z}\,. \tag{2.4.45}$$

- $g + g \to H + g$

$$\hat{G}_{gg}^{(1)}(z) = C_{\mathrm{A}}\,\hat{g}_{gg}^{(1)}(z)\,, \qquad \hat{g}_{gg}^{(1)}(z) = \hat{g}_{gg}^{\mathrm{U}(1)}(z) + \hat{g}_{gg}^{\mathrm{R}(1)}(z)\,, \tag{2.4.46}$$

where

$$
\begin{aligned}
\hat{g}_{gg}^{\mathrm{U}(1)}(z) = {} & \delta(1-z)\log^2(a) - 2\,p_{gg}(z)\log(a) \\
& - \frac{\pi^2}{3}\delta(1-z) - 2\,\hat{p}_{gg}(z)\log(z) + 4\,(1-z)\,\hat{p}_{gg}(z)\left[\frac{\log(1-z)}{1-z}\right]_+ \\
& + \Big\{12\,\delta(1-z) - 8\,\delta^{(1)}(1-z) + 2\,\delta^{(2)}(1-z)\Big\}\,a\log(a) \\
& + \left\{-6\,\delta(1-z) + 4\,\delta^{(1)}(1-z) - 4\,z\,(1-z)\,\hat{p}_{gg}(z)\left[\frac{1}{(1-z)^3}\right]_{3+}\right\} a \\
& + \left\{18\,\delta(1-z) - 30\,\delta^{(1)}(1-z) + 15\,\delta^{(2)}(1-z) - 3\,\delta^{(3)}(1-z)\right. \\
& \qquad \left. + \frac{1}{4}\,\delta^{(4)}(1-z)\right\} a^2\log(a) \\
& + \left\{-\frac{15}{2}\,\delta(1-z) + 3\,\delta^{(1)}(1-z) + \frac{5}{2}\,\delta^{(2)}(1-z) - \delta^{(3)}(1-z)\right. \\
& \qquad \left. + \frac{1}{6}\,\delta^{(4)}(1-z) - 6\,z^2\,(1-z)\,\hat{p}_{gg}(z)\left[\frac{1}{(1-z)^5}\right]_{5+}\right\} a^2 \\
& + \mathcal{O}\Big(a^{\frac{5}{2}}\log(a)\Big)\,,
\end{aligned}
\tag{2.4.47}
$$

$$
\begin{aligned}
\hat{g}_{gg}^{\mathrm{R}(1)}(z) = {} & -\frac{11}{3z}\,(1-z)^3 + 8\,(1-z)\,a + 6\,z\left[\frac{1}{1-z}\right]_+ a^2 \\
& - 3\,\delta(1-z)\,a^2\log(a) - \frac{5}{2}\,\delta(1-z)\,a^2 + \mathcal{O}\Big(a^{\frac{5}{2}}\log(a)\Big)\,,
\end{aligned}
\tag{2.4.48}
$$

and

$$
\hat{p}_{gg}(z) = \frac{2(z^2-z+1)^2}{z(1-z)}\,. \tag{2.4.49}
$$

In eq. (2.4.47) we have written the $2(z^2-z+1)^2/z$ terms coming from the numerator of the $\hat{p}_{gg}(z)$ splitting function as

$$
\frac{2(z^2-z+1)^2}{z} = (1-z)\,\hat{p}_{gg}(z)\,, \tag{2.4.50}
$$

in order to keep track of the universal origin of those terms.

Comments on $\hat{G}_{ab}^{(1)}(z)$

The leading-logarithmic (LL) and next-to-leading-logarithmic (NLL) coefficients of the $\hat{G}_{ab}^{(1)}(z)$ functions that we have computed agree with the ones in the literature, along with the finite term. Their values have been known for a while [42, 45] and are related to the perturbative coefficients of the transverse-momentum subtraction/resummation formulae for Z [44] and Higgs boson production [88], as pointed

out in Sec. 2.4.2. The coefficients of the terms of order $a\log(a)$ and a, and of order $a^2\log(a)$ and a^2 are instead the new results. Notice, however, that all the $\mathcal{O}(a)$ terms, for both Drell–Yan and Higgs production, were already computed fully differentially in the Born phase-space, i.e. in both invariant mass and rapidity of the color singlet, in ref. [81] within a different framework with respect to ours. The $\mathcal{O}(a^2)$ terms are instead completely new.

The general form of the $\hat{G}^{(1)}_{ab}(z)$ functions we have computed reads[5]

$$\begin{aligned}\hat{G}^{(1)}_{ab}(z) = {} & \log^2(a)\,\hat{G}^{(1,2,0)}_{ab}(z) + \log(a)\,\hat{G}^{(1,1,0)}_{ab}(z) + \hat{G}^{(1,0,0)}_{ab}(z) \\ & + a\log(a)\,\hat{G}^{(1,1,2)}_{ab}(z) + a\,\hat{G}^{(1,0,2)}_{ab}(z) \\ & + a^2\log(a)\,\hat{G}^{(1,1,4)}_{ab}(z) + a^2\,\hat{G}^{(1,0,4)}_{ab}(z) + \mathcal{O}\left(a^{\frac{5}{2}}\log(a)\right), \end{aligned} \tag{2.4.51}$$

all the other coefficients being zero.

We will refer to the terms in the first line of eq. (2.4.51) as leading terms (LT). These terms are either logarithmically divergent or finite in the $a \to 0$ limit. We name the terms in the sum in the second line of eq. (2.4.51) as next-to-leading terms (NLT), and the first two terms in the third line as next-to-next-to-leading terms (N^{2}LT), and so forth.

We notice that the NLT and N^{2}LT terms are at most linearly dependent on $\log(a)$, consistently with the fact that the LL contribution is a squared logarithm. In addition, no odd-power corrections of $\sqrt{a} = q_{\mathrm{T}}^{\mathrm{cut}}/Q$ appear in the NLT and N^{2}LT terms. This behaviour is in agreement with what found, for example, in ref. [81], i.e. that, at NLO, the power expansion of the differential cross section for colour-singlet production is in $(q_{\mathrm{T}}^{\mathrm{cut}})^2$. We do not expect this to be true in general when cuts are applied to the final state. In fact, this was verified after our paper by ref. [73], both for transverse momentum and N-jettiness.

Soft behaviour of the universal part

The origin of some of the terms in the diagonal channels, i.e. the $q\bar{q}$ channel for Z production and the gg channel for H production, can be traced back to the behaviour of the Altarelli–Parisi splitting functions in the soft limit, i.e. $z \to 1$. In fact, in this limit,

$$\hat{P}_{qq}(z) \approx \frac{2C_{\mathrm{F}}}{1-z}\,, \qquad\qquad \hat{P}_{gg}(z) \approx \frac{2C_{\mathrm{A}}}{1-z}\,, \tag{2.4.52}$$

[5] The notation for the expansion of $G^{(1)}_{ab}(z)$ follows from the number of powers of α_{S}, $\log(a)$ and $a^{\frac{1}{2}}$ (in the same way as for $\hat{R}^{(1)}_{ab}(z)$), i.e.

$$\hat{G}^{(1)}_{ab}(z) = \sum_{m,r} \log^m(a)\,\left(a^{\frac{1}{2}}\right)^r \hat{G}^{(1,m,r)}_{ab}(z)\,.$$

so that

$$\hat{p}_{qq}(z) \approx \hat{p}_{gg}(z) \approx \frac{2}{1-z} \equiv \hat{p}(z)\,. \tag{2.4.53}$$

Inserting $\hat{p}_{qq}(z)$ and $\hat{p}_{gg}(z)$ in eqs. (2.4.9) and (2.4.11), respectively, they give rise to a contribution of the form

$$\begin{aligned}&\int_{\tau}^{1-f(a)} \frac{\mathrm{d}z}{z}\,\mathcal{L}\left(\frac{\tau}{z}\right)\,2\,\hat{p}(z)\,\log\frac{1+\sqrt{1-\pi_{\mathrm{T}}^2}}{1-\sqrt{1-\pi_{\mathrm{T}}^2}}\\ &\quad=\int_0^1 \frac{\mathrm{d}z}{z}\,\mathcal{L}\left(\frac{\tau}{z}\right)\left\{\delta(1-z)\log^2(a)-2\,p(z)\log(a)-\frac{\pi^2}{3}\,\delta(1-z)+\dots\right\},\end{aligned} \tag{2.4.54}$$

where, following the notation of Appendix F, we have defined

$$p(z) = \left[\frac{2}{1-z}\right]_+\,. \tag{2.4.55}$$

The details for the derivation of eq. (2.4.54), along with the full result, are collected in Appendix C.6. Inspecting the first three terms of the universal function $\hat{g}_{q\bar{q}}^{\mathrm{U}(1)}(z)$ in eq. (2.4.38) and $\hat{g}_{gg}^{\mathrm{U}(1)}(z)$ in eq. (2.4.47), we recognize exactly the three terms on the right-hand side of eq. (2.4.54).

In addition, we point out that the subleading terms of order $a\log(a)$ originating from eq. (2.4.54) present a second-derivative behaviour with respect to the luminosity function, and those of order $a^2\log(a)$ a fourth-derivative behaviour. This is reflected by the results for the universal part of the diagonal channels, eqs. (2.4.38) and (2.4.47), whereas the origin of such terms can be particularly traced back to the contribution of eq. (C.6.5).

The NLT ($\mathrm{N^2LT}$) logarithmic contributions to the off-diagonal channels present instead a first (third)-derivative behaviour, evident from eqs. (2.4.34) and (2.4.43). The same holds for the real-virtual contribution to the NNLO cross section for the qg-initiated channel, that is analysed in the next section. In fact, that contribution has the same kinematics of the tree-level one, and this is reflected by the results of order a presented in Appendix E, where second-derivative terms are absent.

Aside from these comments, it is useful to remark that our findings for the q_{T} power corrections hold at inclusive level. Corresponding results for N-jettiness, such as the power corrections computed by refs. [68] and [72], are given instead at a more differential level, e.g. as functions of the rapidity, and present at the first subleading order only a first-derivative behaviour.

The non-universal part

It is also interesting to notice that the non-universal part of the $\hat{G}_{ab}^{(1)}(z)$ functions contains terms proportional to $\log(a)$, multiplied by powers of a. These powers are controlled by the form of the non-universal parts in eqs. (2.4.8)–(2.4.11), and to the

way they enter in our generating procedure described in Section 2.4.3. In fact, by inspecting eq. (2.4.29), we see that they contribute to $\hat{g}_{ab}^{\mathrm{R}(1)}$ with terms of the form

$$\int_{\tau}^{1-f(a)} \mathrm{d}z\,(1-z)^n\sqrt{1-\pi_{\mathrm{T}}^2} = \begin{cases} +\,a^2\log(a) + a\log(a) + \dots & n=1 \\ -\,2\,a^2\log(a) + \dots & n=2 \\ +\,a^2\log(a) + \dots & n=3 \\ -\,6\,a^3\log(a) + \dots & n=4 \\ +\,2\,a^3\log(a) + \dots & n=5 \end{cases} \tag{2.4.56}$$

where the dots stand for power terms in a with no logarithms attached. This also explains why, for Z production, $\hat{g}_{qg}^{\mathrm{R}(1)}(z)$ in eq. (2.4.35) and $\hat{g}_{q\bar{q}}^{\mathrm{R}(1)}(z)$ in eq. (2.4.39) contain both terms $a\log(a)$ and $a^2\log(a)$: they receive contributions from all the terms in eq. (2.4.56) starting from $n=1$, since eqs. (2.4.8) and (2.4.9) contain a term proportional to $(1-z)\sqrt{1-\pi_{\mathrm{T}}^2}$. Instead, $\hat{g}_{gq}^{\mathrm{R}(1)}(z)$ in eq. (2.4.44) and $\hat{g}_{gg}^{\mathrm{R}(1)}(z)$ in eq. (2.4.48) contain only the term $a^2\log(a)$, since they receive contributions from the terms in eq. (2.4.56) starting from $n=2$, due to the fact that eqs. (2.4.10) and (2.4.11) contain a term proportional to $(1-z)^2\sqrt{1-\pi_{\mathrm{T}}^2}$ and $(1-z)^3\sqrt{1-\pi_{\mathrm{T}}^2}$, respectively.

As far as the finite term in the diagonal channels is concerned, we notice that, in the $q\bar{q}$ channel of DY production, the first term in eq. (2.4.39) happens to correspond to the first-order collinear coefficient function defined in the "hard-resummation scheme", introduced in ref. [89, 90] within the q_{T}-subtraction formalism. Instead, the first term in the gg channel of H production in eq. (2.4.48) has no connection with the first-order collinear coefficient function, that is zero for this production channel. In conclusion, the structure of the terms in the non-universal part depends on the peculiar form of the differential cross sections.

Higher-order soft behaviour of the squared amplitudes

In this section, we extend the study performed in Sec. 2.4.4 in order to investigate the origin of the power-suppressed terms $a\log(a)$ and $a^2\log(a)$, present both in the universal and in the non-universal parts. We will show that their origin can be connected to the higher-order soft behaviour of the squared amplitudes. To this aim, we have performed a Laurent expansion in the energy k^0 of the final-state parton of the exact squared amplitudes of eqs. (A.3), (A.9), (A.14) and (A.19). In the following, we call leading soft (LS) the term proportional to the highest negative power of k^0, next-to-leading soft (N^{1}LS) the subsequent term, and so on. All the technical details and expressions of the expansion terms are collected in Appendix A.

We have then applied the algorithm previously described to each of the terms of the expansions that we have calculated, in order to compute their behaviour as a function of a. This has allowed us to trace the origin of the $a\log(a)$ and $a^2\log(a)$ terms. Our findings are collected in the following:

- $q(\bar{q}) + g \to Z + q(\bar{q})$

  We reproduce the $a\log(a)$ behaviour of $\hat{g}^{(1)}_{qg}(z)$ in eq. (2.4.33) if we consider the soft-expansion of the exact amplitude up to the N^{1}LS level, i.e. if we sum eqs. (A.4) and (A.5), and the $a^2\log(a)$ behaviour if we consider the soft-expansion up to the N^{3}LS level, i.e. if we sum eqs. (A.4)–(A.7).

- $q + \bar{q} \to Z + g$

  We reproduce the $a\log(a)$ behaviour of $\hat{g}^{(1)}_{q\bar{q}}(z)$ in eq. (2.4.37) if we consider the soft-expansion of the exact amplitude up to the N^{1}LS level, i.e. if we sum eqs. (A.10) and (A.11), and the $a^2\log(a)$ behaviour if we consider the soft-expansion up to the N^{2}LS level, i.e. if we sum eqs. (A.10)–(A.12).

- $g + q(\bar{q}) \to H + q(\bar{q})$

  We reproduce the $a\log(a)$ behaviour of $\hat{g}^{(1)}_{gq}(z)$ in eq. (2.4.42) if we consider the soft-expansion of the exact amplitude up to the N^{1}LS level, i.e. if we sum eqs. (A.15) and (A.16), and the $a^2\log(a)$ behaviour if we consider the soft-expansion up to the N^{2}LS level, i.e. if we sum eqs. (A.15)–(A.17).

- $g + g \to H + g$

  We reproduce the $a\log(a)$ behaviour of $\hat{g}^{(1)}_{gg}(z)$ in eq. (2.4.46) if we consider the soft-expansion of the exact amplitude up to the N^{2}LS level, i.e. if we sum eqs. (A.20)–(A.22), and the $a^2\log(a)$ behaviour if we consider the soft-expansion up to the N^{4}LS level, i.e. if we sum eqs. (A.20)–(A.24).

Collecting our result in a table, we have:

	Z		H	
	$\hat{g}^{(1)}_{qg}(z)$	$\hat{g}^{(1)}_{q\bar{q}}(z)$	$\hat{g}^{(1)}_{gq}(z)$	$\hat{g}^{(1)}_{gg}(z)$
$a\log(a)$	N^{1}LS	N^{1}LS	N^{1}LS	N^{2}LS
$a^2\log(a)$	N^{3}LS	N^{2}LS	N^{2}LS	N^{4}LS

In summary, the next-to-leading-soft approximation of the exact amplitudes reproduces the $a\log(a)$ term only for Z production and for the qg-initiated channel of H production. For the gg-initiated channel of H production, only the expansion up to next-to-next-to-leading-soft order reproduces the $a\log(a)$ term. We would like to point out that, of the three terms contributing to the N^{2}LS of eq. (A.22), only the constant one, i.e. the number 16, is needed to reproduce the $a\log(a)$ coefficient. The u/t and t/u terms do not give rise to any $a\log(a)$ contribution.

Moreover, only the expansion up to next-to-next-to-leading-soft order in the $q\bar{q}$ channel for Z production and in the qg-initiated channel for H production reproduces

the $a^2 \log(a)$ coefficient. Higher orders in the expansion in the softness of the final-state parton are needed for the qg-initiated channel of Z production and for the gg-initiated channel of H production.

q_{T}-subtraction method

In the original paper on the q_{T}-subtraction method [4], the expansion in α_{S} of the transverse-momentum resummation formula generates exactly the three terms in eq. (2.4.16), plus extra power-correction terms.

In the formula for $\hat{R}^{(1)}_{ab}(z)$ that we can build from our expression of $\hat{G}^{(1)}_{ab}(z)$, by changing the overall sign and adding the $\delta(1-z)$ contribution from the virtual correction, the power-correction terms are exactly those produced by the expansion of the real amplitudes. If one is interested in using our formula for $\hat{R}^{(1)}_{ab}(z)$ to reduce the dependence on the transverse-momentum cutoff, within the q_{T}-subtraction method, the aforementioned extra terms need then to be subtracted from our expression of $\hat{R}^{(1)}_{ab}(z)$.

Numerical results

As previously pointed out, NLO (and NNLO) cross sections computed with the q_{T}-subtracted formalism exhibit a residual dependence on $q_{\mathrm{T}}^{\mathrm{cut}}$, i.e. the parameter a we have introduced in eq. (2.4.6). This residual dependence is due to power terms which remain after the subtraction of the IR singular contributions, and vanish only in the limit $a \to 0$ (limit which is unattainable in a numerical computation). In this section we discuss the residual systematic dependence on $q_{\mathrm{T}}^{\mathrm{cut}}$ due to terms beyond LT, NLT and N^{2}LT accuracy.

We present our results for Z and H production at the LHC, at a center-of-mass energy of $\sqrt{S} = 13$ TeV. In our NLO calculations we have set the renormalisation and factorisation scales equal to the mass of the corresponding produced boson, and we have used the `MSTW2008nlo` parton-distribution function set [91]. The mass of the Z boson m_{Z} and of the Higgs boson m_{H} have been set to the values 91.1876 GeV and 125 GeV, respectively.

As an overall check of our calculation, we compared the results obtained with the analytically q_{T}-integrated cross sections in eqs. (2.4.8)–(2.4.11) with the numerically-integrated results computed with both the `DYqT-v1.0` [92, 93] and `HqT2.0` [5, 94] codes, and found an excellent agreement.

Then, in order to study the residual $q_{\mathrm{T}}^{\mathrm{cut}}$ dependence of the NLO cross sections for all the partonic subprocesses, we insert the expansion in eq. (2.4.51) into eq. (2.4.19),

and we introduce the following definitions

$$\sigma_{ab}^{\mathrm{LT}} \equiv \tau \int_\tau^1 \frac{\mathrm{d}z}{z}\, \mathcal{L}_{ab}\Big(\frac{\tau}{z}\Big)\, \hat{\sigma}^{(0)} \left[\log^2(a)\, \hat{G}_{ab}^{(1,2,0)}(z) + \log(a)\, \hat{G}_{ab}^{(1,1,0)}(z) + \hat{G}_{ab}^{(1,0,0)}(z)\right], \tag{2.4.57}$$

$$\sigma_{ab}^{\mathrm{NLT}} \equiv \tau \int_\tau^1 \frac{\mathrm{d}z}{z}\, \mathcal{L}_{ab}\Big(\frac{\tau}{z}\Big)\, \hat{\sigma}^{(0)} \left[a \log(a)\, \hat{G}_{ab}^{(1,1,2)}(z) + a\, \hat{G}_{ab}^{(1,0,2)}(z)\right], \tag{2.4.58}$$

$$\sigma_{ab}^{\mathrm{N^2LT}} \equiv \tau \int_\tau^1 \frac{\mathrm{d}z}{z}\, \mathcal{L}_{ab}\Big(\frac{\tau}{z}\Big)\, \hat{\sigma}^{(0)} \left[a^2 \log(a)\, \hat{G}_{ab}^{(1,1,4)}(z) + a^2\, \hat{G}_{ab}^{(1,0,4)}(z)\right], \tag{2.4.59}$$

where we have dropped the $^>$ and $^{(1)}$ superscripts for ease of notation, since there is no possibility of misunderstanding in this section, because we present only the NLO results we have computed for the $\hat{G}_{ab}^{(1)}(z)$ functions.

The $\hat{G}_{ab}^{(1,n,m)}(z)$ functions in eqs. (2.4.57)–(2.4.59) contain plus distributions up to order 5 and to compute these cross sections we have first built interpolations of the luminosity functions $\mathcal{L}_{ab}(y)$, defined in eq. (2.2.28), for the channels that contribute to Z and H production at NLO. We have expanded the luminosity functions on the basis of the Čebyšëv polynomials up to order 30, namely we used them to fit the previously evaluated luminosity functions. In this way, the computation of the derivatives of the (fitted) luminosity functions can be performed in a fast and sound way, as the derivatives of the polynomial basis are completely under control. See Appendix H for further details.

In the forthcoming figures, we plot the following quantities as a function of $q_{\mathrm{T}}^{\mathrm{cut}}$ (the corresponding value of a is given on top of each figure):

1. $(\sigma_{ab}^{>(1)} - \sigma_{ab}^{\mathrm{LT}})$,
2. $(\sigma_{ab}^{>(1)} - \sigma_{ab}^{\mathrm{LT}} - \sigma_{ab}^{\mathrm{NLT}})$,
3. $(\sigma_{ab}^{>(1)} - \sigma_{ab}^{\mathrm{LT}} - \sigma_{ab}^{\mathrm{NLT}} - \sigma_{ab}^{\mathrm{N^2LT}})$,

where $\sigma_{ab}^{>(1)}$ is the cumulative cross section defined on the left-hand side of eq. (2.4.19), obtained by integrating the exact differential cross sections of eqs. (2.4.8)–(2.4.11). We expect that, by adding higher-power terms in a, these differences tend to zero more and more quickly when $q_{\mathrm{T}}^{\mathrm{cut}} \to 0$. And in fact, the results shown in the following figures confirm this behaviour.

We first present our findings separated according to the partonic production channels. In all the figures presented in this section, the statistical errors of the integration procedure are also displayed, but they are always totally negligible on the scales of the figures.

In fig. 2.1 we collect the results for the aforementioned cross-section differences, as a function of $q_{\mathrm{T}}^{\mathrm{cut}}$, for the $qg \to Zq$ (left) and $q\bar{q} \to Zg$ (right) channels, and in fig. 2.2 we collect similar results for the $gq \to Hq$ (left) and $gg \to Hg$ (right)

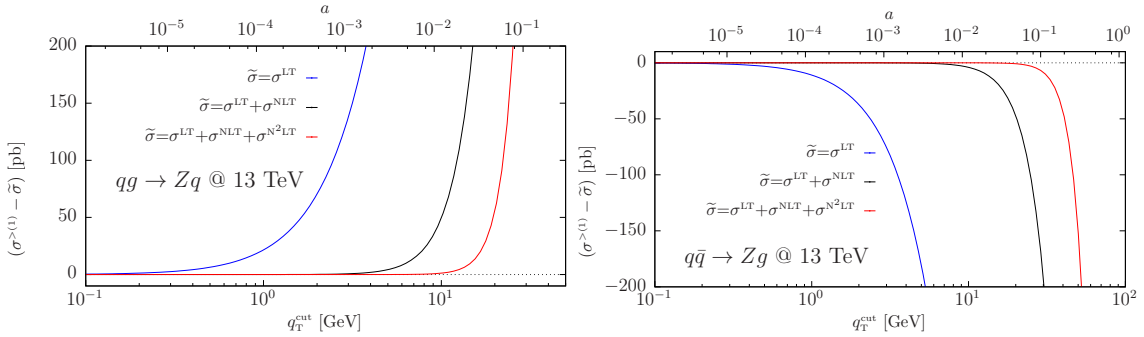

Figure 2.1. Difference of the total cross sections $(\sigma^{>(1)} - \widetilde{\sigma})$ as a function of $q_{\rm T}^{\rm cut}$, for Z boson production, in the $qg \to Zq$ (left pane) and in the $q\bar{q} \to Zg$ channel (right pane). The three curves correspond to the three possible choices of $\widetilde{\sigma}$: results for $\widetilde{\sigma} = \sigma^{\rm LT}$ are displayed in blue, for $\widetilde{\sigma} = \sigma^{\rm LT} + \sigma^{\rm NLT}$ are displayed in black and for $\widetilde{\sigma} = \sigma^{\rm LT} + \sigma^{\rm NLT} + \sigma^{\rm N^2LT}$ are displayed in red. The corresponding values of $a = (q_{\rm T}^{\rm cut}/m_{\rm Z})^2$ are displayed on the top of the figure. The statistical errors of the integration are also shown, but they are totally negligible on the scale of the figure.

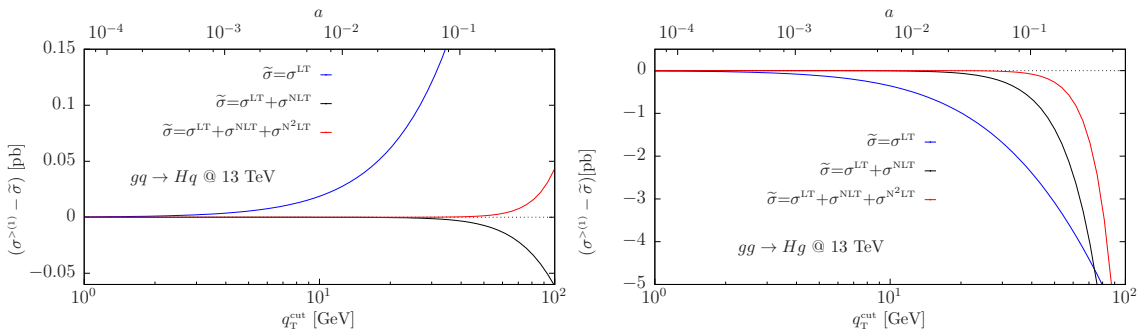

Figure 2.2. Difference of the total cross sections $(\sigma^{>(1)} - \widetilde{\sigma})$ as a function of $q_{\rm T}^{\rm cut}$, for H boson production, in the $qg \to Hq$ (left pane) and in the $gg \to Hg$ channel (right pane). Same legend as in fig. 2.1. The corresponding values of $a = (q_{\rm T}^{\rm cut}/m_{\rm H})^2$ are displayed on the top of the figure.

channels. As expected, NLT and N^{2}LT contributions increase the accuracy of the expanded cross section, with respect to the exact one.

To give a more quantitative estimation of the power-suppressed corrections, we present results for the total hadronic cross section, normalised with respect to the corresponding exact NLO cross section $\sigma_{\rm NLO}$ (i.e. including also the virtual contributions). The results are shown in figs. 2.3 and 2.4, where we have used $\sigma_{\rm NLO} = 55668.1$ pb for Z production and 31.52 pb for H production. On the left panes we plot results in a smaller $q_{\rm T}^{\rm cut}$ region, while, on the right panes, we extend the $q_{\rm T}^{\rm cut}$ interval to higher values.

These plots show exactly how the residual cutoff dependence of the cross sections

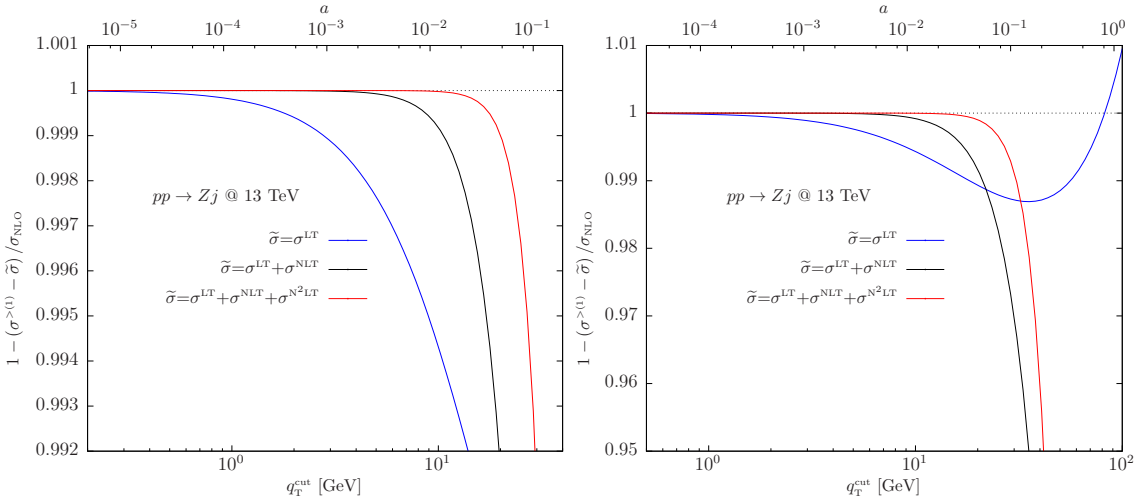

Figure 2.3. Results for $1-(\sigma^{>(1)}-\widetilde{\sigma})/\sigma_{\rm NLO}$ as a function of $q_{\rm T}^{\rm cut}$, for Z boson production, in $pp \to Zj$. Same legend as in fig. 2.1. In the left pane, the low-$q_{\rm T}^{\rm cut}$ region is displayed, while, in the right pane, a larger region in $q_{\rm T}^{\rm cut}$ is shown. The total cross section at NLO for Z production, $\sigma_{\rm NLO}$, has been taken equal to 55668.1 pb.

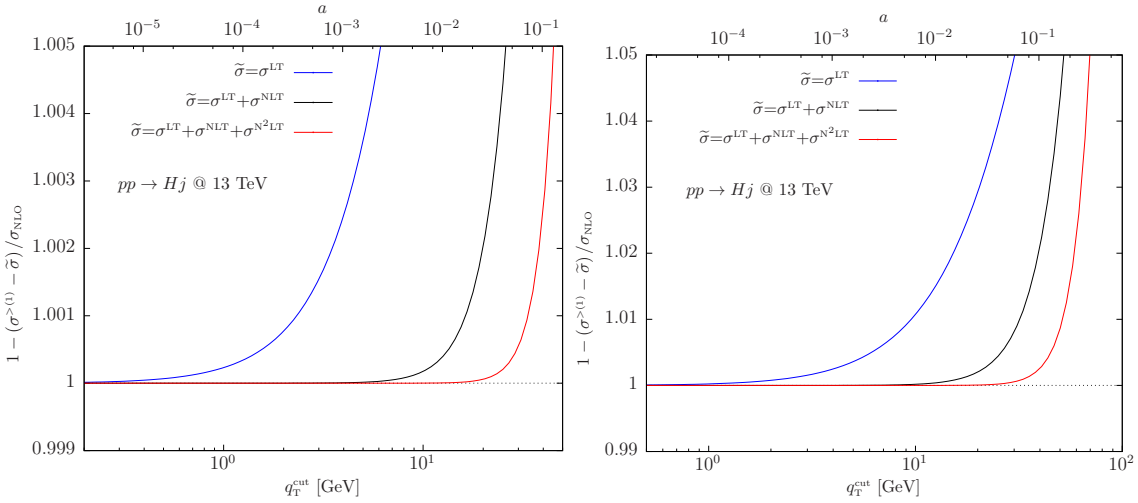

Figure 2.4. Results for $1-(\sigma^{>(1)}-\widetilde{\sigma})/\sigma_{\rm NLO}$ as a function of $q_{\rm T}^{\rm cut}$, for H boson production, in $pp \to Hj$. Same legend as in fig. 2.1. In the left pane, the low-$q_{\rm T}^{\rm cut}$ region is displayed, while, in the right pane, a larger region in $q_{\rm T}^{\rm cut}$ is shown. The total cross section at NLO for H production, $\sigma_{\rm NLO}$, has been taken equal to 31.52 pb.

changes when the $q_{\rm T}$-subtraction counterterm is corrected by the NLT and N^{2}LT power terms. For example, for Z production and for $q_{\rm T}^{\rm cut}=10$ GeV, corresponding to $a=0.012$, the LT cross section gives an estimate of the exact cross section within the 5‰, that reduces to below the 1‰ when the NLT contribution is added and becomes less than 0.01‰ when also the N^{2}LT is present. For Higgs boson production, the

residual cutoff dependence is even more pronounced: in fact, at $q_{\rm T}^{\rm cut} = 10$ GeV, corresponding to $a = 0.0064$, the LT is precise within the 1% level. When the NLT is added, the precision reaches the 0.2‰, and is below 0.001‰ with the addition of the N^{2}LT.

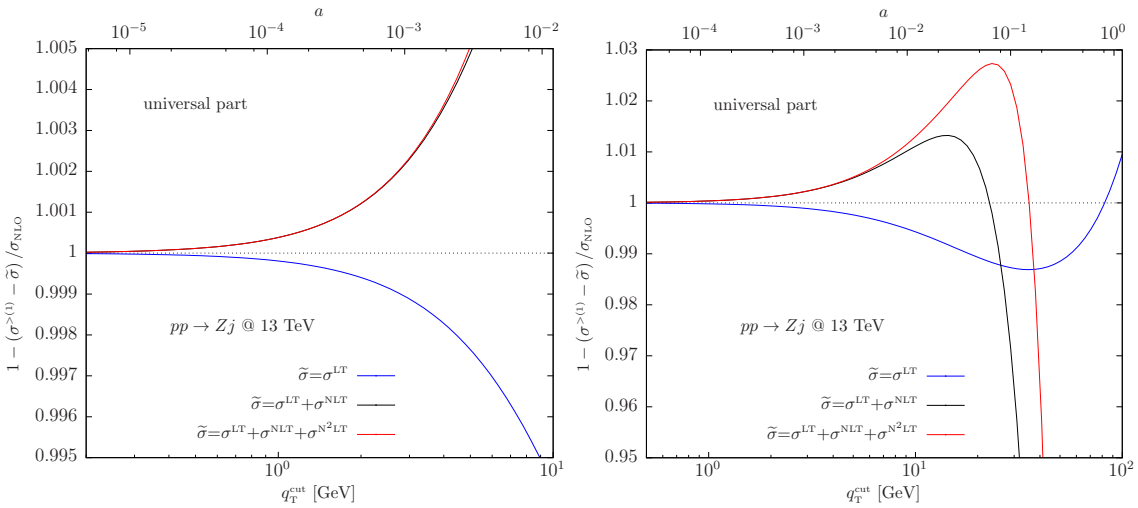

Figure 2.5. Same as fig. 2.3, but using only the universal part of $\hat{G}_{ab}^{(1,n,m)}(z)$ in computing the cross sections of eqs. (2.4.57)–(2.4.59).

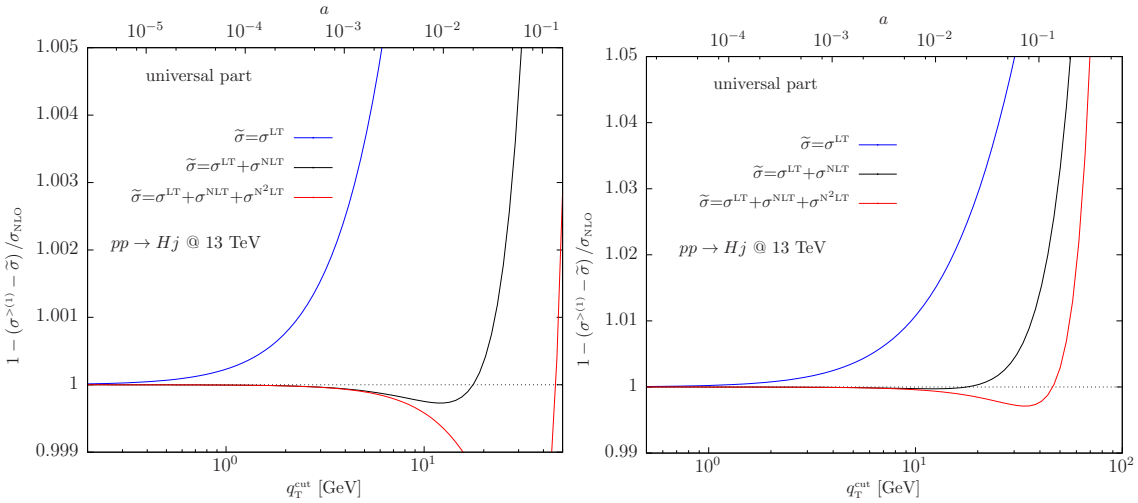

Figure 2.6. Same as fig. 2.5 but for Higgs boson production.

An interesting question is to estimate the impact of the universal parts of the $\hat{G}_{ab}^{(1,n,m)}(z)$ functions, with respect to the non-universal ones. We have then computed the cross sections in eqs. (2.4.57)–(2.4.59), taking into account only the universal parts of the $\hat{G}_{ab}^{(1,n,m)}(z)$ functions. Our results are displayed in fig. 2.5, for Z production, and in fig. 2.6, for H production.

Comparing these figures with the corresponding ones with the full $\hat{G}_{ab}^{(1,n,m)}(z)$ functions, i.e. figs. 2.3 and 2.4, we see that the non-universal contributions play a crucial role for Z production, while their role is minor in Higgs boson production. This is due to the fact that the non-universal part in eqs. (2.4.10) and (2.4.11) is suppressed by higher powers of $(1-z)$, with respect to the corresponding expression for Z production, in eqs. (2.4.8) and (2.4.9), confirming the conclusions drawn in Sec. 2.4.4.

2.5 NNLO subleading power corrections

In the previous sections we presented our results for the subleading power corrections relevant to inclusive Z and H production at NLO in QCD. The calculation is useful to deepen our knowledge about the subleading and universal behaviour of scattering amplitudes in the infrared limits. In order to elaborate even more about that, it is essential to push our effort to the next order in $\alpha_{\rm S}$, also in view of the fact that, as shown in refs. [23, 50], the sensitivity to the numerical value of the cutoff increases at higher orders.

2.5.1 V + jet production

In this thesis we consider the NNLO corrections to the production of a vector boson V, i.e. a $W^{\pm}$, a Z or a virtual photon γ^*. In particular, we deal with the qg-initiated partonic channel

$$q(p_1) + g(p_2) \;\to\; V(q) + X(k)\,, \tag{2.5.1}$$

where the quadri-momenta are given in parentheses. In Sec. 2.4, among other contributions, we considered the NLO cross section for V production, i.e.

$$q(p_1) + g(p_2) \;\to\; V(q) + q(k)\,, \tag{2.5.2}$$

The standard Mandelstam invariants, defined as in eq. (2.2.5), are related by

$$s + t + u = Q^2 + s_2\,, \tag{2.5.3}$$

where Q^2 and s_2 are the squared invariant masses of the V boson and of the system recoiling against V at parton level.

In the following, we use the same notation and the expressions computed in ref. [95]. The couplings appearing in the differential cross sections follow this convention: if an electroweak boson V is emitted by a quark with flavour $f_1 = \{u,\, d,\, s,\, c,\, b\}$ which then changes into f_2, the vertex is described by the Feynman rule

$$-ie\gamma^{\mu}\left[\ell_{f_2 f_1}\,\frac{1-\gamma_5}{2} + r_{f_2 f_1}\,\frac{1+\gamma_5}{2}\right], \tag{2.5.4}$$

where the definitions of the left- and right-handed couplings ℓ and r depend on the V boson

$$W^- \,:\, \ell_{f_2 f_1} = \frac{1}{\sqrt{2}\,\sin\theta_W}\,(\sigma_+)_{f_2 f_1}\,U_{f_2 f_1}\,, \quad r_{f_2 f_1} = 0\,, \tag{2.5.5}$$

$$W^+ \,:\, \ell_{f_2 f_1} = \frac{1}{\sqrt{2}\,\sin\theta_W}\,(\sigma_-)_{f_2 f_1}\,U^\dagger_{f_2 f_1}\,, \quad r_{f_2 f_1} = 0\,, \tag{2.5.6}$$

$$Z \,:\, \ell_{f_2 f_1} = \frac{1}{\sin 2\theta_W}\,(\sigma_3)_{f_2 f_2} - \delta_{f_2 f_1}\,e_{f_1}\tan\theta_W\,, \quad r_{f_2 f_1} = -\delta_{f_2 f_1}\,e_{f_1}\tan\theta_W\,, \tag{2.5.7}$$

$$\gamma^* \,:\, \ell_{f_2 f_1} = r_{f_2 f_1} = \delta_{f_2 f_1}\,e_{f_1}\,, \tag{2.5.8}$$

where θ_W is the Weinberg angle, e_f is the fractional electric charge of the quark with flavour f, $\sigma_\pm = (\sigma_1 \pm i\sigma_2)/2$ and σ_3 are the weak isospin Pauli matrices and U is the unitary Cabibbo–Kobayashi–Maskawa mixing matrix. In addition, in the following we abbreviate $\ell_{f_2 f_1}$ to ℓ_{21}, and the same for $r_{f_2 f_1}$.

The QCD NLO corrections to eq. (2.5.1) were computed in ref. [95]. We report here eq. (2.12) of this reference, since we are going to use their results in $d = 4$ space-time dimensions, after correcting for some known typos[6]

$$\begin{aligned} E_q\,\frac{d\hat{\sigma}_{qg}}{d^3 q} = \frac{1}{s}\,\frac{C_\mathrm{F}}{N_\mathrm{c}^2-1}\,\alpha\,\alpha_\mathrm{S}\Bigg\{ & \delta(s_2)\,A^{qg}(s,t,u)\sum_f \left(|\ell_{f1}|^2 + |r_{f1}|^2\right) \\ & + \frac{\alpha_\mathrm{S}}{2\pi}\Bigg\{\Bigg[\delta(s_2)\Big(B_1^{qg}(s,t,u) + n_\mathrm{f}\,B_2^{qg}(s,t,u) + C_1^{qg}(s,t,u) + C_2^{qg}(s,t,u)\Big) \\ & \qquad + C_3^{qg}(s,t,u,s_2)\Bigg]\sum_f \left(|\ell_{f1}|^2 + |r_{f1}|^2\right) \\ & \qquad + \delta(s_2)\,B_3^{qg}(s,t,u)\,(\ell_{11} - r_{11})\sum_f (\ell_{ff} - r_{ff})\Bigg\}\Bigg\}\,, \end{aligned} \tag{2.5.9}$$

where E_q is the energy of the V boson, $N_\mathrm{c} = 3$ is the number of colours and $C_\mathrm{F} = (N_\mathrm{c}^2-1)/(2N_\mathrm{c}) = 4/3$. The functions A^{qg}, B_i^{qg}, C_i^{qg} are defined in eqs. (A4)–(A6), (A10)–(A12) of ref. [95]. In particular, A^{qg} is the contribution from the Born-level diagrams, i.e. of the process in eq. (2.5.2), considered in detail in Sec. 2.4. The functions B_i^{qg} receive contributions from the interference of one-loop virtual corrections to eq. (2.5.2) with the Born-level diagrams. In particular, B_2^{qg} originates from the renormalisation counterterm, while B_3^{qg} is the contribution from the virtual diagrams with a triangular quark loop, which are present only for Z/γ^* production. These contributions are then multiplied by a $\delta(s_2)$ term, since the system recoiling against the F boson only comprises a single quark with momentum k, so that $s_2 = k^2 = 0$.

[6] See footnote § of ref. [86].

The functions C_i^{qg} originate from the diagrams contributing to the real corrections. In particular, C_1^{qg} and C_2^{qg} are the coefficient of a $\delta(s_2)$ term, leftovers of the subtraction method when dealing with initial- and final-state radiation. C_3^{qg} contributes instead for non-zero values of s_2, and corresponds to the double-real radiation contribution to qg-initiated F boson production. In the following we neglect all the infrared divergences appearing as poles in eqs. (A4)–(A6), (A10)–(A12) of ref. [95], since they cancel out when summing real and virtual contributions at this order in $\alpha_{\rm S}$. The B_i^{qg} and C_i^{qg} are analytic functions of the kinematic invariants and contain logarithmic and dilogarithmic functions.

In this section we present results for the calculation of the power corrections for all the terms proportional to $\delta(s_2)$ in eq. (2.5.9), i.e. the virtual-correction terms and terms from the regularisation of the double-real radiation contributions.

Since the kinematics of these terms is equivalent to the one discussed in Sec. 2.4, we follow the same procedure, and we integrate all the terms proportional to $\delta(s_2)$ in eq. (2.5.9), writing them in the form suitable to be inserted in eq. (2.2.29), i.e.

$$\left.\frac{d\hat{\sigma}_{qg}(q_{\rm T},z)}{dq_{\rm T}^2}\right|_{\delta(s_2)} = \frac{1}{16\pi}\frac{z^2}{Q^4}\frac{1}{\sqrt{(1-z)^2-4z\,\dfrac{q_{\rm T}^2}{Q^2}}}\left[\left|\mathcal{M}\left(z,t_+,q_{\rm T}\right)\right|^2+\left|\mathcal{M}\left(z,t_-,q_{\rm T}\right)\right|^2\right], \tag{2.5.10}$$

where $\mathcal{M}(s,t,u)$ is the sum of the functions $A^{qg}, B_1^{qg}, B_2^{qg}, B_3^{qg}, C_1^{qg}, C_2^{qg}$, as they appear in eq. (2.5.9), together with the global factor in front, evaluated at

$$u = Q^2 - s - t\,, \qquad s = \frac{Q^2}{z}\,, \qquad t = t_\pm\,, \tag{2.5.11}$$

where

$$t_\pm = \frac{Q^2}{2z}\left[z-1\pm\sqrt{(1-z)^2-4z\,\frac{q_{\rm T}^2}{Q^2}}\right], \tag{2.5.12}$$

so that $\mathcal{M}$ becomes a function of z and $q_{\rm T}$, for a given vector-boson virtuality Q^2.

We can write eq. (2.5.9), manipulated according to the previous steps, in a compact notation as

$$\frac{d\hat{\sigma}_{qg}(q_{\rm T},z)}{dq_{\rm T}^2} = \frac{\alpha_{\rm S}}{2\pi}\frac{d\hat{\sigma}_{qg}^{(1)}(q_{\rm T},z)}{dq_{\rm T}^2} + \left(\frac{\alpha_{\rm S}}{2\pi}\right)^2\frac{d\hat{\sigma}_{qg}^{(2)}(q_{\rm T},z)}{dq_{\rm T}^2}, \tag{2.5.13}$$

where the superscript $^{(1)}$ denotes the tree-level cross section, while the superscript $^{(2)}$ the virtual and real contributions. The choice is made in order to make contact with the labeling of the transverse-momentum resummation coefficients, that refer to V production as the zeroth term, to its NLO corrections as the first term, and to the NNLO corrections, i.e. the QCD NLO corrections to $V+1$ parton, as the second one.

From now on we focus on the contribution

$$\left.\frac{d\hat{\sigma}^{(2)}_{qg}(q_{\mathrm{T}},z)}{dq^2_{\mathrm{T}}}\right|_{\delta(s_2)} \tag{2.5.14}$$

and, with a little abuse of notation, when referring to eq. (2.5.14), we sometimes drop the $|_{\delta(s_2)}$, to ease the notation.

2.5.2 Real-virtual power corrections

In this section we collect fully-analytic results for the NNLO power corrections in the transverse-momentum cutoff, up to order a. The results refer to the $\delta(s_2)$ contributions of the qg-initiated channel in eq. (2.5.9).

We label the different contributions of eq. (2.5.9) with the letter K, so that

$$K = \{A^{qg},\, B_1^{qg},\, B_2^{qg},\, B_3^{qg},\, C_1^{qg},\, C_2^{qg}\}\,. \tag{2.5.15}$$

Using eq. (2.5.10) and following the discussion in Sec. 2.2.1, we integrate $K(s,t,u)$ in t to obtain a function of the transverse momentum of the vector boson, q_{T}, and z

$$\int dt\, K(s,t,u) = K(q_{\mathrm{T}},z)\,. \tag{2.5.16}$$

As explained in Sec. 2.4, the functions K are then to be integrated in q_{T} from an arbitrary value, $q_{\mathrm{T}}^{\mathrm{cut}}$, up to the maximum transverse momentum $q_{\mathrm{T}}^{\mathrm{max}}$ allowed by the kinematics of the event.

We further split the contributions of B_1^{qg} and C_1^{qg} according to their colour factor, C_{A} and C_{F}. We then introduce a further index, $c = \{C_{\mathrm{A}}, C_{\mathrm{F}}\}$, relevant for B_1^{qg} and C_1^{qg}, in order to distinguish the coefficients of the different colour factors.

The general procedure described in Sec. 2.4.3 is applied to the q_{T}-integrated K functions. In order to present the structure of the results, we refer to the definitions of I, $\tilde{I}_1$, $\tilde{I}_2$ and $\tilde{I}_3$ of eqs. (2.4.27)–(2.4.30). Moreover, we present the results for the sum $\tilde{I}_{23} \equiv \tilde{I}_2 + \tilde{I}_3$, and we do not give the two terms separately.

After dropping the qg superscript for ease of notation, we can then write

$$I^H = \tilde{I}_1^H + \tilde{I}_{23}^H\,, \qquad\qquad H = \{A,\, B_1,\, B_2,\, B_3,\, C_1,\, C_2\}\,, \tag{2.5.17}$$

where, if $H = \{B_1,\, C_1\}$,

$$\tilde{I}_1^H = \sum_{c=\{C_{\mathrm{A}},C_{\mathrm{F}}\}} c \left\{ \int_0^1 dz\, l(z)\, {}^c g_0^H(z) + \int_0^1 dz\, l(z) \left[\frac{{}^c g_1^H(z)}{1-z}\right]_+ + \int_0^1 dz\, l(z) \left[\frac{{}^c g_2^H(z)}{1-z}\right]_{++} \right\}, \tag{2.5.18}$$

$$\tilde{I}_{23}^H = \sum_{c=\{C_{\mathrm{A}},C_{\mathrm{F}}\}} c\; {}^c\mathcal{J}_{23}^H\,, \tag{2.5.19}$$

while, if $H = \{A,\, B_2,\, B_3,\, C_2\}$,

$$\tilde{I}_1^H = \int_0^1 dz\, l(z)\; g_0^H(z) + \int_0^1 dz\, l(z) \left[\frac{g_1^H(z)}{1-z}\right]_+ + \int_0^1 dz\, l(z) \left[\frac{g_2^H(z)}{1-z}\right]_{++} \tag{2.5.20}$$

$$\tilde{I}_{23}^H = \mathcal{J}_{23}^H\,, \tag{2.5.21}$$

where $l(z)$ is given in terms of the parton luminosity in eq. (2.2.28), where we have dropped any subscript for ease of notation

$$l(z) \equiv \frac{1}{z}\,\mathcal{L}\left(\frac{\tau}{z}\right)\,. \tag{2.5.22}$$

The functions ${}^c g_0^H(z)$, ${}^c g_1^H(z)$, ${}^c g_2^H(z)$, $g_0^H(z)$, $g_1^H(z)$, $g_2^H(z)$, ${}^c\mathcal{J}_{23}^H$ and $\mathcal{J}_{23}^H$ are the main results of this section and are collected in Appendix E.

2.5.3 Technical details

We have written dedicated MATHEMATICA parallel codes in order to apply the whole method to the different contributions. As already pointed out for the NLO calculation, the hardest integrals are those to compute $\tilde{I}_2$, which requires the calculation of exact integrals in z, between 0 e $1 - f(a)$, where $f(a)$ is defined in eq. (2.4.13).

The integrand functions have been classified into five groups, according to the number of logarithmic and polylogarithmic functions that appear at the integrand level. A sample of these integrals is collected in Appendix D. We have integrated $\mathcal{O}(800)$ integrals in order to compute the expressions in eqs. (2.4.29) and (2.4.30) of ref. [82], for all the contributions in eq. (2.5.17). In general, the integrals require dedicated changes of variables and iterated integrations by parts, peculiarly for the ones involving polylogarithms and logarithms to the third power, that turned out to be the most difficult ones.

2.5.4 Comments

Due to the length of the intermediate results, in Appendix E we report only the final results, i.e. the functions ${}^c g_0^H(z)$, ${}^c g_1^H(z)$, ${}^c g_2^H(z)$, $g_0^H(z)$, $g_1^H(z)$, $g_2^H(z)$, ${}^c\mathcal{J}_{23}^H$ and $\mathcal{J}_{23}^H$ that appear in eqs. (2.5.17)–(2.5.21).[7]

In agreement with what is found for the NLO calculation, no odd-power corrections of $q_{\rm T}^{\rm cut}/Q = \sqrt{a}$ appear, i.e. the power expansion of the real-virtual interference terms for F production in the qg channel is in $(q_{\rm T}^{\rm cut})^2$.

In addition, we can define the $\hat{G}_{qg}^{(2)}(z)\Big|_{\delta(s_2)}$ function, starting from the integral of the cumulative cross section in eq. (2.4.8), as

$$\sigma_{qg}^{>(2)}\big|_{\delta(s_2)} = \tau \int_\tau^{1-f(a)} \frac{dz}{z}\,\mathcal{L}_{qg}\left(\frac{\tau}{z}\right) \frac{1}{z}\,\sigma_{qg}^{>(2)}(z)\big|_{\delta(s_2)} \equiv \tau \int_\tau^1 \frac{dz}{z}\,\mathcal{L}_{qg}\left(\frac{\tau}{z}\right) \hat{\sigma}^{(0)}\,\hat{G}_{qg}^{(2)}(z)\Big|_{\delta(s_2)}\,, \tag{2.5.23}$$

[7] The intermediate results are available upon request to the authors.

and, from the structure of the power corrections we have computed here, the general form of this function is given by[8]

$$\begin{aligned}\hat{G}_{qg}^{(2)}(z)\Big|_{\delta(s_2)} = {} & \log^3(a)\,\hat{G}_{qg}^{(2,3,0)}(z) + \log^2(a)\,\hat{G}_{qg}^{(2,2,0)}(z) + \log(a)\,\hat{G}_{qg}^{(2,1,0)}(z) + \hat{G}_{qg}^{(2,0,0)}(z) \\ & + a\log^2(a)\,\hat{G}_{qg}^{(2,2,2)}(z) + a\log(a)\,\hat{G}_{qg}^{(2,1,2)}(z) + a\,\hat{G}_{qg}^{(2,0,2)}(z) \\ & + \mathcal{O}\Big(a^{\frac{3}{2}}\log(a)\Big)\,, \end{aligned} \tag{2.5.24}$$

all the other coefficients being zero.

This also agrees with the calculation done in ref. [64], although the observable is different. In fact, analytic results are therein obtained for the dominant $\alpha_{\mathrm{S}}\,\tau\log(\tau)$ and $\alpha_{\mathrm{S}}^2\,\tau\log^3(\tau)$ subleading terms for 0-jettiness (τ) for $q\bar{q}$-initiated Drell–Yan-like processes.

We do not expect this behaviour to be true in general when cuts are applied to the final-state boson. This was verified in ref. [73, 74], both for transverse momentum and N-jettiness. In fact, power corrections proportional to $\sqrt{a}$ and $\sqrt{\tau}$ are found therein.

2.6 Conclusions

In the first part of the thesis we considered the production of a colourless system at next-to-leading order in the strong coupling constant α_{S}. We imposed a transverse-momentum cutoff, $q_{\mathrm{T}}^{\mathrm{cut}}$, on the colour-singlet final state and we computed the power corrections for the inclusive cross section in the cutoff, up to the fourth power. We also considered the same production process at next-to-next-to-leading order in α_{S}, restricting ourselves to the real-virtual contribution plus other terms with the same kinematics, and we computed the power corrections up to the second power in the cutoff for the inclusive cross section. Although we studied Drell–Yan vector boson production and Higgs boson production in gluon fusion, the procedure we followed is general and can be applied to other similar cases, up to any order in the powers of $q_{\mathrm{T}}^{\mathrm{cut}}$.

We presented analytic results at next-to-leading order and next-to-next-to-leading order in α_{S}, reproducing the known logarithmic terms from collinear and soft regions of the phase space, along with the finite contribution, and adding new terms as power corrections in $q_{\mathrm{T}}^{\mathrm{cut}}$. We found that the logarithmic terms in $q_{\mathrm{T}}^{\mathrm{cut}}$ show up at most

[8] The notation for the expansion of $\hat{G}_{ab}^{(2)}(z)\Big|_{\delta(s_2)}$ follows from the number of powers of α_{S}, $\log(a)$ and $a^{\frac{1}{2}}$, according to

$$\hat{G}_{ab}^{(2)}(z)\Big|_{\delta(s_2)} = \sum_{m,r} \log^m(a)\,\left(a^{\frac{1}{2}}\right)^r \hat{G}_{ab}^{(2,m,r)}(z)\,.$$

linearly (to the third power) in the next-to-leading (next-to-next-to-leading) order power-correction contributions, consistently with the fact that the LL contribution is a squared (fourth-power) logarithm. In addition, no odd-power corrections in $q_{\mathrm{T}}^{\mathrm{cut}}$ appeared in our calculation, both at next-to-leading and next-to-next-to-leading order, in agreement with known results in the literature for the NLO differential cross section in colour-singlet production. We do not expect this to be true in general when cuts are applied to the final state.

Along the calculation at next-to-leading order we kept track of the origin of the newly-computed terms, so that we were able to separate them into a universal part, and a part that depends on the process at stake. In particular we derived and identified the contribution to the universal part coming from soft radiation, present in the diagonal partonic channels for Z and H production. We could also explain some features about the presence of power-suppressed logarithmic terms, appearing in the non-universal part of the power corrections. Furthermore we showed that the knowledge of the squared amplitudes at the next-to-leading-soft approximation is not enough to predict the $(q_{\mathrm{T}}^{\mathrm{cut}})^2 \log q_{\mathrm{T}}^{\mathrm{cut}}$ behaviour of the power corrections. The same conclusion can be drawn for the knowledge of the next-to-next-to-leading-soft approximation in predicting the $(q_{\mathrm{T}}^{\mathrm{cut}})^4 \log q_{\mathrm{T}}^{\mathrm{cut}}$ power correction.

We also studied the numerical impact of the next-to-leading-order power terms in the hadronic cross sections for Z and H production at the LHC at 13 TeV, both by keeping track of the different partonic production channels and by summing over all of them. We plotted the behaviours of the cross sections while adding more and more orders of the power-correction terms, as a function of $q_{\mathrm{T}}^{\mathrm{cut}}$, and comparing them with the exact cross sections. For example, in Z production and for a value of $q_{\mathrm{T}}^{\mathrm{cut}} = 10$ GeV, the sensitivity on the cutoff can be reduced from 1‰ to 0.01‰, when adding the $(q_{\mathrm{T}}^{\mathrm{cut}})^4$ contributions to the $(q_{\mathrm{T}}^{\mathrm{cut}})^2$ ones. Higgs boson production suffers from a larger sensitivity on the cutoff, and the dependence goes from 1% to 0.2‰, when all the power corrections we computed are added. By performing the same numerical comparisons for just the universal part of the power corrections, we showed that the non-universal contributions play a crucial role for Z production, while their role is minor in Higgs boson production.

The knowledge of the power terms is crucial for understanding both the non-trivial behaviour of cross sections at the boundaries of the phase space, and the resummation structure at subleading orders. Within the q_{T}-subtraction method, the knowledge of the power terms helps in reducing the cutoff dependence of the cross sections. We recall here that at next-to-next-to-leading order the q_{T}-subtraction method still plays a major role, also in view of the fact that, as shown in refs. [23, 50], the sensitivity to the numerical value of the cutoff increases at higher orders. Thus it is mandatory to conclude our study aimed at computing analytic results for next-to-next-to-leading-order power corrections. In fact, besides improving the efficiency of the method, the newly-computed terms can help in order to obtain a local version of

the q_{T}-subtraction. This would earn a major technical income from the application of a pointwise subtraction, at variance with a non-local one, whose big cancellations often lead to numerical difficulties and slower integrations.

Chapter 3

A new interface for NLO+parton shower generators

3.1 Introduction

Next-to-leading-order (NLO) calculations for Standard Model (SM) and, sometimes, beyond-the-SM (BSM) processes, interfaced to parton shower (PS) generators, generally dubbed NLO+PS generators, are by now the methods of choice for the generation of event samples for signal and background processes at the LHC. This state of the art has been made possible, on the one side, by the formulations of general methods for computing NLO corrections [2, 3], and, on the other, by the theoretical development of algorithms for interfacing fixed order calculations with parton shower generators [10–12, 96–98]. These algorithms were implemented in software packages for the automatic computation of NLO corrections [20, 99–102], and for the automatic implementation of NLO+PS generators [14, 15, 20, 47, 103] that considerably ease the construction of generators for new processes.

MadGraph5_aMC@NLO, often abbreviated to MG5_aMC in the following, is a framework where automation has been pushed to the highest level. In fact, a user without any knowledge of NLO calculations or NLO+PS implementations can easily generate samples of parton-level events with NLO+PS accuracy, within the MC@NLO procedure. These events can be then directly fed into a PS generator, such as Pythia or Herwig. The MG5_aMC framework is not restricted to the case of SM processes. In fact, it is possible to employ any user-defined model if this is provided in the so-called UFO format [104], for example as generated by FeynRules [105, 106]. In particular, in order to undertake an NLO computation, the model should include the relevant UV and rational counterterms (both needed for the numerical evaluation of the one-loop matrix elements), which can be also automatically computed with FeynRules+NLOCT [107]. Furthermore, the FeynRules+MG5_aMC framework has been recently extended in order to fully support the supersymmetric case, including the implementation of different renormalisation conditions [108], and the

use of the so-called diagram removal and diagram subtraction techniques when intermediate resonances are present. NLO capabilities for BSM processes have been proven successful for a number of processes, see ref. [108] and references therein.

The POWHEG method allows to generate events with positive weights and, because of this, it has become the method of choice when large samples of events are needed. In fact, in view of the large amount of computer resources needed for detector simulation, the experimental collaborations cannot afford to use the larger samples that are required when negative weights are present.[1] The method has been also extended with the introduction of some theoretical developments of general interest. One of them deals with the generation of multijet samples that maintain a certain level of accuracy, even when some of the jets become unresolved [110, 111]. This approach has also led to the development of NNLO+PS generators, i.e. generators where next-to-next-to-leading-order (NNLO) calculations are interfaced to parton showers [112–114].[2] Another development has been the extension of the POWHEG method for the inclusion of processes with decaying coloured resonances, which is capable of handling the interference of the emitted radiation generated in production and decay [118].[3]

The POWHEG BOX framework automatises the construction of NLO+PS generators, once the matrix elements are available. In the early POWHEG BOX processes, the matrix elements were obtained from the authors of specific calculations. A considerable leap in the construction of the matrix elements took place when an interface of the POWHEG BOX to MADGRAPH4 was set up [16], allowing for the implementation of all tree-level ingredients required by a given NLO process. After this development, the only missing ingredient for an NLO calculation in the POWHEG BOX was the virtual contribution. Later, interfaces to automatic generators of virtual processes were also developed in refs. [17, 18] for GOSAM, and in ref. [19] for OPENLOOPS.

As of now, an interface to the matrix-element generator that is available within the MG5_AMC package has not been developed. The main obstacle is the fact that MG5_AMC is built as a single package that aims at the production of partonic events, at difference with MADGRAPH4, that was initially conceived for the generation of tree-level matrix elements. An interface between the matrix-element generator of MG5_AMC and the POWHEG BOX is also highly desirable since many BSM processes are available within MG5_AMC. In order to exploit the full capabilities of the MG5_AMC package, such interface should also build, in addition to the virtual contribution, all the necessary tree-level matrix elements: the Born, the colour- and spin-correlated Born, and the real matrix elements.

[1] A variant of the MC@NLO method for drastically reducing the negative weight fraction has appeared in ref. [109].

[2] Alternative methods for multijet merging have been presented in refs. [97, 98, 115]. Alternative methods for NNLO+PS accuracy have been proposed in refs. [116, 117].

[3] See also ref. [119].

The purpose of the present work is to present an interface between the MG5_aMC matrix-element generator and the POWHEG BOX. The structure of the interface is such that developments in MG5_aMC and POWHEG can remain independent to a large extent. For this reason, our aim is not to construct a framework that is automatised at the same level as the full MG5_aMC package itself, but rather to build an MG5_aMC extension that makes the NLO matrix elements readily available to POWHEG. Thus, progresses on the POWHEG BOX side and on the MG5_aMC side can take place independently, which is a considerable advantage in view of the way in which theoretical projects are developed. Furthermore, this kind of interface allows generalisations to other NLO+PS frameworks, that may also benefit from it for the implementation of the matrix elements.

The second part of the thesis is then organised as follows. In Sec. 3.2 we describe the interface and we give some technical details on how to use it and how to distribute the generated code. In Sec. 3.3 we consider, as a case study, the production of a spin-0 boson X_0 plus two jets. In particular, we present a few distributions able to characterise the X_0 boson CP properties and we discuss some features connected to the POWHEG BOX reweighting feature. We also show a few distributions obtained with the MiNLO approach. Finally, in Sec. 3.4 we draw our conclusions.

3.2 Interface to MG5_aMC

The new interface between POWHEG and MG5_aMC uses the capability of the latter to provide tree-level and one-loop matrix elements to be used by the former. The interface itself is a plugin for MG5_aMC: as such, it does not require any modification of the core code and it works with any recent version of MG5_aMC.[4] It re-organises the output of MG5_aMC in a format which is suitable for the POWHEG BOX [15], closely following what is described in ref. [16]. At variance with what is discussed there, no external providers for the one-loop matrix elements are needed. Rather, one-loop matrix elements are directly generated by MG5_aMC thanks to the MADLOOP module [20, 121], which encapsulates several different strategies, such as integrand reduction [122], Laurent-series expansion [123] and tensor-integral reduction [124–126], as implemented in different computer libraries [127–130] and improved by an in-house implementation of the OPENLOOPS method [99]. Thus, by fully exploiting the capabilities of MADLOOP, the evaluation of virtual matrix elements and the assessment of the numerical stability of the results are granted. Along with the matrix elements, the relevant helicity routines are also provided, in the ALOHA format [131].

[4] Versions 2.6 and onward are fully supported, for what concerns QCD corrections. The extension of the interface to more recent releases able to deal with electro-weak corrections (from version 3) [120] is left for future work.

3.2.1 Technical details

The interface plugin, dubbed MG5aMC-PWG, is publicly available.[5] Its usage is very simple, as one only needs to copy (or link) the `MG5aMC_PWG` folder inside the `PLUGIN` directory of MG5_aMC. Please refer to the `README` file enclosed in the package for conditions of usage and instructions.

The plugin can be loaded by launching, within the MG5_aMC installation directory,

```
./bin/mg5_aMC --mode=MG5aMC_PWG
```

in a command shell. In order to generate the code for a specific process at NLO QCD accuracy, the usual syntax of MG5_aMC should be employed. For example, in the case of top-pair production, the syntax is the following:

```
generate p p > t t~ [QCD]
output pp_ttx
```

where `pp_ttx` is the name (chosen by the user) of the directory where the code will be created. During the execution of the `generate` command, the MG5aMC-PWG plugin checks whether an installation of the Powheg Box V2 is available on the system and asks for its installation path (this is needed only once).

When this stage is concluded, the user can `quit` MG5_aMC and finds the MG5_aMC code for the Born, real and virtual contributions in the `pp_ttx` directory, in addition to a few basic Powheg Box V2 files. In particular, the `Born.f`, `real.f` and `virtual.f` files are ready to be used. Also the `init_processes.f` file can be used as it is, but can be also modified if particular features of the Powheg Box V2 need to be activated and initialised.

A few comments about the other files are in order:

- The `Born_phsp.f` file is just a place holder. It needs to be replaced by the actual phase-space generator for the process at hand. Examples of `Born_phsp.f` implementations can be found in the processes already implemented in the Powheg Box V2. In the current setup, a subroutine `born_suppression` should be also implemented in the `Born_phsp.f` file. This function is used at the integration stage to suppress divergences when present at the Born level, i.e. when there are jets and photons.

- The call of the `setpara("param_card.dat")` routine in the `init_couplings.f` file initialises the parameters listed in the `Cards/param_card.dat` file to the

[5] See https://code.launchpad.net/~mg5amc-pwg-team/mg5amc-pwg/v0, while the code can be downloaded with the command: `bzr branch lp:~mg5amc-pwg-team/mg5amc-pwg/v0`. The installation of the revision control system `bazaar` is required.

corresponding values, according to the UFO model [104] used in MG5_aMC.[6] It is also possible to assign a value to a MG5_aMC parameter at execution time. An example of this can be found in the `init_couplings.f` file for the process X_0jj, that we discuss in Sec. 3.3. In this file we reassign the value of $\cos\alpha$, the CP-mixing parameter that appears in the Lagrangian of eq. (3.3.3). This parameter is indicated with `cosa` in the `Cards/param_card.dat` file, and is initialised to the value specified in this file, if no further action is taken. In order to reassign its value at execution time, we change the values of the internal MG5_aMC variables, `mdl_cosa` and `mp__mdl_cosa` (for double and quadruple precision), that encode this parameter.

After any reassignment of the MG5_aMC parameters, the user has to call the `coup` routine in order to recompute all the dependent variables.

- In order to have full consistency between the MG5_aMC amplitudes and what is computed by the POWHEG BOX V2, all the physical parameters used by the POWHEG BOX V2 should be set starting from those assigned or computed by MG5_aMC. An example of this is the list of the external-particle masses, `kn_masses`, used by POWHEG BOX V2 when generating the kinematics of the event. Using $t\bar{t}$ production as example, `kn_masses` should be set to

  ```
  (\ 0, 0, mdl_mt, mdl_mt, 0 \)
  ```

  in `init_couplings.f` or `Born_phsp.f`, where `mdl_mt` is the mass of the top quark used inside MG5_aMC, the first two entries are the masses of the incoming particles, and the last massless particle is the radiated one, when computing the real contribution.

- The interface also builds a script file, `prepare_run_dir`, that is useful to create a directory where the produced code can be executed. For example, by typing the command

  ```
  ./prepare_run_dir test
  ```

  a directory `test` is created. This directory contains all the relevant links to the MG5_aMC code and a template of the `powheg.input` file, required by the POWHEG BOX V2. This last file should then be changed and modified according to the process at hand.

[6] It should be noted that the `Cards/param_card.dat` file is not read at execution time. Rather, it is parsed at compilation time into a FORTRAN include file, which is then compiled together with the code. Hence, after any parameter modification within this file, the main executable has to be recompiled.

The POWHEG process generated along these lines can be completed with all sorts of features that are commonly used in the POWHEG BOX V2. For example, one can activate the MiNLO option for processes with associated jets, or use the damping option to separate the real contributions into two parts, along the lines of what was suggested in the original POWHEG paper [11], and applied for the first time in ref. [132].

3.2.2 Distribution of the code

A process generated with this interface to MG5_aMC cannot be distributed as a usual POWHEG BOX process, since the searching path of the linked libraries are written in several files at generation time.

An author can distribute the instructions for MG5_aMC, needed in order to generate the process, and the actual files, that overwrite the place holders created by the interface plugin. In this way, all relevant paths point to the right directories in the user computer.

Alternatively, the author of the process may provide a script file that automatically executes all these tasks, helping the installation phase.

3.3 A case study: X_0jj production with CP-violating couplings

For our case study, we considered the production of a spin-0 boson X_0 (a Higgs-like boson) that couples to a massive top quark, produced via gluon fusion, and accompanied by two jets, in the heavy-top-mass limit. We discuss a few distributions able to characterise the X_0 boson CP properties, and discuss a few results obtained using the POWHEG BOX V2 reweighting feature. We also present a few distributions obtained with the MiNLO method.

3.3.1 Theoretical setup

The theoretical framework of this study is fully inherited from what was done in ref. [133], where the process was studied at NLO in QCD. In particular, in the heavy-top-mass limit, the CP structure of the X_0-top interaction characterises the effective ggX_0 vertex. The starting point is the effective Lagrangian

$$\mathcal{L}_0^t = -\bar{\psi}_t \left(k_{Htt}\, g_{Htt}\, \cos\alpha + i\, k_{Att}\, g_{Att}\, \sin\alpha\, \gamma_5\right) \psi_t\, X_0\,, \tag{3.3.1}$$

where X_0 is the spin-0 boson, ψ_t the top-quark spinor, α the CP-mixing angle parameter ($0 \leq \alpha \leq \pi$), k_{Htt} and k_{Att} the real coupling parameters and

$$g_{Htt} = g_{Att} = \frac{m_t}{v} = \frac{y_t}{\sqrt{2}} \tag{3.3.2}$$

the Yukawa couplings, with v the vacuum expectation value.

The CP-even case, that will be labeled 0^+, corresponds to the assignment $\cos\alpha = 1$, namely to the SM scenario, while the CP-odd case, labeled 0^-, to $\cos\alpha = 0$. A CP-mixed case, $0^\pm$, where the spin-0 boson receives contributions from both a scalar and a pseudoscalar state, is also taken into account by setting $\cos\alpha = 1/\sqrt{2}$.

For our purposes, it will suffice to notice that the Higgs interaction with the gluons originates as an effective coupling induced by a top-quark loop. The relevant effective Lagrangian, in the *Higgs Characterisation* framework [134], reads

$$\mathcal{L}_{0,g}^{\text{loop}} = -\frac{1}{4}\left(k_{Hgg}\, g_{Hgg}\, \cos\alpha\; G^a_{\mu\nu}\, G^{a,\mu\nu} + k_{Agg}\, g_{Agg}\, \sin\alpha\; \epsilon^{\mu\nu\rho\sigma}\, G^a_{\mu\nu}\, G^a_{\rho\sigma}\right) X_0\,, \qquad (3.3.3)$$

where $G^a_{\mu\nu}$ is the gluon field strength and

$$k_{Hgg} = -\frac{\alpha_S}{3\pi v}\,, \qquad k_{Agg} = \frac{\alpha_S}{2\pi v}\,. \qquad (3.3.4)$$

The theoretical setup is made available online in the FeynRules [106] repository as a UFO model named `HC_NLO_X0` [133, 135–137], which is in fact the one used for our case study.

3.3.2 Generation of the code

In order to generate the code, we have first to install the UFO model `HC_NLO_X0_UFO.zip` under the `models` directory of the MG5_aMC version being used. We have then followed the procedure described in Sec. 3.2.1 for the generation of the code, and given the following commands to MG5_aMC:

```
import model HC_NLO_X0_UFO-heft
generate p p > x0 j j / t [QCD]
install ninja
install collier
output X0jj
```

where we have also inserted the command lines to install ninja [128] and collier [130], that are optional and need to be installed just once.

We have then overwritten the `Born_phsp.f` file generated by the interface with the `Born_phsp.f` from the *Hjj* Powheg Box V2 process, taking care of assigning to the Powheg variables `hmass` and `hwidth` (the mass and width of the Higgs-like boson) the MG5_aMC values, `mdl_mx0` and `mdl_wx0` respectively.

In order to ease the installation procedure, we provide a tarball file that needs to be inflated in the installation directory. This file contains all the modified files that replace the place holders.

3.3.3 Simulation parameters

We have performed a simulation for the LHC, running at a centre-of-mass energy of $\sqrt{S} = 13$ TeV. The mass of the spin-0 boson X_0 has been set equal to 125 GeV. We have chosen the NNPDF2.3 (NLO) set [138] for the parton distribution functions, within the LHAPDF interface [139, 140].

The differential cross section for X_0jj production is already divergent at the Born level, unless a minimum set of generation cuts is imposed on the transverse momentum of the final-state jets and on their invariant mass. Alternatively, the divergences can be avoided if the code is executed with the MiNLO option activated. We have generated the kinematics of the underlying Born configurations imposing the following minimum set of cuts

$$p_{\rm T}^{j_k} > 10 \text{ GeV}\,, \quad k = 1, 2\,, \qquad\qquad m_{j_1 j_2} > 10 \text{ GeV}\,. \tag{3.3.5}$$

In the phenomenological study we perform in Sec. 3.3.4, we apply more stringent cuts, and we have checked that the results we present are insensitive to the generation cuts.

In order to integrate the divergent underlying Born cross section, the POWHEG BOX V2 can further apply a suppression factor at the integrand level. We stress that the final kinematic distributions are independent of this factor.[7]

3.3.4 Phenomenology

In this section we present results produced by the POWHEG BOX V2 at the Les Houches Event (LHE) level, i.e. after the emission of the first radiation, accurate at NLO for large transverse momentum, and with leading-logarithmic accuracy at small $p_{\rm T}$, due to the presence of the POWHEG Sudakov form factor. The results are computed on samples of 3.2 M events.

The renormalisation and factorisation scales are set to

$$\mu_{\rm R} = \mu_{\rm F} = \frac{H_{\rm T}}{2}\,, \tag{3.3.6}$$

where $H_{\rm T}$ is the sum of the transverse masses of the particles in the final state.

Jets are reconstructed employing the anti-$k_{\rm T}$ algorithm [141] via the FASTJET implementation [142], with distance parameter $R = 0.4$, and the two leading jets are required to have transverse momentum and pseudorapidity such that

$$p_{\rm T}^{j_k} > 30 \text{ GeV}\,, \qquad |\eta_{j_k}| < 4.5\,, \qquad k = 1, 2\,. \tag{3.3.7}$$

Events that do not pass this minimum set of acceptance cuts are discarded.

In Fig. 3.1 we plot the differential cross section for X_0jj production as a function of the invariant mass of the two leading jets, $m_{j_1 j_2}$, for three different CP scenarios:

[7] We have set `bornsuppfact` to 30 GeV in our simulation.

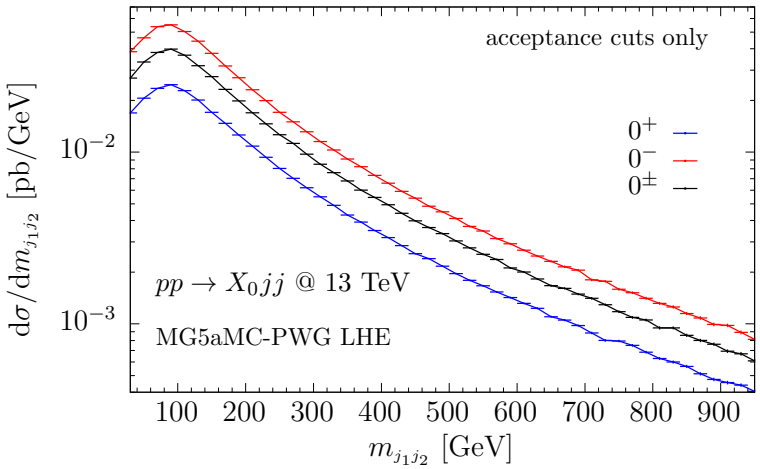

Figure 3.1. Differential cross section as a function of the invariant-mass distribution of the two leading jets in $pp \to X_0 jj$ for the three CP scenarios. The blue curve corresponds to the CP-even scenario with $\cos\alpha = 1$, the red curve to the CP-odd scenario with $\cos\alpha = 0$ and the black curve to the mixture of the 0^+ and 0^- scenarios with $\cos\alpha = 1/\sqrt{2}$.

CP even (0^+), CP odd (0^-) and a mixture of the two ($0^\pm$). The shapes of the three spectra are very similar among each other. Since a cut on the invariant mass of the dijet system enhances the discriminating power among different CP scenarios [143], the fact that the three spectra have similar shapes implies that the cut acts in a similar way on each of them. Typically a cut on $m_{j_1 j_2}$ enhances the contributions coming from the exchange of a gluon in the t channel, and these contributions are more sensitive to the CP properties of the X_0 boson.

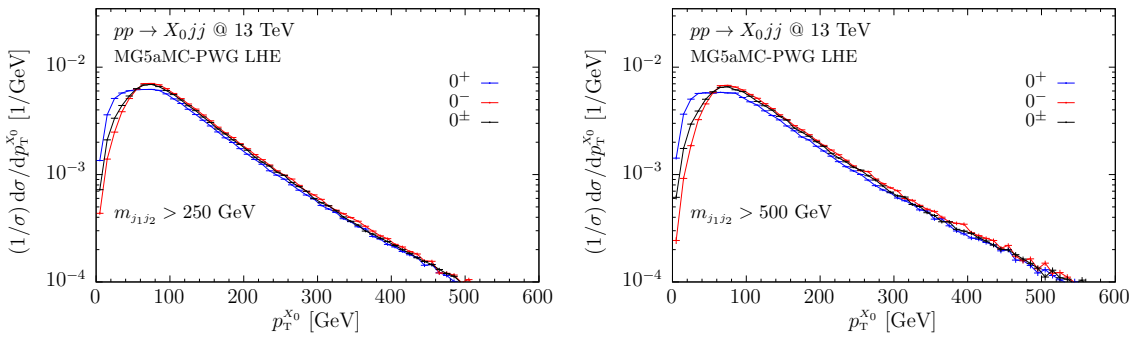

Figure 3.2. Normalised differential cross section as a function of the transverse momentum of the spin-0 boson X_0, for the three CP scenarios. On the left panel, a cut of 250 GeV is imposed on the dijet mass, while on the right panel a cut of 500 GeV is applied. The colour code is the same as in Fig. 3.1.

In the following plots we impose an additional cut on the dijet mass. In partic-

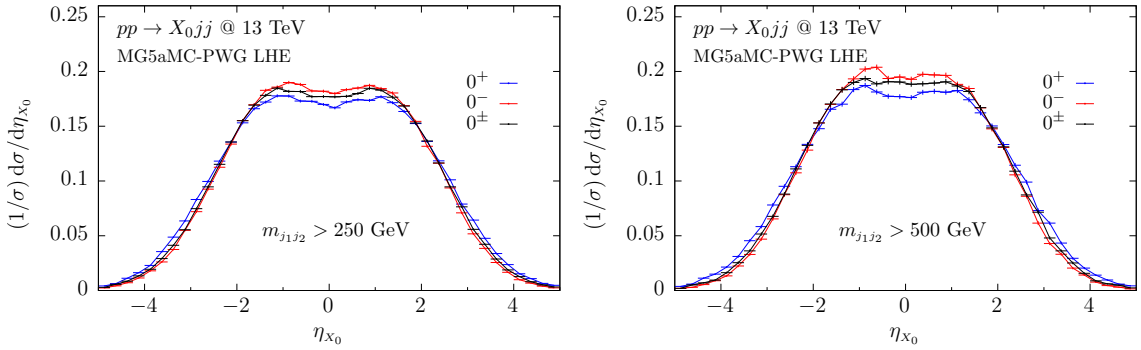

Figure 3.3. Normalised differential cross section as a function of the pseudorapidity of the spin-0 boson X_0, for the three CP scenarios. On the left panel, a cut of 250 GeV is imposed on the dijet mass, while on the right panel a cut of 500 GeV is applied. The colour code is the same as in Fig. 3.1.

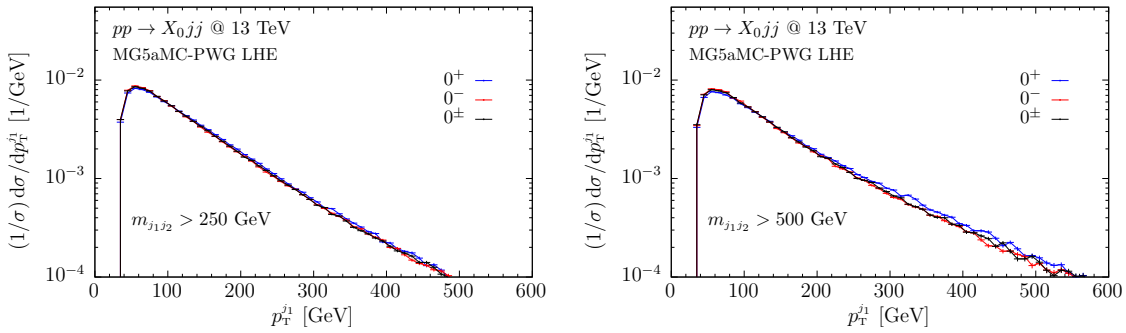

Figure 3.4. Normalised differential cross section as a function of the transverse momentum of the leading jet, for the three CP scenarios. On the left panel, a cut of 250 GeV is imposed on the dijet mass, while on the right panel a cut of 500 GeV is applied. The colour code is the same as in Fig. 3.1.

ular, we consider the two cases where

$$m_{j_1 j_2} > 250 \text{ GeV} \qquad \text{and} \qquad m_{j_1 j_2} > 500 \text{ GeV}\,. \tag{3.3.8}$$

In addition, since we are interested in shape comparisons among different CP scenarios, we normalise each curve to one.

In Figs. 3.2 and 3.3 we plot the transverse momentum and pseudorapidity of the X_0 boson, and in Figs. 3.4 and 3.5 we show the transverse momentum and pseudorapidity of the leading jet. The increase of the cut on the dijet mass hardens the p_T spectrum of the X_0 boson and the leading jet j_1. Moreover, there are only mild differences among the three CP scenarios in the X_0 distributions at low transverse momentum and in the central pseudorapidity region, with a modest enhancement when the dijet-mass cut increases. No substantial differences are present in $p_\mathrm{T}^{j_1}$ and

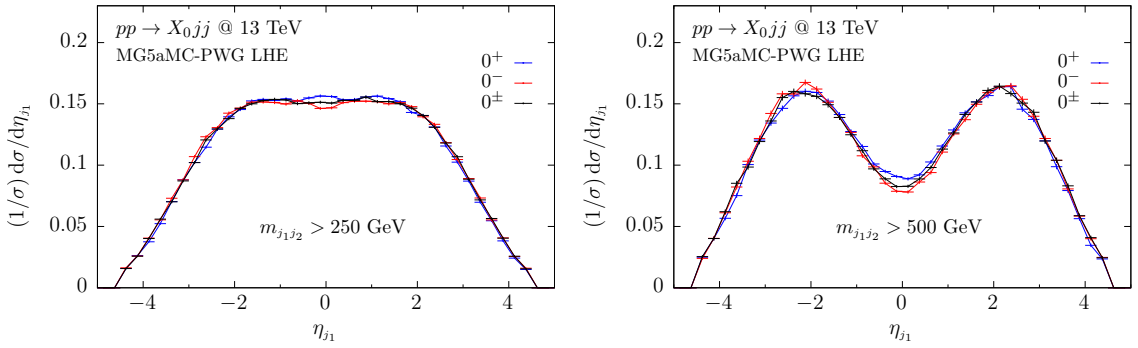

Figure 3.5. Normalised differential cross section as a function of the pseudorapidity of the leading jet, for the three CP scenarios. On the left panel, a cut of 250 GeV is imposed on the dijet mass, while on the right panel a cut of 500 GeV is applied. The colour code is the same as in Fig. 3.1.

η_{j_1}, also in agreement with what is found in ref. [133].[8]

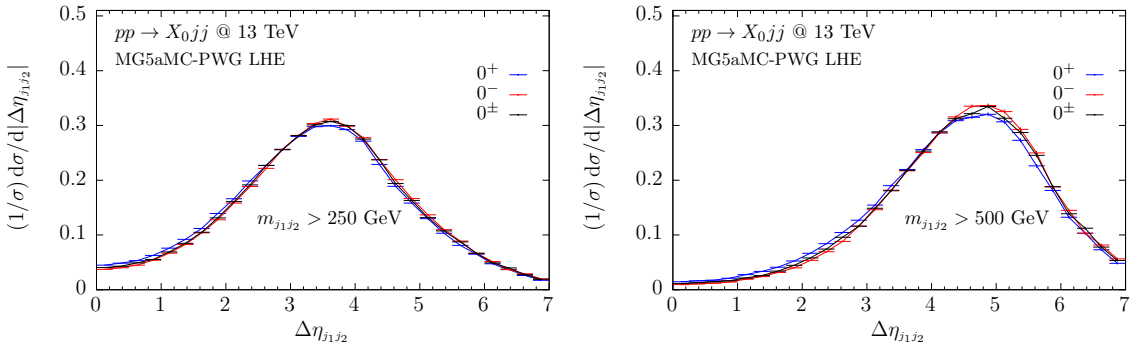

Figure 3.6. Normalised differential cross section as a function of the pseudorapidity separation of the two leading jets (see eq. (3.3.9)), for the three CP scenarios. On the left panel, a cut of 250 GeV is imposed on the dijet mass, while on the right panel a cut of 500 GeV is applied. The colour code is the same as in Fig. 3.1.

The most sensitive observables to the CP coupling of the X_0 boson to the top quark in gluon fusion are dijet-correlation variables [143, 146–152]. As displayed in Fig. 3.6, no significant differences are seen in the differential cross sections as a

[8] A possible concern is to what extent the effective-field-theory (EFT) Lagrangian of eq. (3.3.3) produces sound results in the high-energy regimes, since it describes the full theory in the heavy-top-quark limit. From the exact calculation of ref. [144], it is known that the EFT closely reproduces the $m_{j_1 j_2}$ spectrum even in the very high invariant-mass region. However, the EFT approximation breaks down when the transverse momenta of the jets are larger than the top mass [145], overestimating the exact prediction when $p_{\mathrm{T}}^{j_1}$ is larger than the top mass. Since the region of interest for discriminating the CP properties is at low transverse momentum, we can trust the results obtained within the EFT approach.

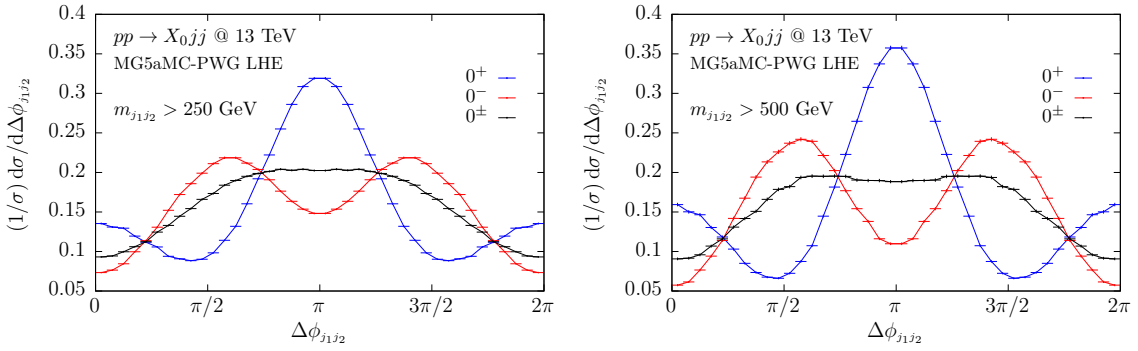

Figure 3.7. Normalised differential cross section as a function of the azimuthal separation of the two leading jets (see eq. (3.3.10)), for the three CP scenarios. On the left panel, a cut of 250 GeV is imposed on the dijet mass, while on the right panel a cut of 500 GeV is applied. The colour code is the same as in Fig. 3.1.

function of the pseudorapidity separation of the two leading jets

$$\Delta\eta_{j_1 j_2} = |\eta_{j_1} - \eta_{j_2}| \,. \tag{3.3.9}$$

Instead, when the differential cross sections are expressed as a function of the azimuthal-angle separation, the CP nature of the coupling is more evident [143]. In fact, the shape of the differential cross sections as a function of $\Delta\phi_{j_1 j_2}$ are very different, as shown in Fig. 3.7, where we have defined (modulo 2π)

$$\Delta\phi_{j_1 j_2} = |\phi_{j_1} - \phi_{j_2}| \,, \tag{3.3.10}$$

where the azimuth of a jet is computed as

$$\phi_{j_k} = \arg\left(\mathbf{p}^{j_k} \cdot \hat{y} + i\, \mathbf{p}^{j_k} \cdot \hat{x}\right), \quad k = 1, 2 \,, \tag{3.3.11}$$

with $\mathbf{p}^{j_k}$ the tri-momentum of the jet k and $\hat{x}$ ($\hat{y}$) the unit vector along the x (y)-axis direction. In the following figure, z is the beam axis.

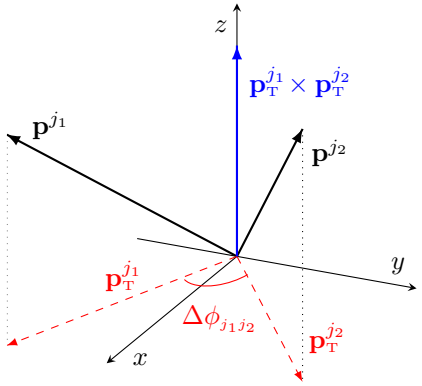

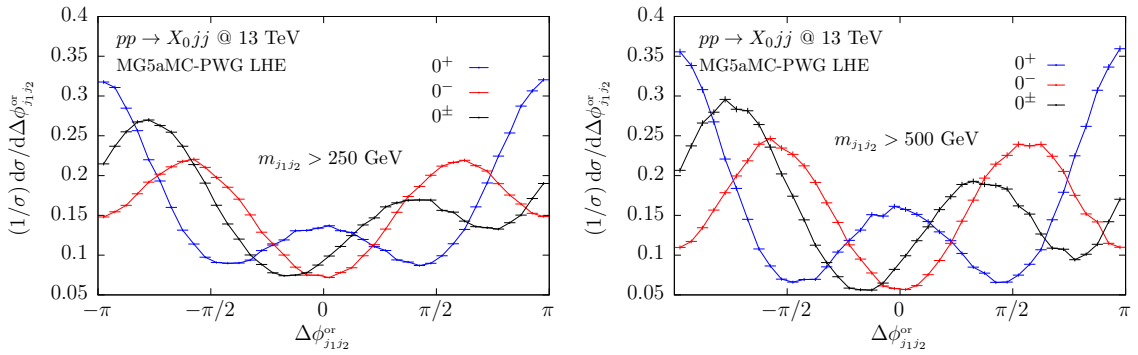

Figure 3.8. Normalised differential cross section as a function of the oriented azimuthal separation of the two leading jets, defined in eq. (3.3.12), for the three CP scenarios. On the left panel, a cut of 250 GeV is imposed on the dijet mass, while on the right panel a cut of 500 GeV is applied. The colour code is the same as in Fig. 3.1.

As pointed out in refs. [147, 153], a more CP-sensitive observable (especially for the maximal mixing scenario of $\cos\alpha = 1/\sqrt{2}$ considered here) is the oriented azimuthal separation of the two hardest jets. This variable contains information not only on the azimuthal separation of the two jets but also on the sign of the azimuthal angle. We have adopted the definition of this variable of ref. [154], namely

$$\Delta\phi^{\mathrm{or}}_{j_1 j_2} \equiv \frac{\left(\hat{\mathbf{p}}^{j_1}_{\mathrm{T}} \times \hat{\mathbf{p}}^{j_2}_{\mathrm{T}}\right)\cdot\hat{z}}{\left|\left(\hat{\mathbf{p}}^{j_1}_{\mathrm{T}} \times \hat{\mathbf{p}}^{j_2}_{\mathrm{T}}\right)\cdot\hat{z}\right|}\,\frac{\left(\mathbf{p}^{j_1}-\mathbf{p}^{j_2}\right)\cdot\hat{z}}{\left|\left(\mathbf{p}^{j_1}-\mathbf{p}^{j_2}\right)\cdot\hat{z}\right|}\,\Delta\phi_{j_1 j_2} \tag{3.3.12}$$

where $\hat{\mathbf{p}}^{j_k}_{\mathrm{T}}$ is the jet transverse momentum, normalised to one, and $\hat{z}$ is the unit vector along the z-axis direction.

The differential cross sections for the three different CP scenarios considered in this study, as a function of $\Delta\phi^{\mathrm{or}}_{j_1 j_2}$, are shown in Fig. 3.8, and their shapes are visibly different.

In particular, the oriented azimuthal separation can also distinguish between the two scenarios with $\cos\alpha = 1/\sqrt{2}$ and $\cos\alpha = -1/\sqrt{2}$, as illustrated in Fig. 3.9, while $\Delta\phi_{j_1 j_2}$cannot distinguish between them.

3.3.5 Reweighting

In this section we present a few results obtained with the POWHEG BOX V2 reweighting feature. We have reweighted two of the event samples that we have produced: the scalar and the mixed one. We have then compared the reweighted distributions with the original ones, i.e. those computed from the beginning with a given value of $\cos\alpha$. In particular, we have reweighted the scalar sample to the pseudoscalar and CP mixed cases, and we have reweighted the mixed sample to the scalar and pseudoscalar ones. We have found an overall good agreement between the reweighted and

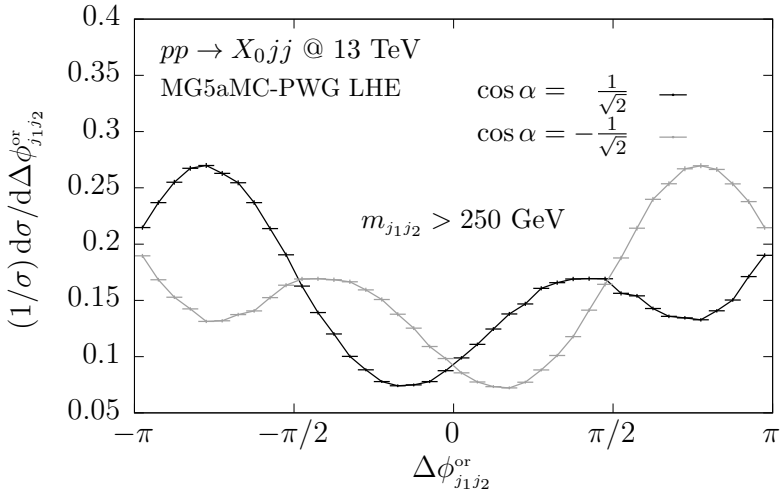

Figure 3.9. Normalised differential cross section as a function of the oriented azimuthal separation of the two leading jets, defined in eq. (3.3.12), for the two mixed CP scenarios with $\cos\alpha = 1/\sqrt{2}$ (black curve) and $\cos\alpha = -1/\sqrt{2}$ (grey curve). A cut of 250 GeV is imposed on the dijet mass.

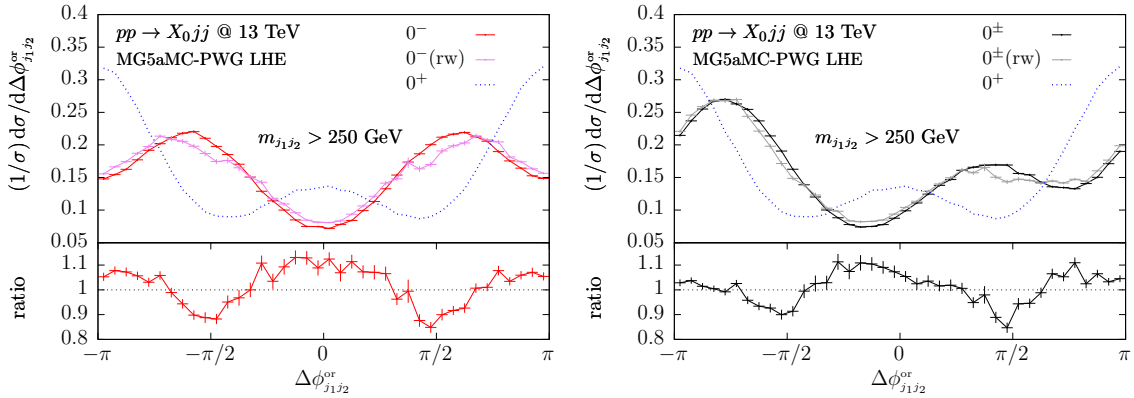

Figure 3.10. Normalised differential cross section as a function of the oriented azimuthal separation of the two leading jets, defined in eq. (3.3.12), with a cut of 250 GeV imposed on the dijet mass. On the left panel, the pseudoscalar original distribution in red, the pseudoscalar as obtained by reweighting (rw) in pink, and the scalar one in dotted blue. On the right panel, the CP mixed original distribution in black, the mixed as obtained by reweighting (rw) in grey, and the scalar one in dotted blue. The ratios between the distributions obtained by reweighting and the original ones are also shown.

the original distributions, see Appendix I for further plots, except for the distribution of the differential cross section expressed as a function of the oriented azimuthal angle, i.e. the distributions most sensitive to the value of the CP parameter $\cos\alpha$.

In Fig. 3.10 we compare three curves. The $\Delta\phi^{\mathrm{or}}_{j_1 j_2}$ distribution obtained from the

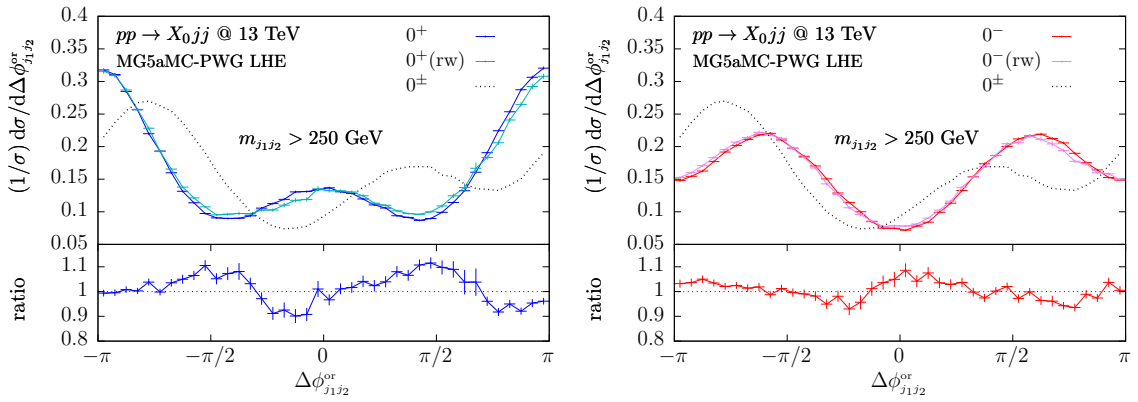

Figure 3.11. Same as Fig. 3.10 but for the reweighting of the CP mixed sample to the scalar case (on the left) and to the pseudoscalar one (on the right).

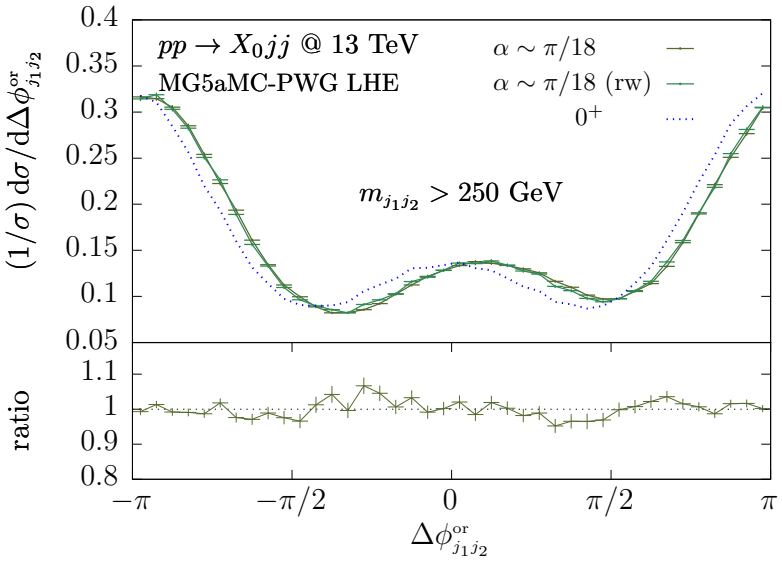

Figure 3.12. Same as Fig. 3.10 but for the reweighting of the scalar sample to the CP scenario defined by $\cos\alpha = 0.985$.

original scalar sample is plotted in dotted blue, on both panels. This curve corresponds to the 0^+ line on the left panel of Fig. 3.8. The scalar sample is reweighted to the pseudoscalar scenario on the left panel and to the mixed scenario on the right panel. The reweighted sample, indicated with "rw" in the figures, is then compared with the original distribution. The ratio of the last two curves is also plotted. In both cases, in correspondence to the minima of the 0^+ distribution, the discrepancy between the reweighted distribution and the original one is more than -10%, the minus sign to indicate that the distributions obtained by reweighting underestimate the original ones. The opposite is also true: when the 0^+ distribution has maxima that

are not close to the maxima of the 0^- and $0^\pm$ distributions, we have a discrepancy on the opposite side, up to +10%.

Similar conclusions can be drawn by reweighting the $0^\pm$ sample, as illustrated in Fig. 3.11, in order to produce the differential cross section as a function of $\Delta\phi^{\rm or}_{j_1 j_2}$ for the 0^+ and 0^- scenarios.

These differences can be explained by noticing that the minima of the above distributions are actually zeros at LO, and the production of events around these regions is then suppressed. The reweighting procedure is not able to generate the correct distributions, if the starting one is very different from the final one, i.e., for example, going from $\alpha = 0$ to $\alpha = \pi/2$, for the reweighting of the scalar case to the pseudoscalar one.

Otherwise, if the reweighting procedure is used to reweight distributions with similar values of the angle α, the procedure correctly works. This is shown in Fig. 3.12, where the distribution computed with $\alpha = 0$ is reweighted to the distribution with $\alpha \sim 10^\circ \sim \pi/18$, and the agreement with the exact one is very good.

3.3.6 MiNLO

In this section we present a few results for the pseudoscalar X_0 production, obtained within the MiNLO procedure. Although all the cuts applied on the jets in the previous sections are completely removed, the differential cross sections for inclusive quantities are finite, due to the presence of the MiNLO Sudakov form factor.

This is shown, for example, in Fig. 3.13, where we plot the inclusive differential cross section as a function of the transverse momentum of the hardest and of the second-to-hardest jet, on the left panel, and the inclusive rapidity of the X_0 boson, on the right one.

Although finite, we cannot make any claim on the accuracy of these distributions, i.e. they do not reach the NLO accuracy of the MiNLO' method, described in refs. [111, 155].[9]

3.4 Conclusions

In the second part of the thesis we have presented an interface between MadGraph5_aMC@NLOand the Powheg Box V2, able to build a NLO + parton shower generator for Standard Model and many beyond-the-Standard-Model processes, in an automatic way.

[9] Our MG5aMC-PWG implementation is NLO accurate only for quantities involving two detected jets. The MiNLO procedure allows to obtain finite and LO accurate predictions for quantities with one or zero detected jets. Otherwise, the only available method able to reach NLO accuracy for one-jet inclusive distributions, for colour-singlet production with two associated jets within the Powheg-MiNLO method, is the one illustrated in ref. [155].

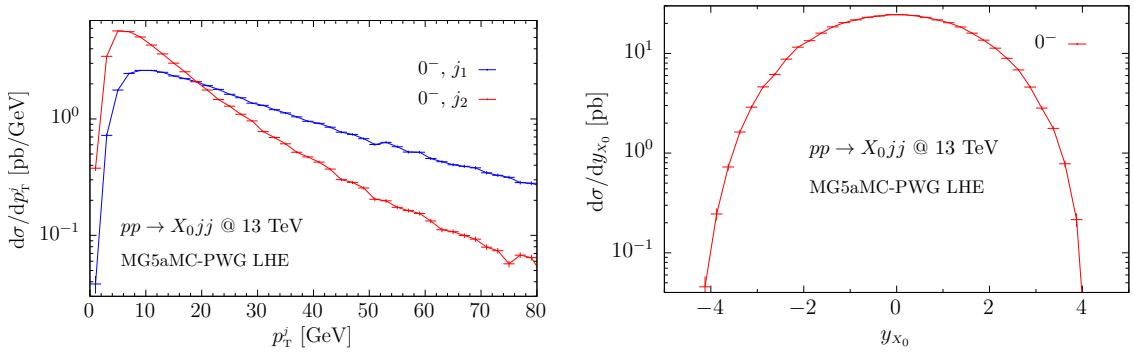

Figure 3.13. On the left panel the inclusive differential cross section as a function of the transverse momentum of the hardest jet, in blue, and of the second-to-hardest one, in red. The CP scenario is defined by $\cos\alpha = 0$, namely, the pseudoscalar case. On the right panel in red, the inclusive rapidity of the X_0 boson, for the same CP scenario as in the left panel. Both plots are obtained with MiNLO.

The structure of the interface is such that future developments in MadGraph5_aMC@NLO and Powheg Box V2 remain independent to a large extent, so that it benefits from all the progresses coming from both sides. In fact, on the one side, MadGraph5_aMC@NLO provides the matrix elements for the Born, the colour- and spin-correlated Born, the real and the virtual contributions. On the other, the Powheg Box uses these ingredients to generate events accurate at the NLO + parton shower level. In addition, the interface writes other files needed by the Powheg Box V2. Some of them, as the list of processes, are fully finalised. Others, such as the phase-space generator, need to be adjusted in order to deal with the process at hand.

By now the interface only deals with processes for which we aim at NLO QCD accuracy. The extension including the electroweak corrections and the interface with the more recent version of the Powheg Box, i.e. the Powheg Box Res, is left as future work.

As a case study, using this interface we have generated the code for the production of a spin-0 boson plus two jets, and we have computed a few kinematic distributions, sensitive to the CP properties of the coupling of the boson with a massive top quark. We have compared these distributions with known results in the literature and found full agreement. We have also presented a few results for the pseudoscalar case, obtained within the MiNLO approach.

Finally, we have tested the Powheg Box reweighting feature. This procedure works fine for every kinematic distributions we have examined, but for the ones most sensitive to the CP nature of the X_0 boson. In fact, we have observed that it works if the reweighting is done from one distribution to another, with values of the mixing angle α not very different from each other.

Appendix A

Squared amplitudes and their soft limit

In this section, for completeness, we collect the squared amplitudes $|\mathcal{M}(s,t,u)|^2$ for Z+jet and H+jet, at the lowest order in $\alpha_{\rm S}$, stripped off of trivial coupling, colour and spin factors. The normalization of the following amplitudes is such that

$$\frac{z}{2}\frac{q_{\rm T}^2}{Q^2}\left[|\mathcal{M}\left(z,t_+,q_{\rm T}\right)|^2+|\mathcal{M}\left(z,t_-,q_{\rm T}\right)|^2\right] \tag{A.1}$$

is exactly the numerator of eqs. (2.2.41)–(2.2.59).

Together with the exact squared matrix elements, we give also the soft behaviour of the amplitudes, using the energy k^0 of the final-state parton as expansion parameter. We have computed the soft expansion adopting the following procedure: we first got rid of s in favour of Q^2, t and u using the identity

$$s = Q^2 - t - u\,. \tag{A.2}$$

In this way, the only dependence on the energy of the final-state parton is through t and u, that are linearly dependent on k^0 (see eq. (2.2.5)). Then we perform a Laurent expansion in k^0, and define leading soft (LS) the term proportional to the highest negative power of k^0, next-to-leading soft (N^{1}LS) the subsequent term, and so on. Finally we re-express all the soft-expansion contributions in terms of t and u. As a result, at each order of the expansion, all the terms proportional to a given power of k^0 are included, and only them. This is an unambiguous way to define the softness order of the expansion.

Z production

- $q(\bar{q}) + g \to Z + q(\bar{q})$

  The exact squared amplitude is given by

$$|\mathcal{M}(s,t,u)|^2 = -2\left[\frac{t}{s}+\frac{s}{t}+2\,\frac{Q^2u}{st}\right] \tag{A.3}$$

with soft-expansion terms

$$|\mathcal{M}|^2_{\rm LS} = -2\,\frac{Q^2}{t} \tag{A.4}$$

$$|\mathcal{M}|^2_{\rm N^1LS} = -2\,\frac{u}{t} + 2 \tag{A.5}$$

$$|\mathcal{M}|^2_{\rm N^2LS} = -\frac{2}{Q^2}\left[2\frac{u^2}{t} + 2u + t\right] \tag{A.6}$$

$$|\mathcal{M}|^2_{\rm N^3LS} = -\frac{2}{Q^4}\left[2\,\frac{u^3}{t} + 4\,u^2 + 3\,tu + t^2\right] \tag{A.7}$$

$$|\mathcal{M}|^2_{\rm N^4LS} = \dots \tag{A.8}$$

- $q + \bar{q} \to Z + g$

  The exact squared amplitude is given by

$$|\mathcal{M}(s,t,u)|^2 = \frac{4\,Q^4}{tu} - 4\left[\frac{Q^2}{u} + \frac{Q^2}{t}\right] + 2\left[\frac{u}{t} + \frac{t}{u}\right] \tag{A.9}$$

  with soft-expansion terms

$$|\mathcal{M}|^2_{\rm LS} = 4\,\frac{Q^4}{t\,u} \tag{A.10}$$

$$|\mathcal{M}|^2_{\rm N^1LS} = -4\left[\frac{Q^2}{t} + \frac{Q^2}{u}\right] \tag{A.11}$$

$$|\mathcal{M}|^2_{\rm N^2LS} = 2\left[\frac{u}{t} + \frac{t}{u}\right] \tag{A.12}$$

$$|\mathcal{M}|^2_{\rm N^nLS} = 0\,, \qquad n \geq 3 \tag{A.13}$$

We notice that, for $q(\bar{q}) + g \to V + q(\bar{q})$ production, the LS term of eq. (A.4) has only one negative power of k^0, while in $q + \bar{q} \to V + g$ the LS term of eq. (A.10) has two negative powers of k^0, in agreement with the eikonal approximation for soft-gluon emission.

H production

- $g + q(\bar{q}) \to H + q(\bar{q})$

  The exact squared amplitude is given by

$$|\mathcal{M}(s,t,u)|^2 = -\frac{2}{Q^2}\,\frac{s^2 + u^2}{t} \tag{A.14}$$

with soft-expansion terms

$$|\mathcal{M}|^2_{\text{LS}} = -2\frac{Q^2}{t} \tag{A.15}$$

$$|\mathcal{M}|^2_{\text{N}^1\text{LS}} = 4\frac{u}{t} + 4 \tag{A.16}$$

$$|\mathcal{M}|^2_{\text{N}^2\text{LS}} = -\frac{2}{Q^2}\left[2\frac{u^2}{t} + 2\,u + t\right] \tag{A.17}$$

$$|\mathcal{M}|^2_{\text{N}^n\text{LS}} = 0\,, \qquad n \geq 3 \tag{A.18}$$

- $g + g \to H + g$

  The exact squared amplitude is given by

$$|\mathcal{M}(s,t,u)|^2 = \frac{2}{Q^2}\frac{(Q^2)^4 + s^4 + t^4 + u^4}{s\,t\,u} \tag{A.19}$$

  with soft-expansion terms

$$|\mathcal{M}|^2_{\text{LS}} = 4\,\frac{Q^4}{t\,u} \tag{A.20}$$

$$|\mathcal{M}|^2_{\text{N}^1\text{LS}} = -4\left[\frac{Q^2}{t} + \frac{Q^2}{u}\right] \tag{A.21}$$

$$|\mathcal{M}|^2_{\text{N}^2\text{LS}} = 8\left[\frac{u}{t} + \frac{t}{u} + 2\right] \tag{A.22}$$

$$|\mathcal{M}|^2_{\text{N}^3\text{LS}} = 0 \tag{A.23}$$

$$|\mathcal{M}|^2_{\text{N}^4\text{LS}} = \frac{4}{Q^4}\frac{(u^2 + t\,u + t^2)^2}{t\,u} \tag{A.24}$$

$$|\mathcal{M}|^2_{\text{N}^5\text{LS}} = \dots \tag{A.25}$$

Similar conclusions to Z production can be drawn for H production: one negative power of k^0 in $g + q(\bar{q}) \to H + q(\bar{q})$, see eq. (A.15), and two negative powers for $g + g \to H + g$, see eq. (A.20).

Appendix B

q_{T}^2 integrals

We recall a couple of definitions in order to present the minimal set of q_{T}^2 integrals that we have found for the NLO calculation:

$$a \equiv \frac{\left(q_{\mathrm{T}}^{\mathrm{cut}}\right)^2}{Q^2}\,, \tag{B.1}$$

$$\pi_{\mathrm{T}}^2 \equiv \frac{4az}{(1-z)^2}\,. \tag{B.2}$$

Hence follow the three results

$$\int_{(q_{\mathrm{T}}^{\mathrm{cut}})^2}^{(q_{\mathrm{T}}^{\mathrm{max}})^2} \frac{\mathrm{d}q_{\mathrm{T}}^2}{q_{\mathrm{T}}^2} \frac{1}{\sqrt{(1-z)^2 - 4z\,\frac{q_{\mathrm{T}}^2}{Q^2}}} = -\frac{1}{1-z}\,\log\frac{\pi_{\mathrm{T}}^2}{4} + \frac{2}{1-z}\,\log\frac{1+\sqrt{1-\pi_{\mathrm{T}}^2}}{2}\,, \tag{B.3}$$

$$\int_{(q_{\mathrm{T}}^{\mathrm{cut}})^2}^{(q_{\mathrm{T}}^{\mathrm{max}})^2} \frac{\mathrm{d}q_{\mathrm{T}}^2}{q_{\mathrm{T}}^2} \frac{\frac{q_{\mathrm{T}}^2}{Q^2}}{\sqrt{(1-z)^2 - 4z\,\frac{q_{\mathrm{T}}^2}{Q^2}}} = \frac{1-z}{2z}\,\sqrt{1-\pi_{\mathrm{T}}^2}\,, \tag{B.4}$$

$$\int_{(q_{\mathrm{T}}^{\mathrm{cut}})^2}^{(q_{\mathrm{T}}^{\mathrm{max}})^2} \frac{\mathrm{d}q_{\mathrm{T}}^2}{q_{\mathrm{T}}^2} \frac{\left(\frac{q_{\mathrm{T}}^2}{Q^2}\right)^2}{\sqrt{(1-z)^2 - 4z\,\frac{q_{\mathrm{T}}^2}{Q^2}}} = \frac{1-z}{2z}\,\frac{(1-z)^2}{6z}\,\sqrt{1-\pi_{\mathrm{T}}^2}\,\left(1+\frac{\pi_{\mathrm{T}}^2}{2}\right). \tag{B.5}$$

Appendix C

Detailed derivation of the results for Z and H production

C.1 Introduction

In this appendix we present in detail how we applied the method described in Section 2.4.3 to perform the series expansion in a for every production channel of the processes at stake. In particular, we specify for each channel which functions are assumed to be the $l(z)$ and $g(z)$ functions of eq. (2.4.20).

For ease of notation, in the following sections, the subscripts of the parton luminosities are suppressed, since any misunderstanding is prevented by the title of the section itself.

Also, in the summary of each of the following sections, a distinction is made while separating the final result in a universal and a non-universal part. As detailed in Section 2.4.1, the contributions proportional to the Altarelli–Parisi splitting functions constitute what we call the universal part of the results. The remaining ones constitute the non-universal one.

Finally, a note on the integrals we have dealt with is in order. None of them poses particular issues, except for one that we quote here, along with the method we

used in order to solve it. The final result, with $f(a) = 2\sqrt{a}\left(\sqrt{1+a}-\sqrt{a}\right)$, is

$$
\begin{aligned}
I &= \int_0^{1-f(a)} \mathrm{d}z\, \frac{1}{1-z}\, \log\frac{1}{2}\left(\sqrt{1-\frac{4a\,z}{(1-z)^2}}+1\right) \\
&\equiv \int_0^{1-f(a)} \mathrm{d}z\, \mathcal{J}(a,z) \\
&= \pi\, \arctan\left(\frac{1}{\sqrt{1+a}-\sqrt{a}}\right) - \arctan^2\left(\frac{1}{\sqrt{1+a}-\sqrt{a}}\right) \\
&\quad + \frac{1}{4}\log^2 2 + \frac{1}{2}\log 2\, \log a - \frac{5}{2}\log 2\, \log\left(\sqrt{1+a}+\sqrt{a}\right) \\
&\quad - \frac{5}{16}\log^2(1+a) - \frac{1}{4}\log 2\, \log(1+a) + \frac{1}{2}\log(1+a)\, \log\left(\sqrt{1+a}+\sqrt{a}\right) \\
&\quad - \frac{3}{4}\log(1+a)\, \log\left(\sqrt{1+a}-\sqrt{a}\right) \\
&\quad + \log\left(2a+1+2\sqrt{a}\sqrt{1+a}\right)\, \log\left(\sqrt{1+a}+\sqrt{a}\right) \\
&\quad - \frac{1}{2}\log(1+a)\, \log\left(2a+1+2\sqrt{a}\sqrt{1+a}\right) \\
&\quad - \frac{3}{4}\log^2\left(\sqrt{1+a}-\sqrt{a}\right) - \frac{1}{2}\log^2\left(\sqrt{1+a}+\sqrt{a}\right) \\
&\quad - 3\,\mathrm{Li}_2\left(\frac{\sqrt{1+a}-\sqrt{a}-i}{2\sqrt{1+a}}\right) - 3\,\mathrm{Li}_2\left(\frac{\sqrt{1+a}-\sqrt{a}+i}{2\sqrt{1+a}}\right) \\
&\quad - \mathrm{Li}_2\left(\frac{\sqrt{1+a}+\sqrt{a}+i}{2\sqrt{1+a}}\right) - \mathrm{Li}_2\left(\frac{\sqrt{1+a}+\sqrt{a}-i}{2\sqrt{1+a}}\right) \\
&\quad + \mathrm{Li}_2\left(\frac{\sqrt{1+a}-\sqrt{a}-i}{\sqrt{1+a}}\right) + \mathrm{Li}_2\left(\frac{\sqrt{1+a}-\sqrt{a}+i}{\sqrt{1+a}}\right) \\
&\quad + \mathrm{Li}_2\left(\frac{1+i\sqrt{a}}{1+a+\sqrt{a}\sqrt{1+a}}\right) + \mathrm{Li}_2\left(\frac{1-i\sqrt{a}}{1+a+\sqrt{a}\sqrt{1+a}}\right) \\
&\quad + \mathrm{Li}_2\left(-i\sqrt{1+a}+i\sqrt{a}\right) + \mathrm{Li}_2\left(i\sqrt{1+a}-i\sqrt{a}\right) \\
&\quad + \mathrm{Li}_2\left(\frac{\sqrt{a}-\sqrt{1+a}}{2\sqrt{a}}\right) + \mathrm{Li}_2\left(\frac{\sqrt{1+a}-\sqrt{a}}{2\sqrt{1+a}}\right) \\
&\quad - \mathrm{Li}_2\left(\frac{1}{2}\left(1+i\sqrt{1+a}-i\sqrt{a}\right)\right) - \mathrm{Li}_2\left(\frac{1}{2}\left(1-i\sqrt{1+a}+i\sqrt{a}\right)\right) \\
&\quad + \mathrm{Li}_2\left(1-i\left(\sqrt{1+a}-\sqrt{a}\right)\right) + \mathrm{Li}_2\left(1+i\left(\sqrt{1+a}-\sqrt{a}\right)\right) \\
&\quad - \mathrm{Li}_2\left(1+a-\sqrt{a}\sqrt{1+a}\right) + \frac{1}{2}\log^2\left(\frac{\sqrt{a}}{\sqrt{1+a}}\right). \qquad \text{(C.1.1)}
\end{aligned}
$$

In order to solve the integral I, two changes of variable were used. First, we introduced a new variable y such that

$$
y^2 = 1 - \frac{4a\,z}{(1-z)^2} \quad \leftrightarrow \quad z(y) = \frac{1+2a-y^2-2\sqrt{a+a^2-a\,y^2}}{1-y^2} \qquad \text{(C.1.2)}
$$

and we chose the z-root with the proper sign, such that $z(0) = 1 - f(a)$. Notice that the z-interval $[0, 1 - f(a)]$ is thus mapped onto the y-interval $[1, 0]$. Therefore, the first change of variable leads to the replacement

$$\int_0^{1-f(a)} \mathrm{d}z\, \mathcal{J}(z,a) \quad \to \quad -\int_0^1 \mathrm{d}y\, \frac{\mathrm{d}z(y)}{\mathrm{d}y}\, \mathcal{J}(z(y),a)\,. \tag{C.1.3}$$

Then, we dealt with the square roots appearing in eq. (C.1.3) via a second change of variable inspired by Appendix A of ref. [156], namely

$$y(u) = \frac{2u}{c - d\,(2u)^2}\,, \qquad c = 1, \quad d = -\frac{1}{4\,(1+a)}\,. \tag{C.1.4}$$

This is such that, by setting $0 < y(\bar{u}) < 1$, where $\bar{u}$ is the new integration extrema different from zero, the y-interval $[0, 1]$ is mapped onto the u-interval $[0, 1 + a - \sqrt{a + a^2}] \equiv [0, \bar{u}]$. The final replacement is then

$$-\int_0^1 \mathrm{d}y\, \frac{\mathrm{d}z(y)}{\mathrm{d}y}\, \mathcal{J}(z(y),a) \quad \to \quad -\int_0^{\bar{u}} \mathrm{d}u\, \frac{\mathrm{d}y(u)}{\mathrm{d}u}\, \frac{\mathrm{d}z(y)}{\mathrm{d}y}\, \mathcal{J}(z(y(u)),a)\,, \tag{C.1.5}$$

where

$$\frac{\mathrm{d}y(u)}{\mathrm{d}u}\, \frac{\mathrm{d}z(y)}{\mathrm{d}y}\, \mathcal{J}(u,a) = \frac{4b\,u\,[u^2\,(b+\beta) - b\,(b-\beta)]}{(u^2+b)\,(u^2+2b\,u+b)\,(u^2-2b\,u+b)}\, \log\frac{u^2+2b\,u+b}{2\,(u^2+b)} \tag{C.1.6}$$

with

$$b = 1 + a\,, \qquad \beta = \sqrt{b(b-1)}\,. \tag{C.1.7}$$

The second integral of eq. (C.1.5) is part of a known and solvable class of integrals.

C.2 Z production: qg channel

The relevant integral, corresponding to that in eq. (2.4.20), is

$$\begin{aligned} I = \int_\tau^{1-f(a)} \mathrm{d}z\, \mathcal{L}\left(\frac{\tau}{z}\right) \Bigg\{ & \frac{1}{2z}\,(1+3z)(1-z)\,\sqrt{1 - \frac{4az}{(1-z)^2}} \\ & + p_{qg}(z)\frac{1}{z}\left[-\log\frac{az}{(1-z)^2} + 2\log\frac{1}{2}\left(\sqrt{1-\frac{4az}{(1-z)^2}} + 1\right)\right]\Bigg\}\,, \end{aligned} \tag{C.2.1}$$

where

$$p_{qg}(z) = 2z^2 - 2z + 1\,. \tag{C.2.2}$$

We can express I as the sum of three integrals

$$I = I^a + I^b + I^c\,, \tag{C.2.3}$$

where

$$I^a = \int_\tau^{1-f(a)} \mathrm{d}z\, \frac{1}{2z}\,(1+3z)(1-z)\,\mathcal{L}\left(\frac{\tau}{z}\right)\sqrt{1-\frac{4az}{(1-z)^2}}\,, \tag{C.2.4}$$

$$I^b = -\int_\tau^{1-f(a)} \mathrm{d}z\, p_{qg}(z)\,\frac{1}{z}\,\mathcal{L}\left(\frac{\tau}{z}\right)\log\frac{az}{(1-z)^2}\,, \tag{C.2.5}$$

$$I^c = \int_\tau^{1-f(a)} \mathrm{d}z\, p_{qg}(z)\,\frac{2}{z}\,\mathcal{L}\left(\frac{\tau}{z}\right)\log\frac{1}{2}\left(\sqrt{1-\frac{4az}{(1-z)^2}}+1\right), \tag{C.2.6}$$

and for each of the three integrals we apply the procedure detailed in Section 2.4.

Integral I^a

We define

$$l(z) = \frac{1}{2z}\,(1+3z)\,\mathcal{L}\left(\frac{\tau}{z}\right), \tag{C.2.7}$$

$$g(z) = (1-z)\sqrt{1-\frac{4az}{(1-z)^2}}\,, \tag{C.2.8}$$

and expanding $g(z)$ according to eq. (2.4.21), we have

$$g(z) = (1-z) - \frac{2az}{1-z} - \frac{2a^2z^2}{(1-z)^3} + \mathcal{O}\big(a^3\big) \tag{C.2.9}$$

so that

$$g_0(z,a) = 1-z\,, \qquad g_1(z,a) = -2az\,, \qquad g_2(z,a) = 0\,, \qquad g_3(z,a) = -2a^2z^2\,. \tag{C.2.10}$$

With this assignment of the different terms of the expansion of $g(z)$, we perform the integrations in eqs. (2.4.28)–(2.4.30).

Integral I^b

The integrand of I^b is defined up to $z=1$. For this reason, the computation of this contribution is easier than the previous one. In particular we can write

$$I^b \equiv I^b_1 + I^b_2\,, \tag{C.2.11}$$

where

$$I^b_1 = -\int_0^1 \mathrm{d}z\, p_{qg}(z)\,\frac{1}{z}\log\frac{az}{(1-z)^2}\,\mathcal{L}\left(\frac{\tau}{z}\right), \tag{C.2.12}$$

$$I^b_2 = +\int_{1-f(a)}^1 \mathrm{d}z\, p_{qg}(z)\,\frac{1}{z}\log\frac{az}{(1-z)^2}\,\mathcal{L}\left(\frac{\tau}{z}\right). \tag{C.2.13}$$

Defining

$$l(z) = \left(2z^2 - 2z + 1\right) \frac{1}{z} \mathcal{L}\left(\frac{\tau}{z}\right), \tag{C.2.14}$$

we expand it as a power series in $(z-1)$, so that

$$I_2^b = \sum_{n=0}^{\infty} \frac{1}{n!} l^{(n)}(1) \int_{1-f(a)}^{1} \mathrm{d}z\, (z-1)^n \log \frac{az}{(1-z)^2} \tag{C.2.15}$$

and the integration becomes straightforward.

Integral I^c

We define

$$l(z) = \frac{2}{z}\left(2z^2 - 2z + 1\right) \mathcal{L}\left(\frac{\tau}{z}\right), \tag{C.2.16}$$

$$g(z) = \log \frac{1}{2}\left(\sqrt{1 - \frac{4az}{(1-z)^2}} + 1\right), \tag{C.2.17}$$

and expanding $g(z)$ according to eq. (2.4.21), we have

$$g(z) = -\frac{az}{(1-z)^2} - \frac{3}{2}\frac{a^2 z^2}{(1-z)^4} + \mathcal{O}\left(a^3\right), \tag{C.2.18}$$

so that

$$Bg_0(z,a) = g_1(z,a) = g_3(z,a) = 0\,, \qquad g_2(z,a) = -az\,, \qquad g_4(z,a) = -\frac{3}{2}a^2 z^2\,. \tag{C.2.19}$$

We then perform the integrations in eqs. (2.4.28)–(2.4.30).

C.2.1 Summary

Summarising our results, and writing I in eq. (C.2.1) as a sum of the universal and the non-universal part, we have

$$I = I^{\mathrm{U}} + I^{\mathrm{R}}\,, \tag{C.2.20}$$

where

$$\begin{aligned}
I^{\mathrm{U}} = & -\log(a) \int_0^1 \mathrm{d}z\, \frac{1}{z} p_{qg}(z)\, \mathcal{L}\left(\frac{\tau}{z}\right) - \int_0^1 \mathrm{d}z\, \frac{1}{z} p_{qg}(z) \log \frac{z}{(1-z)^2}\, \mathcal{L}\left(\frac{\tau}{z}\right) \\
& - 2\,a \int_0^1 \mathrm{d}z\, p_{qg}(z)\, \mathcal{L}\left(\frac{\tau}{z}\right) \left[\frac{1}{(1-z)^2}\right]_{2+} - 3\,a^2 \int_0^1 \mathrm{d}z\, z\, p_{qg}(z)\, \mathcal{L}\left(\frac{\tau}{z}\right) \left[\frac{1}{(1-z)^4}\right]_{4+} \\
& + \left\{-2\,\mathcal{L}(\tau) + \tau\,\mathcal{L}^{(1)}(\tau)\right\} a \log(a) + \mathcal{L}(\tau)\, a \\
& + \left\{-3\,\mathcal{L}(\tau) + 3\,\tau\,\mathcal{L}^{(1)}(\tau) - \frac{3}{4}\tau^2\,\mathcal{L}^{(2)}(\tau) + \frac{1}{4}\tau^3\,\mathcal{L}^{(3)}(\tau)\right\} a^2 \log(a) \\
& + \left\{\frac{9}{4}\mathcal{L}(\tau) - \frac{1}{4}\tau\,\mathcal{L}^{(1)}(\tau) + \frac{1}{4}\tau^2\,\mathcal{L}^{(2)}(\tau) + \frac{1}{6}\tau^3\,\mathcal{L}^{(3)}(\tau)\right\} a^2 \\
& + \mathcal{O}\left(a^{\frac{5}{2}} \log(a)\right),
\end{aligned} \tag{C.2.21}$$

$$
\begin{aligned}
I^{\mathrm{R}} = &+ \int_0^1 \mathrm{d}z\, \frac{1}{2z}\,(1+3z)(1-z)\,\mathcal{L}\left(\frac{\tau}{z}\right) - a\int_0^1 \mathrm{d}z\,(1+3z)\,\mathcal{L}\left(\frac{\tau}{z}\right)\left[\frac{1}{1-z}\right]_+ \\
&- a^2\int_0^1 \mathrm{d}z\, z\,(1+3z)\,\mathcal{L}\left(\frac{\tau}{z}\right)\left[\frac{1}{(1-z)^3}\right]_{3+} \\
&+ 2\,\mathcal{L}(\tau)\,a\log(a) - 2\,\mathcal{L}(\tau)\,a \\
&+ \left\{\frac{3}{2}\,\mathcal{L}(\tau) - \frac{3}{2}\,\tau\,\mathcal{L}^{(1)}(\tau) + \tau^2\,\mathcal{L}^{(2)}(\tau)\right\} a^2\log(a) \\
&+ \left\{-\frac{7}{4}\,\mathcal{L}(\tau) + \frac{5}{4}\,\tau\,\mathcal{L}^{(1)}(\tau) + \frac{1}{2}\,\tau^2\,\mathcal{L}^{(2)}(\tau)\right\} a^2 + \mathcal{O}\left(a^{\frac{5}{2}}\log(a)\right). \qquad \text{(C.2.22)}
\end{aligned}
$$

Then, writing I^{U} and I^{R} in the form

$$
I^{\mathrm{U}} = \int_0^1 \frac{\mathrm{d}z}{z}\,\mathcal{L}\left(\frac{\tau}{z}\right)\hat{g}_{qg}^{\mathrm{U}(1)}(z)\,, \qquad I^{\mathrm{R}} = \int_0^1 \frac{\mathrm{d}z}{z}\,\mathcal{L}\left(\frac{\tau}{z}\right)\hat{g}_{qg}^{\mathrm{R}(1)}(z)\,, \qquad \text{(C.2.23)}
$$

we get the expression of $\hat{g}_{qg}^{\mathrm{U}(1)}(z)$ and $\hat{g}_{qg}^{\mathrm{R}(1)}(z)$ in eqs. (2.4.34) and (2.4.35), respectively.

C.3 Z production: $q\bar{q}$ channel

The relevant integral, corresponding to that in eq. (2.4.20), is

$$
\begin{aligned}
I = \int_\tau^{1-f(a)} \mathrm{d}z\,\mathcal{L}\left(\frac{\tau}{z}\right)\Bigg\{&-\frac{2}{z}\,(1-z)\sqrt{1-\frac{4az}{(1-z)^2}} \\
&+ \frac{2}{z}\,\hat{p}_{qq}(z)\left[-\log\frac{az}{(1-z)^2} + 2\log\frac{1}{2}\left(\sqrt{1-\frac{4az}{(1-z)^2}}+1\right)\right]\Bigg\}, \qquad \text{(C.3.1)}
\end{aligned}
$$

where

$$
\hat{p}_{qq}(z) = \frac{1+z^2}{1-z}\,. \qquad \text{(C.3.2)}
$$

We can express I as the sum of three integrals

$$
I = I^a + I^b + I^c\,, \qquad \text{(C.3.3)}
$$

where

$$
I^a = -\int_\tau^{1-f(a)} \mathrm{d}z\,\mathcal{L}\left(\frac{\tau}{z}\right)\frac{2}{z}(1-z)\sqrt{1-\frac{4az}{(1-z)^2}}\,, \qquad \text{(C.3.4)}
$$

$$
I^b = -\int_\tau^{1-f(a)} \mathrm{d}z\,\frac{2}{z}\,\hat{p}_{qq}(z)\,\mathcal{L}\left(\frac{\tau}{z}\right)\log\frac{az}{(1-z)^2}\,, \qquad \text{(C.3.5)}
$$

$$
I^c = \int_\tau^{1-f(a)} \mathrm{d}z\,\frac{4}{z}\,\hat{p}_{qq}(z)\,\mathcal{L}\left(\frac{\tau}{z}\right)\log\frac{1}{2}\left(\sqrt{1-\frac{4az}{(1-z)^2}}+1\right), \qquad \text{(C.3.6)}
$$

and for each of the three integrals we apply the procedure detailed in Section 2.4.

Integral I^a

We define

$$l(z) = -\frac{2}{z}\,\mathcal{L}\left(\frac{\tau}{z}\right), \tag{C.3.7}$$

$$g(z) = (1-z)\sqrt{1-\frac{4az}{(1-z)^2}}, \tag{C.3.8}$$

and expanding $g(z)$ according to eq. (2.4.21), we have

$$g(z) = (1-z) - \frac{2az}{1-z} - \frac{2a^2z^2}{(1-z)^3} + \mathcal{O}\big(a^3\big), \tag{C.3.9}$$

so that

$$g_0(z,a) = 1-z\,, \qquad g_1(z,a) = -2az\,, \qquad g_2(z,a) = 0\,, \qquad g_3(z,a) = -2a^2z^2\,. \tag{C.3.10}$$

We then perform the integrations in eqs. (2.4.28)–(2.4.30).

Integral I^b

We start by separating I^b into two further integrals, writing

$$I^b = I^{b1} + I^{b2}\,, \tag{C.3.11}$$

where

$$I^{b1} = -\int_\tau^{1-f(a)} \mathrm{d}z\,\frac{2}{z}\,\hat{p}_{qq}(z)\,\mathcal{L}\left(\frac{\tau}{z}\right)\log(az)\,, \tag{C.3.12}$$

$$I^{b2} = +\int_\tau^{1-f(a)} \mathrm{d}z\,\frac{4}{z}\,\hat{p}_{qq}(z)\,\mathcal{L}\left(\frac{\tau}{z}\right)\log(1-z)\,, \tag{C.3.13}$$

and for each of them we follow our integration and expansion procedure.

- **Integral I^{b1}**

  We define

  $$l(z) = -\frac{2}{z}\left(1+z^2\right)\log(az)\,\mathcal{L}\left(\frac{\tau}{z}\right), \tag{C.3.14}$$

  $$g(z) = \frac{1}{1-z}\,, \tag{C.3.15}$$

  and we deal with this case as with a case with $g_0 = 0$, $g_1(z,a) = 1$ and all the other g_i functions equal to 0. Then, we perform the integrations in eqs. (2.4.28)–(2.4.30).

- **Integral I^{b2}**

  We define

$$l(z) = \frac{4}{z}\left(1+z^2\right)\mathcal{L}\left(\frac{\tau}{z}\right), \tag{C.3.16}$$

$$g(z) = \frac{\log(1-z)}{1-z}, \tag{C.3.17}$$

  and we deal with this case as with a case with $g_0 = 0$, $g_1(z,a) = \log(1-z)$ and all the other g_i functions equal to 0. Then, we perform the integrations in eqs. (2.4.28)–(2.4.30).

Integral I^c

We define

$$l(z) = \frac{4}{z}\left(1+z^2\right)\mathcal{L}\left(\frac{\tau}{z}\right), \tag{C.3.18}$$

$$g(z) = \frac{1}{1-z}\log\frac{1}{2}\left(\sqrt{1-\frac{4az}{(1-z)^2}}+1\right), \tag{C.3.19}$$

and expanding $g(z)$ according to eq. (2.4.21), we have

$$g(z) = -\frac{az}{(1-z)^3} - \frac{3}{2}\frac{a^2z^2}{(1-z)^5} + \mathcal{O}\left(a^3\right), \tag{C.3.20}$$

so that

$$g_0(z,a) = g_1(z,a) = g_2(z,a) = g_4(z,a) = 0\,, \quad g_3(z,a) = -az\,, \quad g_5(z,a) = -\frac{3}{2}a^2z^2\,. \tag{C.3.21}$$

We then perform the integrations in eqs. (2.4.28)–(2.4.30).

C.3.1 Summary

Summarising our results, and writing I in eq. (C.3.1) as a sum of a universal and non-universal part, we have

$$I = I^{\mathrm{U}} + I^{\mathrm{R}}\,, \tag{C.3.22}$$

where

$$
\begin{aligned}
I^{\mathrm{U}} = & -2\log(a)\int_0^1 \mathrm{d}z\,\frac{1}{z}\,\mathcal{L}\left(\frac{\tau}{z}\right)p_{qq}(z) \\
& -2\int_0^1 \mathrm{d}z\,\frac{1}{z}\,\hat{p}_{qq}(z)\log(z)\,\mathcal{L}\left(\frac{\tau}{z}\right)+\int_0^1 \mathrm{d}z\,\frac{4}{z}\,(1-z)\,\hat{p}_{qq}(z)\mathcal{L}\left(\frac{\tau}{z}\right)\left[\frac{\log(1-z)}{1-z}\right]_+ \\
& -4a\int_0^1 \mathrm{d}z\,(1-z)\,\hat{p}_{qq}(z)\mathcal{L}\left(\frac{\tau}{z}\right)\left[\frac{1}{(1-z)^3}\right]_{3+} \\
& -6a^2\int_0^1 \mathrm{d}z\,z\,(1-z)\,\hat{p}_{qq}(z)\mathcal{L}\left(\frac{\tau}{z}\right)\left[\frac{1}{(1-z)^5}\right]_{5+} \\
& +\mathcal{L}(\tau)\log(a)^2-\frac{\pi^2}{3}\,\mathcal{L}(\tau) \\
& +\left\{\mathcal{L}(\tau)+2\,\tau^2\,\mathcal{L}^{(2)}(\tau)\right\}a\log(a)+\left\{-2\,\mathcal{L}(\tau)+4\,\tau\,\mathcal{L}^{(1)}(\tau)\right\}a \\
& +\left\{\frac{3}{2}\,\tau^2\,\mathcal{L}^{(2)}(\tau)+\tau^3\,\mathcal{L}^{(3)}(\tau)+\frac{1}{4}\,\tau^4\,\mathcal{L}^{(4)}(\tau)\right\}a^2\log(a) \\
& +\left\{-\mathcal{L}(\tau)+2\,\tau\,\mathcal{L}^{(1)}(\tau)+\frac{5}{2}\,\tau^2\,\mathcal{L}^{(2)}(\tau)+\frac{5}{3}\,\tau^3\,\mathcal{L}^{(3)}(\tau)+\frac{1}{6}\,\tau^4\,\mathcal{L}^{(4)}(\tau)\right\}a^2 \\
& +\mathcal{O}\left(a^{\frac{5}{2}}\log(a)\right), \qquad \text{(C.3.23)}
\end{aligned}
$$

$$
\begin{aligned}
I^{\mathrm{R}} = & -\int_0^1 \mathrm{d}z\,\frac{2}{z}\,(1-z)\,\mathcal{L}\left(\frac{\tau}{z}\right)+4a\int_0^1 \mathrm{d}z\,\mathcal{L}\left(\frac{\tau}{z}\right)\left[\frac{1}{1-z}\right]_+ \\
& +4a^2\int_0^1 \mathrm{d}z\,z\,\mathcal{L}\left(\frac{\tau}{z}\right)\left[\frac{1}{(1-z)^3}\right]_{3+} \\
& -2\,\mathcal{L}(\tau)\,a\log(a)+2\,\mathcal{L}(\tau)\,a-\tau^2\,\mathcal{L}^{(2)}(\tau)\,a^2\log(a) \\
& +\left\{\mathcal{L}(\tau)-2\,\tau\,\mathcal{L}^{(1)}(\tau)-\frac{1}{2}\,\tau^2\,\mathcal{L}^{(2)}(\tau)\right\}a^2+\mathcal{O}\left(a^{\frac{5}{2}}\log(a)\right), \qquad \text{(C.3.24)}
\end{aligned}
$$

where we have written the $(1+z^2)$ terms coming from the numerator of the $q\bar{q}$ splitting function as

$$
1+z^2=(1-z)\,\hat{p}_{qq}(z)\,. \qquad \text{(C.3.25)}
$$

Then, writing I^{U} and I^{R} in the form

$$
I^{\mathrm{U}}=\int_0^1\frac{\mathrm{d}z}{z}\,\mathcal{L}\left(\frac{\tau}{z}\right)\hat{g}^{\mathrm{U}(1)}_{q\bar{q}}(z)\,,\qquad\qquad I^{\mathrm{R}}=\int_0^1\frac{\mathrm{d}z}{z}\,\mathcal{L}\left(\frac{\tau}{z}\right)\hat{g}^{\mathrm{R}(1)}_{q\bar{q}}(z)\,, \qquad \text{(C.3.26)}
$$

we get the expression of $\hat{g}^{\mathrm{U}(1)}_{q\bar{q}}(z)$ and $\hat{g}^{\mathrm{R}(1)}_{q\bar{q}}(z)$ in eqs. (2.4.38) and (2.4.39), respectively.

C.4 H production: gq channel

The relevant integral, corresponding to that in eq. (2.4.20), is

$$I = \int_\tau^{1-f(a)} dz\, \mathcal{L}\left(\frac{\tau}{z}\right) \left\{ -\frac{3(1-z)^2}{2z^2} \sqrt{1-\frac{4az}{(1-z)^2}} + \frac{1}{z}\, p_{gq}(z) \left[-\log\frac{az}{(1-z)^2} + 2\log\frac{1}{2}\left(\sqrt{1-\frac{4az}{(1-z)^2}}+1\right)\right]\right\}, \tag{C.4.1}$$

where

$$p_{gq}(z) = \frac{z^2-2z+2}{z}\,. \tag{C.4.2}$$

We can express I as the sum of three integrals

$$I = I^a + I^b + I^c\,, \tag{C.4.3}$$

where

$$I^a = \int_\tau^{1-f(a)} \mathrm{d}z \left[-\frac{3}{2}\frac{(1-z)^2}{z^2}\right] \mathcal{L}\left(\frac{\tau}{z}\right) \sqrt{1-\frac{4az}{(1-z)^2}}\,, \tag{C.4.4}$$

$$I^b = \int_\tau^{1-f(a)} \mathrm{d}z \left(-\frac{1}{z}\right) p_{gq}(z)\, \mathcal{L}\left(\frac{\tau}{z}\right) \log\frac{az}{(1-z)^2}\,, \tag{C.4.5}$$

$$I^c = \int_\tau^{1-f(a)} \mathrm{d}z\, \frac{2}{z}\, p_{gq}(z)\, \mathcal{L}\left(\frac{\tau}{z}\right) \log\frac{1}{2}\left(\sqrt{1-\frac{4az}{(1-z)^2}}+1\right), \tag{C.4.6}$$

and for each of the three integrals we apply the procedure detailed in Section 2.4.

Integral I^a

We define

$$l(z) = -\frac{3}{2}\,\frac{1}{z^2}\,\mathcal{L}\left(\frac{\tau}{z}\right), \tag{C.4.7}$$

$$g(z) = (1-z)^2 \sqrt{1-\frac{4az}{(1-z)^2}}\,, \tag{C.4.8}$$

and expanding $g(z)$ according to eq. (2.4.21), we have

$$g(z) = (1-z)^2 - 2az - \frac{2a^2z^2}{(1-z)^2} + \mathcal{O}\big(a^3\big)\,, \tag{C.4.9}$$

so that

$$g_0(z,a) = (1-z)^2 - 2az\,, \qquad g_1(z,a) = 0\,, \qquad g_2(z,a) = -2a^2z^2\,, \qquad g_3(z,a) = 0\,. \tag{C.4.10}$$

We then perform the integrations in eqs. (2.4.28)–(2.4.30).

Integral I^b

The integrand of I^b is defined up to $z = 1$. Thus, the computation of this contribution is easier than the previous one. In particular, we can proceed by separating it into two further integrals

$$I^b \equiv I_1^b + I_2^b \,, \tag{C.4.11}$$

where

$$I_1^b = \int_0^1 \mathrm{d}z \left(-\frac{1}{z}\right) p_{gq}(z)\, \mathcal{L}\left(\frac{\tau}{z}\right) \log \frac{az}{(1-z)^2} \,, \tag{C.4.12}$$

$$I_2^b = \int_{1-f(a)}^1 \mathrm{d}z \, \frac{1}{z}\, p_{gq}(z)\, \mathcal{L}\left(\frac{\tau}{z}\right) \log \frac{az}{(1-z)^2} \,. \tag{C.4.13}$$

Then, after defining

$$l(z) = \left[\frac{z^2 - 2z + 2}{z^2}\right] \mathcal{L}\left(\frac{\tau}{z}\right) , \tag{C.4.14}$$

we expand I_2^b as a power series in $(z-1)$, so that

$$I_2^b = \sum_{n=0}^{\infty} \frac{1}{n!}\, l^{(n)}(1) \int_{1-f(a)}^1 \mathrm{d}z \, (z-1)^n \log \frac{az}{(1-z)^2} \,, \tag{C.4.15}$$

and this integration is straightforward to be performed.

Integral I^c

We define

$$l(z) = 2\, \frac{z^2 - 2z + 2}{z^2}\, \mathcal{L}\left(\frac{\tau}{z}\right) , \tag{C.4.16}$$

$$g(z) = \log \frac{1}{2} \left(\sqrt{1 - \frac{4az}{(1-z)^2}} + 1 \right) , \tag{C.4.17}$$

and expanding $g(z)$ according to eq. (2.4.21), we have

$$g(z) = -\frac{az}{(1-z)^2} - \frac{3}{2} \frac{a^2 z^2}{(1-z)^4} + \mathcal{O}\big(a^3\big) \,, \tag{C.4.18}$$

so that

$$g_0(z,a) = g_1(z,a) = g_3(z,a) = 0 \,, \qquad g_2(z,a) = -az \,, \qquad g_4(z,a) = -\frac{3}{2} a^2 z^2 \,. \tag{C.4.19}$$

We then perform the integrations in eqs. (2.4.28)–(2.4.30).

C.4.1 Summary

Summarising our results, and writing I in eq. (C.4.1) as a sum of a universal and non-universal part, we have

$$I = I^{\mathrm{U}} + I^{\mathrm{R}}\,, \tag{C.4.20}$$

where

$$\begin{aligned}
I^{\mathrm{U}} = &-\log(a)\int_0^1 \mathrm{d}z\,\frac{1}{z}\,p_{gq}(z)\,\mathcal{L}\left(\frac{\tau}{z}\right) - \int_0^1 \mathrm{d}z\,\frac{1}{z}\,p_{gq}(z)\,\mathcal{L}\left(\frac{\tau}{z}\right)\log\frac{z}{(1-z)^2}\\
&- 2\,a\int_0^1 \mathrm{d}z\;p_{gq}(z)\,\mathcal{L}\left(\frac{\tau}{z}\right)\left[\frac{1}{(1-z)^2}\right]_{2+}\\
&- 3\,a^2\int_0^1 \mathrm{d}z\,z\,p_{gq}(z)\,\mathcal{L}\left(\frac{\tau}{z}\right)\left[\frac{1}{(1-z)^4}\right]_{4+}\\
&+ \left\{\,\mathcal{L}(\tau) + \,\tau\,\mathcal{L}^{(1)}(\tau)\right\}a\log(a) + \mathcal{L}(\tau)\,a\\
&+ \left\{3\,\tau\,\mathcal{L}^{(1)}(\tau) + \frac{3}{2}\,\tau^2\,\mathcal{L}^{(2)}(\tau) + \frac{1}{4}\,\tau^3\,\mathcal{L}^{(3)}(\tau)\right\}a^2\log(a)\\
&+ \left\{2\,\mathcal{L}(\tau) + \frac{17}{4}\,\tau\,\mathcal{L}^{(1)}(\tau) + \frac{7}{4}\,\tau^2\,\mathcal{L}^{(2)}(\tau) + \frac{1}{6}\,\tau^3\,\mathcal{L}^{(3)}(\tau)\right\}a^2\\
&+ \mathcal{O}\Big(a^{\frac{5}{2}}\log(a)\Big)\,,
\end{aligned} \tag{C.4.21}$$

$$\begin{aligned}
I^{\mathrm{R}} = &-\frac{3}{2}\int_0^1 \mathrm{d}z\,\frac{1}{z^2}(1-z)^2\,\mathcal{L}\left(\frac{\tau}{z}\right) + 3\,a\int_0^1 \mathrm{d}z\,\frac{1}{z}\,\mathcal{L}\left(\frac{\tau}{z}\right)\\
&+ 3\,a^2\int_0^1 \mathrm{d}z\,\mathcal{L}\left(\frac{\tau}{z}\right)\left[\frac{1}{(1-z)^2}\right]_{2+}\\
&- \frac{3}{2}\,\tau\,\mathcal{L}^{(1)}(\tau)\,a^2\log(a) + \left\{-\frac{3}{2}\,\mathcal{L}(\tau) - \frac{3}{4}\,\tau\,\mathcal{L}^{(1)}(\tau)\right\}a^2\\
&+ \mathcal{O}\Big(a^{\frac{5}{2}}\log(a)\Big)\,.
\end{aligned} \tag{C.4.22}$$

Then, writing I^{U} and I^{R} in the form

$$I^{\mathrm{U}} = \int_0^1 \frac{\mathrm{d}z}{z}\,\mathcal{L}\left(\frac{\tau}{z}\right)\hat{g}_{gq}^{\mathrm{U}(1)}(z)\,, \qquad I^{\mathrm{R}} = \int_0^1 \frac{\mathrm{d}z}{z}\,\mathcal{L}\left(\frac{\tau}{z}\right)\hat{g}_{gq}^{\mathrm{R}(1)}(z)\,, \tag{C.4.23}$$

we get the expression of $\hat{g}_{gq}^{\mathrm{U}(1)}(z)$ and $\hat{g}_{gq}^{\mathrm{R}(1)}(z)$ in eqs. (2.4.43) and (2.4.44), respectively.

C.5 H production: gg channel

The relevant integral, corresponding to that in eq. (2.4.20), is

$$I = \int_\tau^{1-f(a)} \mathrm{d}z\, \mathcal{L}\left(\frac{\tau}{z}\right) \left\{ -\frac{11}{3}\frac{(1-z)^3}{z^2}\sqrt{1-\frac{4az}{(1-z)^2}} + \frac{2}{3}\,a\,\frac{1-z}{z}\sqrt{1-\frac{4az}{(1-z)^2}} \right.$$
$$\left. + \frac{2}{z}\,\hat{p}_{gg}(z)\left[-\log\frac{az}{(1-z)^2} + 2\log\frac{1}{2}\left(\sqrt{1-\frac{4az}{(1-z)^2}}+1\right)\right]\right\}, \tag{C.5.1}$$

where

$$\hat{p}_{gg}(z) = \frac{2(z^2-z+1)^2}{z(1-z)}\,. \tag{C.5.2}$$

We can express I as the sum of four integrals

$$I = I^{a1} + I^{a2} + I^b + I^c\,, \tag{C.5.3}$$

where

$$I^{a1} = \int_\tau^{1-f(a)} \mathrm{d}z \left(-\frac{11}{3}\right)\frac{(1-z)^3}{z^2}\,\mathcal{L}\left(\frac{\tau}{z}\right)\sqrt{1-\frac{4az}{(1-z)^2}}\,, \tag{C.5.4}$$

$$I^{a2} = \int_\tau^{1-f(a)} \mathrm{d}z\, \frac{2}{3}\,a\,\frac{1-z}{z}\,\mathcal{L}\left(\frac{\tau}{z}\right)\sqrt{1-\frac{4az}{(1-z)^2}}\,, \tag{C.5.5}$$

$$I^b = \int_\tau^{1-f(a)} \mathrm{d}z \left(-\frac{2}{z}\right)\hat{p}_{gg}(z)\mathcal{L}\left(\frac{\tau}{z}\right)\log\frac{az}{(1-z)^2}\,, \tag{C.5.6}$$

$$I^c = \int_\tau^{1-f(a)} \mathrm{d}z\, \frac{4}{z}\,\hat{p}_{gg}(z)\,\mathcal{L}\left(\frac{\tau}{z}\right)\log\frac{1}{2}\left(\sqrt{1-\frac{4az}{(1-z)^2}}+1\right), \tag{C.5.7}$$

and for each of the four integrals we apply the procedure detailed in Section 2.4.

Integral I^{a1}

We define

$$l(z) = -\frac{11}{3}\,\frac{1}{z^2}\,\mathcal{L}\left(\frac{\tau}{z}\right), \tag{C.5.8}$$

$$g(z) = (1-z)^3\sqrt{1-\frac{4az}{(1-z)^2}}\,, \tag{C.5.9}$$

and expanding $g(z)$ according to eq. (2.4.21), we have

$$g(z) = (1-z)^3 - 2az(1-z) - \frac{2a^2z^2}{1-z} + \mathcal{O}\big(a^3\big)\,, \tag{C.5.10}$$

so that

$$g_0(z,a) = (1-z)^3 - 2az(1-z)\,, \qquad g_1(z,a) = -2a^2z^2\,, \tag{C.5.11}$$

$$g_2(z,a) = 0\,, \qquad g_3(z,a) = \mathcal{O}\big(a^3\big)\,. \tag{C.5.12}$$

We then perform the integrations in eqs. (2.4.28)–(2.4.30).

Integral I^{a2}

We define

$$l(z) = \frac{2}{3}\, a\, \frac{1}{z}\, \mathcal{L}\left(\frac{\tau}{z}\right), \tag{C.5.13}$$

$$g(z) = (1-z)\sqrt{1 - \frac{4az}{(1-z)^2}}, \tag{C.5.14}$$

and expanding $g(z)$ according to eq. (2.4.21), we have

$$g(z) = (1-z) - \frac{2az}{1-z} - \frac{2a^2z^2}{(1-z)^3} + \mathcal{O}\left(a^3\right), \tag{C.5.15}$$

so that

$$g_0(z,a) = (1-z)\,, \qquad g_1(z,a) = -2az\,, \qquad g_2(z,a) = 0\,, \qquad g_3(z,a) = -2a^2z^2\,. \tag{C.5.16}$$

We then perform the integrations in eqs. (2.4.28)–(2.4.30).

Integral I^{b}

We start by separating I^b into two further integrals

$$I^b = I^{b1} + I^{b2}\,, \tag{C.5.17}$$

where

$$I^{b1} = \int_\tau^{1-f(a)} \mathrm{d}z \left(-\frac{2}{z}\right) \hat{p}_{gg}(z)\, \mathcal{L}\left(\frac{\tau}{z}\right) \log(az)\,, \tag{C.5.18}$$

$$I^{b2} = \int_\tau^{1-f(a)} \mathrm{d}z\, \frac{4}{z}\, \hat{p}_{gg}(z)\, \mathcal{L}\left(\frac{\tau}{z}\right) \log(1-z)\,, \tag{C.5.19}$$

and for each of them we follow our integration and expansion procedure.

- **Integral I^{b1}**

  We define

  $$l(z) = -\frac{4\left(z^2 - z + 1\right)^2}{z^2} \log(az)\, \mathcal{L}\left(\frac{\tau}{z}\right), \tag{C.5.20}$$

  $$g(z) = \frac{1}{1-z}\,, \tag{C.5.21}$$

  We deal with this case as with a case with $g_0 = 0$, $g_1(z,a) = 1$ and all the other g_i functions equal to 0. Then, we perform the integrations in eqs. (2.4.28)–(2.4.30).

- **Integral I^{b2}**

  We define

$$l(z) = \frac{8\left(z^2 - z + 1\right)^2}{z^2}\mathcal{L}\left(\frac{\tau}{z}\right) \tag{C.5.22}$$

$$g(z) = \frac{\log(1-z)}{1-z} \tag{C.5.23}$$

  We deal with this case as with a case with $g_0 = 0$, $g_1(z,a) = \log(1-z)$ and all the other g_i functions equal to 0. Then, we perform the integrations in eqs. (2.4.28)–(2.4.30).

Integral I^c

We define

$$l(z) = \frac{8\left(z^2 - z + 1\right)^2}{z^2}\mathcal{L}\left(\frac{\tau}{z}\right), \tag{C.5.24}$$

$$g(z) = \frac{1}{1-z}\log\frac{1}{2}\left(\sqrt{1 - \frac{4az}{(1-z)^2}} + 1\right), \tag{C.5.25}$$

and expanding $g(z)$ according to eq. (2.4.21), we have

$$g(z) = -\frac{az}{(1-z)^3} - \frac{3}{2}\frac{a^2z^2}{(1-z)^5} + \mathcal{O}\left(a^3\right), \tag{C.5.26}$$

so that

$$g_0(z,a) = g_1(z,a) = g_2(z,a) = g_4(z,a) = 0\,, \quad g_3(z,a) = -az\,, \quad g_5(z,a) = -\frac{3}{2}a^2z^2\,. \tag{C.5.27}$$

We then perform the integrations in eqs. (2.4.28)–(2.4.30).

C.5.1 Summary

Summarising our results, and writing I in eq. (C.5.1) as a sum of a universal and non-universal part, we have

$$I = I^{\mathrm{U}} + I^{\mathrm{R}}\,, \tag{C.5.28}$$

where

$$
\begin{aligned}
I^{\mathrm{U}} = & -2\log(a)\int_0^1 \mathrm{d}z\,\frac{1-z}{z}\,\hat{p}_{gg}(z)\mathcal{L}\left(\frac{\tau}{z}\right)\left[\frac{1}{1-z}\right]_+ \\
& -2\int_0^1 \mathrm{d}z\,\frac{1}{z}\,\hat{p}_{gg}(z)\log(z)\mathcal{L}\left(\frac{\tau}{z}\right) \\
& +4\int_0^1 \mathrm{d}z\,\frac{1-z}{z}\,\hat{p}_{gg}(z)\mathcal{L}\left(\frac{\tau}{z}\right)\left[\frac{\log(1-z)}{1-z}\right]_+ \\
& -4\,a\int_0^1 \mathrm{d}z\,(1-z)\,\hat{p}_{gg}(z)\,\mathcal{L}\left(\frac{\tau}{z}\right)\left[\frac{1}{(1-z)^3}\right]_{3+} \\
& -6\,a^2\int_0^1 \mathrm{d}z\,z(1-z)\,\hat{p}_{gg}(z)\mathcal{L}\left(\frac{\tau}{z}\right)\left[\frac{1}{(1-z)^5}\right]_{5+} \\
& +\mathcal{L}(\tau)\,\log^2(a) - \frac{\pi^2}{3}\,\mathcal{L}(\tau) \\
& +\left\{8\,\mathcal{L}(\tau)+2\,\tau^2\,\mathcal{L}^{(2)}(\tau)\right\}a\log(a) + \left\{-2\,\mathcal{L}(\tau)+4\,\tau\,\mathcal{L}^{(1)}(\tau)\right\}a \\
& +\left\{6\,\mathcal{L}(\tau)+6\,\tau^2\,\mathcal{L}^{(2)}(\tau)+\,\tau^3\,\mathcal{L}^{(3)}(\tau)+\frac{1}{4}\,\tau^4\,\mathcal{L}^{(4)}(\tau)\right\}a^2\log(a) \\
& +\left\{-\frac{3}{2}\,\mathcal{L}(\tau)+11\,\tau\,\mathcal{L}^{(1)}(\tau)+\frac{11}{2}\,\tau^2\,\mathcal{L}^{(2)}(\tau)+\frac{5}{3}\,\tau^3\,\mathcal{L}^{(3)}(\tau)+\frac{1}{6}\,\tau^4\,\mathcal{L}^{(4)}(\tau)\right\}a^2 \\
& +\mathcal{O}\Big(a^{\frac{5}{2}}\log(a)\Big)\,,
\end{aligned}
\tag{C.5.29}
$$

$$
\begin{aligned}
I^{\mathrm{R}} = & -\frac{11}{3}\int_0^1 \mathrm{d}z\,\frac{1}{z^2}\,(1-z)^3\,\mathcal{L}\left(\frac{\tau}{z}\right) + 8a\int_0^1 \mathrm{d}z\,\frac{1}{z}(1-z)\,\mathcal{L}\left(\frac{\tau}{z}\right) \\
& +6\,a^2\int_0^1 \mathrm{d}z\,\mathcal{L}\left(\frac{\tau}{z}\right)\left[\frac{1}{1-z}\right]_+ \\
& -3\,\mathcal{L}(\tau)\,a^2\log(a) - \frac{5}{2}\,\mathcal{L}(\tau)\,a^2 + \mathcal{O}\Big(a^{\frac{5}{2}}\log(a)\Big)\,.
\end{aligned}
\tag{C.5.30}
$$

Then, writing I^{U} and I^{R} in the form

$$
I^{\mathrm{U}} = \int_0^1 \frac{\mathrm{d}z}{z}\,\mathcal{L}\left(\frac{\tau}{z}\right)\hat{g}_{gg}^{\mathrm{U}(1)}(z)\,, \qquad I^{\mathrm{R}} = \int_0^1 \frac{\mathrm{d}z}{z}\,\mathcal{L}\left(\frac{\tau}{z}\right)\hat{g}_{gg}^{\mathrm{R}(1)}(z)\,, \tag{C.5.31}
$$

we get the expression of $\hat{g}_{gg}^{\mathrm{U}(1)}(z)$ and $\hat{g}_{gg}^{\mathrm{R}(1)}(z)$ in eqs. (2.4.47) and (2.4.48), respectively.

C.6 Study of a universal term of the form $1/(1-z)$

In this section we apply the procedure described in Section 2.4 to study the universal part of the Altarelli–Parisi splitting functions that accounts for soft radiation, i.e. the

$z \to 1$ limit. In this approximation, the Altarelli–Parisi splitting functions $\hat{p}_{qq}(z)$ and $\hat{p}_{gg}(z)$ behave like $1/(1-z)$. The relevant integral, corresponding to that in eq. (2.4.20), is given by

$$I^{\mathrm{U}} = \int_{\tau}^{1-f(a)} \mathrm{d}z\, \mathcal{L}\left(\frac{\tau}{z}\right) \frac{1}{z}\, p(z) \times \left[-\log \frac{az}{(1-z)^2} + 2 \log \frac{1}{2} \left(\sqrt{1 - \frac{4az}{(1-z)^2}} + 1 \right) \right], \tag{C.6.1}$$

where

$$p(z) = \frac{1}{1-z}\,. \tag{C.6.2}$$

We write I as the sum of two integrals

$$I = I^b + I^c\,, \tag{C.6.3}$$

where

$$I^b = \int_{\tau}^{1-f(a)} \mathrm{d}z \left(-\frac{1}{z}\right) p(z)\, \mathcal{L}\left(\frac{\tau}{z}\right) \log \frac{az}{(1-z)^2}\,, \tag{C.6.4}$$

$$I^c = \int_{\tau}^{1-f(a)} \mathrm{d}z\, \frac{2}{z}\, p(z)\, \mathcal{L}\left(\frac{\tau}{z}\right) \log \frac{1}{2} \left(\sqrt{1 - \frac{4az}{(1-z)^2}} + 1 \right), \tag{C.6.5}$$

and for each of the two integrals we apply the procedure detailed in Section 2.4.

Integral I^b

We write I^b as sum of two further integrals

$$I^b = I^{b1} + I^{b2}\,, \tag{C.6.6}$$

where

$$I^{b1} = \int_{\tau}^{1-f(a)} \mathrm{d}z \left(-\frac{1}{z}\right) p(z)\, \mathcal{L}\left(\frac{\tau}{z}\right) \log(az)\,, \tag{C.6.7}$$

$$I^{b2} = \int_{\tau}^{1-f(a)} \mathrm{d}z\, \frac{2}{z}\, p(z)\, \mathcal{L}\left(\frac{\tau}{z}\right) \log(1-z)\,, \tag{C.6.8}$$

Integral I^{b1}

We define

$$l(z) = -\frac{1}{z} \log(az)\, \mathcal{L}\left(\frac{\tau}{z}\right), \tag{C.6.9}$$

$$g(z) = \frac{1}{1-z}\,, \tag{C.6.10}$$

and we treat this case as the case with $g_0(z,a) = 0$ and $g_1(z,a) = 1$ and all the other g_i functions equal to 0. We then perform the integrations in eqs. (2.4.28)–(2.4.30).

Integral I^{b2}

We define

$$l(z) = \frac{2}{z}\mathcal{L}\left(\frac{\tau}{z}\right), \tag{C.6.11}$$

$$g(z) = \frac{\log(1-z)}{1-z}, \tag{C.6.12}$$

and we treat this case as the case with $g_0(z,a) = 0$ and $g_1(z,a) = \log(1-z)$ and all the other g_i functions equal to 0. We then perform the integrations in eqs. (2.4.28)–(2.4.30).

Integral I^{c}

We define

$$l(z) = \frac{2}{z}\mathcal{L}\left(\frac{\tau}{z}\right), \tag{C.6.13}$$

$$g(z) = \frac{1}{1-z}\log\frac{1}{2}\left(\sqrt{1-\frac{4az}{(1-z)^2}}+1\right), \tag{C.6.14}$$

and expanding $g(z)$ according to eq. (2.4.21), we have

$$g(z) = -\frac{az}{(1-z)^3} - \frac{3}{2}\frac{a^2z^2}{(1-z)^5} + \mathcal{O}\left(a^3\right), \tag{C.6.15}$$

so that

$$g_0(z,a) = g_1(z,a) = g_2(z,a) = g_4(z,a) = 0\,, \quad g_3(z,a) = -az\,, \quad g_5(z,a) = -\frac{3}{2}a^2z^2\,. \tag{C.6.16}$$

We then perform the integrations in eqs. (2.4.28)–(2.4.30).

C.6.1 Summary

Summarising our results, we have

$$
\begin{aligned}
I^{\mathrm{U}} = & -\log(a)\int_0^1 \mathrm{d}z\,\frac{1}{z}\mathcal{L}\left(\frac{\tau}{z}\right)\left[\frac{1}{1-z}\right]_+ \\
& -\int_0^1 \mathrm{d}z\,\frac{1}{z(1-z)}\log(z)\,\mathcal{L}\left(\frac{\tau}{z}\right)+\int_0^1 \mathrm{d}z\,\frac{2}{z}\mathcal{L}\left(\frac{\tau}{z}\right)\left[\frac{\log(1-z)}{1-z}\right]_+ \\
& -2a\int_0^1 \mathrm{d}z\,\mathcal{L}\left(\frac{\tau}{z}\right)\left[\frac{1}{(1-z)^3}\right]_{3+}-3a^2\int_0^1 \mathrm{d}z\,z\,\mathcal{L}\left(\frac{\tau}{z}\right)\left[\frac{1}{(1-z)^5}\right]_{5+} \\
& +\frac{1}{4}\,\mathcal{L}(\tau)\log^2(a)-\frac{\pi^2}{12}\,\mathcal{L}(\tau)+\left\{\tau\,\mathcal{L}^{(1)}(\tau)+\frac{1}{2}\,\tau^2\,\mathcal{L}^{(2)}(\tau)\right\}a\log(a) \\
& +\left\{\frac{1}{2}\,\mathcal{L}(\tau)+\tau\,\mathcal{L}^{(1)}(\tau)\right\}a \\
& +\left\{\frac{3}{4}\,\tau^2\,\mathcal{L}^{(2)}(\tau)+\frac{1}{2}\,\tau^3\,\mathcal{L}^{(3)}(\tau)+\frac{1}{16}\,\tau^4\,\mathcal{L}^{(4)}(\tau)\right\}a^2\log(a) \\
& +\left\{-\frac{1}{8}\,\mathcal{L}(\tau)+\frac{1}{2}\,\tau\,\mathcal{L}^{(1)}(\tau)+\frac{13}{8}\,\tau^2\,\mathcal{L}^{(2)}(\tau)+\frac{7}{12}\,\tau^3\,\mathcal{L}^{(3)}(\tau)+\frac{1}{24}\,\tau^4\,\mathcal{L}^{(4)}(\tau)\right\}a^2 \\
& +\mathcal{O}\Big(a^{\frac{5}{2}}\log(a)\Big)\,. \qquad \text{(C.6.17)}
\end{aligned}
$$

Then, writing I^{U} in the form

$$
I^{\mathrm{U}}=\int_0^1 \mathrm{d}z\,\frac{1}{z}\,\mathcal{L}\left(\frac{\tau}{z}\right)\hat{g}^{\mathrm{U}(1)}(z)\,, \qquad \text{(C.6.18)}
$$

we get

$$
\begin{aligned}
\hat{g}^{\mathrm{U}(1)}(z) = &+\frac{1}{4}\,\delta(1-z)\log^2(a) - \left[\frac{1}{1-z}\right]_+ \log(a) - \frac{\pi^2}{12}\,\delta(1-z) \\
&- \frac{1}{(1-z)}\log(z) + 2\left[\frac{\log(1-z)}{1-z}\right]_+ \\
&+ \left\{\frac{1}{2}\delta^{(2)}(1-z) - \delta^{(1)}(1-z)\right\} a\log(a) \\
&+ \left\{-\frac{1}{2}\,\delta(1-z) + \delta^{(1)}(1-z) - 2z\left[\frac{1}{(1-z)^3}\right]_{3+}\right\} a \\
&+ \left\{\frac{3}{4}\,\delta^{(2)}(1-z) - \frac{1}{2}\,\delta^{(3)}(1-z) + \frac{1}{16}\,\delta^{(4)}(1-z)\right\} a^2\log(a) \\
&+ \left\{\frac{1}{8}\,\delta(1-z) + \frac{1}{2}\,\delta^{(1)}(1-z) - \frac{5}{8}\,\delta^{(2)}(1-z) - \frac{1}{12}\,\delta^{(3)}(1-z)\right. \\
&\qquad \left. + \frac{1}{24}\,\delta^{(4)}(1-z) - 3z^2\left[\frac{1}{(1-z)^5}\right]_{5+}\right\} a^2 \\
&+ \mathcal{O}\Big(a^{\frac{5}{2}}\log(a)\Big)\,. \qquad \text{(C.6.19)}
\end{aligned}
$$

Appendix D

Samples of integrals

According to the procedure presented in Secs. 2.4, in order to compute the power corrections, one has to perform two integrations of the differential cross sections: an integration in $q_{\rm T}$, in general easy to perform, and an integration in z from 0 to $1 - f(a)$. This second integration turned out to be challenging for some integrand functions.

We have classified the integrand functions into five groups, according to the number of logarithms and polylogarithms appearing in the expressions. We present here a sample of integrands for each group.

D.1 Integrand classification

Defining

$$r(z) \equiv \sqrt{(1-z)^2 - 4az}\,, \tag{D.1.1}$$

we have groups containing:

1. one logarithm:

$$\int_0^{1-f(a)} dz\, z^n \,\log\left[(1-z)\,\frac{1+z\pm r(z)}{1-z\pm r(z)}\right] \tag{D.1.2}$$

$$\int_0^{1-f(a)} dz\, z^n \,\frac{r(z)}{1+z\pm r(z)}\,\log\left[\frac{2z}{1-z\pm r(z)}\right] \tag{D.1.3}$$

2. two logarithms:

$$\int_0^{1-f(a)} dz\, z^n\, r(z)\log(z)\log\left[\frac{1-z-r(z)}{2(1-z)}\right] \tag{D.1.4}$$

$$\int_0^{1-f(a)} dz\, z^n\, r(z)\,\log^2\left[\frac{2z}{1-z\pm r(z)}\right] \tag{D.1.5}$$

3. three logarithms:

$$\int_0^{1-f(a)} dz\, z^n\, \log^2\left[\frac{1-z-r(z)}{1-z+r(z)}\right] \log\left[(1-z)\frac{1+z+r(z)}{1-z+r(z)}\right] \tag{D.1.6}$$

$$\int_0^{1-f(a)} dz\, z^n\, \log(z) \log^2\left[\frac{1-z\pm r(z)}{2(1-z)}\right] \tag{D.1.7}$$

$$\int_0^{1-f(a)} dz\, z^n\, \log^3\left[\frac{1\mp z\pm r(z)}{2z}\right] \tag{D.1.8}$$

$$\int_0^{1-f(a)} dz\, z^n\, \log(z)\, \log\frac{1-z\pm r(z)}{2\,(1-z)}\, \log\frac{1-z\mp r(z)}{2z} \tag{D.1.9}$$

4. one polylogarithm of order 2:

$$\int_0^{1-f(a)} dz\, z^n\, r(z)\, \mathrm{Li}_2\left[\frac{2z}{1+z\pm r(z)}\right] \tag{D.1.10}$$

$$\int_0^{1-f(a)} dz\, z^n\, \log\left[\frac{1-z\pm r(z)}{1-z\mp r(z)}\right]\, \mathrm{Li}_2\left[-z\,\frac{1-z\pm r(z)}{1-z\mp r(z)}\right] \tag{D.1.11}$$

5. one polylogarithm of order 3:

$$\int_0^{1-f(a)} dz\, z^n\, \mathrm{Li}_3\left[\frac{2z}{1+z\pm r(z)}\right] \tag{D.1.12}$$

$$\int_0^{1-f(a)} dz\, z^n\, \mathrm{Li}_3\left[-z\,\frac{1-z\pm r(z)}{1-z\mp r(z)}\right] \tag{D.1.13}$$

where $n = 1, \ldots, 4$.

D.2 Sample of integral expansion

After the z integration, the results are functions of a only, and have to be expanded around $a = 0$. A sample of these expansions is given in the following:

- **Example 1**

$$\begin{aligned}\int_0^{1-f(a)} & dz\, z \log^2\left[\frac{1-z-r(z)}{1-z+r(z)}\right] \log\left[(1-z)\frac{1+z+r(z)}{1-z+r(z)}\right] \\ &= \frac{1}{2}\,a\log^3(a) + 2\,a\log^2(a) + \left(\frac{17}{2}+\pi^2\right) a\log(a) + \left[48 - 32\,C - 16\log 2\right]\sqrt{a} \\ &\quad + \left[9\,\zeta(3) - \frac{15}{4} + \frac{4}{3}\pi^2 + 8\log 2\right] a + \mathcal{O}\left(a^{\frac{3}{2}}\right),\end{aligned} \tag{D.2.1}$$

where C is the Catalan constant defined by

$$C = \sum_{n=0}^{\infty} \frac{(-1)^n}{(2n+1)^2} = \frac{1}{1^2} - \frac{1}{3^2} + \frac{1}{5^2} - \frac{1}{7^2} + \ldots \approx 0.915965594\ldots \tag{D.2.2}$$

- **Example 2**

$$\int_0^{1-f(a)} dz\, z^3 \log^2\left[\frac{1-z-r(z)}{1-z+r(z)}\right] \log\left[(1-z)\frac{1+z+r(z)}{1-z+r(z)}\right]$$
$$= \frac{5}{6} a \log^3(a) + \frac{71}{12} a \log^2(a) + \left(\frac{1721}{72} + \frac{5}{3}\pi^2\right) a \log(a)$$
$$+ \left[48 - 32\, C - 16 \log 2\right] \sqrt{a}$$
$$+ \left[16\, \zeta(3) + \frac{8711}{864} + \frac{71}{18}\pi^2 + 16 \log 2\right] a + \mathcal{O}\left(a^{\frac{3}{2}}\right), \quad \text{(D.2.3)}$$

- **Example 3**

$$\int_0^{1-f(a)} dz\, z\, r(z) \log(z) \log\left[\frac{1-z-r(z)}{2(1-z)}\right]$$
$$= -\frac{5}{36}\log(a) + \frac{\pi^2}{18} - \frac{55}{108} + \left(\frac{\pi^2}{3} - \frac{5}{2}\right) a \log(a) + \left(\frac{5}{6}\pi^2 - \frac{25}{4}\right) a + \mathcal{O}\left(a^{\frac{3}{2}}\right), \quad \text{(D.2.4)}$$

- **Example 4**

$$\int_0^{1-f(a)} dz\, z \log(z) \log\left[\frac{1-z+r(z)}{2(1-z)}\right] = a\left[1 - \frac{\pi^2}{12} + 2\log^2 2 - 2\log 2\right] + \mathcal{O}\left(a^{\frac{3}{2}}\right), \quad \text{(D.2.5)}$$

- **Example 5**

$$\int_0^{1-f(a)} dz\, z \log(z) \log^2\left[\frac{1-z-r(z)}{2(1-z)}\right]$$
$$= \frac{1}{2} a \log^2(a) - \frac{\log^2(a)}{4} + a\left(2 + \frac{3}{4}\pi^2 + 2\log^2 2 - 2\log 2\right)$$
$$+ \left(\frac{2}{3}\pi^2 - 4\right) a \log(a) + \left(\frac{\pi^2}{3} - \frac{7}{2}\right)\log(a) + \frac{2}{3}\pi^2 - \frac{59}{8} + \mathcal{O}\left(a^{\frac{3}{2}}\right). \quad \text{(D.2.6)}$$

We note that the intermediate integrals contain $\log(2)$ and $\sqrt{a}$ terms, and also terms proportional to the Catalan constant C. Despite this, once recombined to compose the whole behaviour of the physical cross section, all these terms disappear from the final answer, as illustrated in Appendix E. Something similar happened for the results at NLO.

Appendix E

NNLO final results

In this appendix we collect the results for the NNLO power corrections, up to order a in the transverse-momentum cutoff. The results refer to the $\delta(s_2)$ contribution of the qg-initiated channel to the inclusive cross section for the production of a vector boson F, i.e. the ${}^{c}g_0^H(z)$, ${}^{c}g_1^H(z)$, ${}^{c}g_2^H(z)$, $g_0^H(z)$, $g_1^H(z)$, $g_2^H(z)$, ${}^{c}\mathcal{J}_{23}^H$ and $\mathcal{J}_{23}^H$ functions in eqs. (2.5.18)–(2.5.21).

In the following, we need $l(z)$, defined in eq. (2.5.22), and its first derivative

$$l^{(1)}(z) \equiv \frac{\mathrm{d}}{\mathrm{d}z} l(z) = -\frac{1}{z^2}\,\mathcal{L}\left(\frac{\tau}{z}\right) - \frac{\tau}{z^3}\,\mathcal{L}^{(1)}\left(\frac{\tau}{z}\right), \tag{E.0.1}$$

both evaluated in $z = 1$. For sake of brevity, we introduce the following notation

$$\mathcal{L} \equiv l(1) = \mathcal{L}(\tau), \tag{E.0.2}$$

$$\mathcal{L}' \equiv l^{(1)}(1) = -\mathcal{L}(\tau) - \tau\mathcal{L}^{(1)}(\tau). \tag{E.0.3}$$

The renormalisation and factorisation scales are indicated with μ_{R} and μ_{F}, respectively, and $p_{qg}(z)$ is the zeroth-order Altarelli–Parisi splitting function, defined as

$$P_{qg}(z) = T_{\mathrm{R}}\left[2z^2 - 2z + 1\right] \equiv T_{\mathrm{R}}\, p_{qg}(z). \tag{E.0.4}$$

In addition, we recall the definition of a in eq. (2.4.6): $a = \left(q_{\mathrm{T}}^{\mathrm{cut}}\right)^2 / Q^2$.

E.1 A^{qg}

$$g_0^A(z) = p_{qg}(z)\left[-\log(a) + \log\frac{(1-z)^2}{z}\right] + \frac{1}{2}(1+3z)(1-z) + \mathcal{O}\left(a^{\frac{3}{2}}\log(a)\right) \tag{E.1.1}$$

$$g_1^A(z) = -z(1+3z)\,a + \mathcal{O}\left(a^{\frac{3}{2}}\log(a)\right) \tag{E.1.2}$$

$$g_2^A(z) = -2z\,p_{qg}(z)\,a + \mathcal{O}\left(a^{\frac{3}{2}}\log(a)\right) \tag{E.1.3}$$

$$\mathcal{J}_{23}^A = -\left(\mathcal{L} + \mathcal{L}'\right) a\log(a) - \left(\frac{3}{2}\mathcal{L} + \frac{10}{3}\mathcal{L}'\right) a + \mathcal{O}\left(a^{\frac{3}{2}}\log(a)\right) \tag{E.1.4}$$

E.2 B_1^{qg}: $C_{\rm A}$ coefficient

$$
\begin{aligned}
{}^{C_{\rm A}}g_0^{B_1}(z) = {}& \frac{1}{6}\,p_{qg}(z)\log^3(a) - p_{qg}(z)\log(z)\log^2(a) \\
&+ \left[z - p_{qg}(z)\left(\log^2\frac{z}{1-z} - 2\log(1-z)\log(z) + \frac{7}{6}\pi^2\right)\right]\log(a) \\
&+ p_{qg}(z)\left(\frac{2}{3}\log^3(1-z) - \frac{1}{6}\log^3(z) + \log(1-z)\log^2(z)\right) \\
&- \left(6z^2 - 5z + \frac{5}{2}\right)\log^2(1-z)\log(z) - \left(\frac{15}{2}\,z^2 - 5z + 1\right)\log(1-z)\log(z) \\
&+ \left(\frac{21}{4}\,z^2 - \frac{3}{2}\,z - \frac{1}{4}\right)\log^2(z) + \left(3z^2 - 4z + 1\right)\log^2(1-z) \\
&+ \left(\frac{14}{3}\,\pi^2\,z^2 + \frac{9}{2}\,z^2 - \frac{9}{2}\,\pi^2\,z - 8z + \frac{9}{4}\,\pi^2 + \frac{3}{2}\right)\log(1-z) \\
&- \left(\frac{4}{3}\,\pi^2\,z^2 + \frac{3}{2}\,z^2 - \frac{3}{2}\,\pi^2\,z - 3z + \frac{3}{4}\,\pi^2 - \frac{1}{2}\right)\log(z) \\
&- \left(\frac{3}{2}\,z^2 + 3z - 1 + \frac{1}{2}(2z-1)\,\log\frac{z}{1-z}\right)\Big(\mathrm{Li}_2(1-z) - \mathrm{Li}_2(z)\Big) \\
&- 2(2z-1)\,\mathrm{Li}_3(1-z) - \left(4z^2 - 2z + 1\right)\mathrm{Li}_3(z) \\
&+ \zeta(3)\left(4z^2 - 2z + 1\right) - \frac{15}{4}\,\pi^2\,z^2 - \frac{13}{4}\,z^2 + \frac{23}{6}\,\pi^2\,z + \frac{9}{2}\,z - \frac{2}{3}\,\pi^2 - \frac{5}{4} \\
&+ \left[\frac{11}{6}\,p_{qg}(z)\left(-\log(a) + \log\frac{(1-z)^2}{z}\right) + \frac{11}{12}\,(1-z)\,(3z+1)\right]\log\frac{\mu_{\rm R}^2}{Q^2} \\
&- 2\,(1+z)\,a\log^2(a) \\
&+ \left[\frac{39}{8}\,z - \frac{45}{16} + (11z+10)\,\log(1-z) - (16z+19)\,\log(z)\right]a\log(a) \\
&+ \Bigg[-\left(\frac{13}{8}\,z^3 + 9z^2 + \frac{27}{16}\,z - \frac{1}{16}\right)\log(1-z) + \left(\frac{5}{2}\,z + 2\right)\log^2(1-z) \\
&\quad + \left(\frac{13}{8}\,z^3 + 9\,z^2 - \frac{63}{8}\,z - \frac{11}{2}\right)\log(z) - \left(\frac{19}{2}\,z + 5\right)\log^2(z) \\
&\quad - (z+9)\log(1-z)\log(z) + 2\,(1+z)\Big(\mathrm{Li}_2(1-z) - \mathrm{Li}_2(z)\Big) \\
&\quad + \frac{23}{8}z^2 - \frac{165}{16}z + \frac{\pi^2}{3}z - 3 + \frac{5}{6}\pi^2\Bigg]\,a + \mathcal{O}\Big(a^{\frac{3}{2}}\log(a)\Big)
\end{aligned}
\tag{E.2.1}
$$

$$
\begin{aligned}
{}^{C_{\mathrm{A}}}g_1^{B_1}(z) = &\left[-2z^3 - \frac{1}{2}\,z^2 + z + \frac{1}{2}\right] a\log^2(a) \\
&+ \Bigg[\Big(8z^3 + 12z^2 - 8z - 4\Big)\log(1-z) + \Big(-4z^3 - 11z^2 + 6z + 1\Big)\log(z) \\
&\quad + 4z^3 - \frac{43}{8}\,z^2 - \frac{75}{16}\,z + \frac{61}{16}\Bigg] a\log(a) \\
&+ \Bigg[\left(-8z^3 + \frac{1}{2}\,z^2 + \frac{15}{2}\,z - 8\right)\log^2(1-z) + \left(6z^3 - 10z^2 + \frac{11}{2}\,z\right)\log^2(z) \\
&\quad + \left(12z^3 - \frac{23}{2}\,z^2 - 2z + 15\right)\log(1-z)\log(z) \\
&\quad - (1+z)\left(\frac{13}{8}\,z^3 + \frac{31}{4}\,z^2 - \frac{177}{16}\,z + \frac{65}{16}\right)\log(1-z) \\
&\quad + \left(\frac{9}{2}\,z^2 - z - 2\right)\Big(\mathrm{Li}_2(1-z) - \mathrm{Li}_2(z)\Big) \\
&\quad + \left(\frac{13}{8}\,z^4 + \frac{43}{8}\,z^3 - \frac{29}{8}\,z^2 - \frac{43}{8}\,z + \frac{17}{2}\right)\log(z) \\
&\quad + 2\pi^2\,z^3 - \frac{63}{16}\,z^3 - \frac{79}{12}\,\pi^2\,z^2 - \frac{11}{4}\,z^2 - \frac{\pi^2}{2}\,z + \frac{79}{16}\,z + \frac{4}{3}\,\pi^2 + 4 \\
&\quad - \frac{11}{6}z\,(3z+1)\log\frac{\mu_{\mathrm{R}}^2}{Q^2}\Bigg] a + \mathcal{O}\Big(a^{\frac{3}{2}}\log(a)\Big)
\end{aligned}
\tag{E.2.2}
$$

$$
\begin{aligned}
{}^{C_{\mathrm{A}}}g_2^{B_1}(z) = &\left[\frac{1}{2}(1-z)(z+1)\left(4z^2-6z+3\right)\right] a\log^2(a)\\
&+\left[(z-1)\left(4z^3-\frac{21}{4}z^2-2z+3\right)+2\left(4z^4-4z^3-3z^2+7z-3\right)\log(1-z)\right.\\
&\quad\left.+\left(-4z^4+10z^3+2z^2-29z+18\right)\log(z)\right] a\log(a)\\
&+\left[\left(12z^4-25z^3+\frac{43}{2}z^2+2z-6\right)\log(1-z)\log(z)\right.\\
&\quad-2\left(4z^4-4z^3-3z^2+7z-3\right)\log^2(1-z)\\
&\quad+\left(6z^4-5z^3-\frac{3}{2}z^2-5z+5\right)\log^2(z)\\
&\quad+\frac{1}{4}\left(16z^4-11z^3-32z^2+31z-12\right)\log(z)\\
&\quad+(1-z)\left(8z^3-4z^2-\frac{25}{4}z+6\right)\log(1-z)\\
&\quad+\frac{z^2}{2}(2z-1)\Big(\mathrm{Li}_2(1-z)-\mathrm{Li}_2(z)\Big)+\frac{\pi^2}{12}\big(24z^4-94z^3+45z^2+24z-26\big)\\
&\quad\left.+\frac{1}{16}\left(-109z^4+132z^3+83z^2-122z+48\right)-\frac{11}{3}z\,p_{qg}(z)\log\frac{\mu_{\mathrm{R}}^2}{Q^2}\right]a\\
&+\mathcal{O}\Big(a^{\frac{3}{2}}\log(a)\Big)
\end{aligned}
\tag{E.2.3}
$$

$$
\begin{aligned}
{}^{C_{\mathrm{A}}}\mathcal{J}_{23}^{B_1} = &\frac{1}{6}\left[\mathcal{L}+\mathcal{L}'\right]a\log^3(a)+\frac{1}{4}\left[15\,\mathcal{L}-\frac{11}{3}\,\mathcal{L}'\right]a\log^2(a)\\
&+\left[\left(-\frac{11}{6}\,\log\frac{\mu_{\mathrm{R}}^2}{Q^2}-\frac{5}{3}\,\pi^2-\frac{43}{8}\right)\mathcal{L}\right.\\
&\quad\left.+\left(-\frac{11}{6}\,\log\frac{\mu_{\mathrm{R}}^2}{Q^2}-\frac{5}{3}\,\pi^2+\frac{79}{6}\right)\mathcal{L}'\right]a\log(a)\\
&+\left[\left(-\frac{11}{4}\,\log\frac{\mu_{\mathrm{R}}^2}{Q^2}-5\zeta(3)-\frac{11}{3}\,\pi^2+\frac{897}{32}\right)\mathcal{L}\right.\\
&\quad\left.+\left(-\frac{55}{9}\,\log\frac{\mu_{\mathrm{R}}^2}{Q^2}-5\zeta(3)-\frac{185}{36}\,\pi^2+\frac{565}{192}\right)\mathcal{L}'\right]a+\mathcal{O}\Big(a^{\frac{3}{2}}\log(a)\Big)
\end{aligned}
\tag{E.2.4}
$$

E.3 B_1^{qg}: C_F coefficient

$$
\begin{aligned}
{}^{C_F}g_0^{B_1}(z) = {} & p_{qg}(z)\log\frac{z}{1-z}\log^2(a) \\
& + \Bigg[16z^2-17z+8+p_{qg}(z)\Bigg(\frac{11}{6}\pi^2+\mathrm{Li}_2(z)-\mathrm{Li}_2(1-z) \\
& \quad + 2\log^2\frac{z}{1-z}+\log^2(1-z)-\log(1-z)\log(z)\Bigg)\Bigg]\log(a) \\
& - 2p_{qg}(z)\left(\log^3(1-z)-\frac{2}{3}\log^3(z)+2\log(1-z)\log^2(z)\right) \\
& + \left(8z^2-6z+3\right)\log^2(1-z)\log(z) \\
& + \left(-\frac{9}{2}z^2+7z-\frac{5}{2}\right)\log^2(1-z)+\left(-6z^2+3z-2\right)\log^2(z) \\
& + \left(-7\pi^2z^2-42z^2+\frac{20}{3}\pi^2z+48z-\frac{10}{3}\pi^2-20\right)\log(1-z) \\
& + \left(\frac{8}{3}\pi^2z^2+\frac{47}{2}z^2-3\pi^2z-24z+\frac{3}{2}\pi^2+9\right)\log(z) \\
& + \left(\frac{21}{2}z^2-10z+\frac{9}{2}\right)\log(1-z)\log(z)+\Bigg[\frac{3}{2}z^2+4z-\frac{1}{2} \\
& \quad + \left(6z^2-8z+4\right)\log(1-z)-\left(4z^2-6z+3\right)\log(z)\Bigg]\Big(\mathrm{Li}_2(1-z)-\mathrm{Li}_2(z)\Big) \\
& - 8(1-z)^2\,\mathrm{Li}_3(1-z)+2\,(2z-1)\,\mathrm{Li}_3(z)+\frac{27}{4}\pi^2z^2+\frac{37}{2}z^2 \\
& - 4z\,\zeta(3)-\frac{23}{3}\pi^2z-\frac{33}{2}z+2\zeta(3)+\frac{7}{4}\pi^2-2+\frac{1}{2}z\,a\log^2(a) \\
& + \left[-\frac{73}{8}z+\frac{25}{4}-(21z+20)\,\log(1-z)+(33z+38)\,\log(z)\right]a\log(a) \\
& + \Bigg[\left(\frac{19}{8}z^3+14z^2+3z-2\right)\log(1-z)-12\,(1+z)\log^2(1-z) \\
& \quad + \left(-\frac{19}{8}z^3-14\,z^2+\frac{141}{8}z+\frac{31}{2}\right)\log(z)+(16z+8)\log^2(z) \\
& \quad + \left(-\frac{9}{2}z+14\right)\log(1-z)\log(z)-\left(\frac{7}{2}z+4\right)\Big(\mathrm{Li}_2(1-z)-\mathrm{Li}_2(z)\Big) \\
& \quad - \frac{43}{8}z^2+\frac{175}{8}z+\frac{23}{12}\pi^2z+\frac{47}{8}+\pi^2\Bigg]a+\mathcal{O}\Big(a^{\frac{3}{2}}\log(a)\Big) \qquad \text{(E.3.1)}
\end{aligned}
$$

$$
\begin{aligned}
{}^{C_{\mathrm{F}}}g_1^{B_1}(z) = {} & \left[4z^3 - \frac{1}{2}\,z^2 - \frac{5}{2}\,z + 3\right] a\log^2(a) \\
& + \left[\left(-16z^3 - 27z^2 + 15z + 8\right)\log(1-z) + \left(8z^3 + 19z^2 - 13z - 2\right)\log(z)\right. \\
& \quad \left. - 8z^3 + \frac{13}{8}\,z^2 + \frac{69}{8}\,z - \frac{25}{4}\right] a\log(a) \\
& + \left[\left(16z^3 - 5z^2 - 15z + 24\right)\log^2(1-z) + \left(-8z^3 + 19z^2 - 8z\right)\log^2(z)\right. \\
& \quad + \left(-22z^3 + \frac{37}{2}\,z^2 + \frac{11}{2}\,z - 26\right)\log(1-z)\log(z) \\
& \quad + \left(\frac{19}{8}\,z^4 + \frac{125}{8}\,z^3 + 2z^2 - 12z + 8\right)\log(1-z) \\
& \quad + \left(-\frac{19}{8}\,z^4 - \frac{61}{8}\,z^3 + \frac{51}{8}\,z^2 + \frac{89}{8}\,z - \frac{37}{2}\right)\log(z) \\
& \quad + \left(2z^3 - \frac{25}{2}\,z^2 + \frac{5}{2}\,z + 4\right)\Big(\mathrm{Li}_2(1-z) - \mathrm{Li}_2(z)\Big) \\
& \quad - \frac{13}{3}\,\pi^2\,z^3 + \frac{125}{16}\,z^3 + \frac{169}{12}\,\pi^2\,z^2 + \frac{599}{16}\,z^2 + \frac{5}{4}\,\pi^2\,z - \frac{51}{16}\,z \\
& \quad \left. - \frac{17}{3}\,\pi^2 - \frac{55}{8}\right] a + \mathcal{O}\Big(a^{\frac{3}{2}}\log(a)\Big)
\end{aligned}
\tag{E.3.2}
$$

$$
\begin{aligned}
{}^{C_{\mathrm{F}}}g_2^{B_1}(z) = {} & \left(4z^4-4z^3-3z^2+7z-3\right) a\log^2(a) \\
& + \Big[4\left(2z^4-6z^3+14z-9\right)\log(z) + \frac{1}{4}(1-z)\left(32z^3-35z^2-13z+24\right) \\
& \quad - 2\left(8z^4-6z^3-8z^2+15z-6\right)\log(1-z)\Big] a\log(a) \\
& + \Big[2z\left(z^3-4z^2+3z-1\right)\ \Big(\mathrm{Li}_2(1-z)-\mathrm{Li}_2(z)\Big) \\
& \quad + 2\left(8z^4-6z^3-8z^2+15z-6\right)\log^2(1-z) \\
& \quad + \left(-8z^4+10z^3-z^2+10z-8\right)\log^2(z) \\
& \quad - 2\left(11z^4-24z^3+21z^2+2z-6\right)\log(z)\log(1-z) \\
& \quad + 4(z-1)(z+1)\left(4z^2-6z+3\right)\log(1-z) \\
& \quad + \frac{1}{4}\left(-32z^4-z^3+74z^2-65z+12\right)\log(z) \\
& \quad + \frac{\pi^2}{3}\left(-13z^4+42z^3-15z^2-17z+14\right) \\
& \quad + \frac{1}{16}\left(211z^4+208z^3-566z^2+467z-96\right)\Big] a + \mathcal{O}\Big(a^{\frac{3}{2}}\log(a)\Big)
\end{aligned}
\tag{E.3.3}
$$

$$
\begin{aligned}
{}^{C_{\mathrm{F}}}\mathcal{J}_{23}^{B_1} = {} & \left[-\frac{3}{4}\,\mathcal{L}+\frac{7}{2}\,\mathcal{L}'\right] a\log^2(a) \\
& + \left[\left(\frac{8}{3}\,\pi^2+\frac{429}{16}\right)\mathcal{L}+\left(\frac{8}{3}\,\pi^2-\frac{821}{72}\right)\mathcal{L}'\right] a\log(a) \\
& + \left[\left(8\zeta(3)+\frac{\pi^2}{3}+\frac{4627}{192}\right)\mathcal{L}+\left(8\zeta(3)+\frac{64}{9}\,\pi^2+\frac{75667}{1728}\right)\mathcal{L}'\right] a + \mathcal{O}\Big(a^{\frac{3}{2}}\log(a)\Big)
\end{aligned}
\tag{E.3.4}
$$

E.4 B_2^{qg}

$$
g_i^{B_2}(z) = -\frac{1}{3}\log\frac{\mu_{\mathrm{R}}^2}{Q^2}\; g_i^A(z) \qquad\qquad i=0,1,2 \tag{E.4.1}
$$

$$
\mathcal{J}_{23}^{B_2} = -\frac{1}{3}\log\frac{\mu_{\mathrm{R}}^2}{Q^2}\; \mathcal{J}_{23}^A \tag{E.4.2}
$$

E.5 B_3^{qg}

$$
\begin{aligned}
g_0^{B_3}(z) = {} & \frac{1}{2}\, z\, \log^2(z) + 2z\,(1-z)\log\frac{z}{1-z} \\
& - \frac{1}{2}\, z\, \log(1-z)\log(z) - \frac{1}{2}\, z\, \Big(\mathrm{Li}_2(1-z) - \mathrm{Li}_2(z)\Big) \\
& - \frac{1}{12}\,\pi^2\, z - z + 1 + \Big[(1+z)\log(1-z)\Big]a + \mathcal{O}\Big(a^{\frac{3}{2}}\log(a)\Big)
\end{aligned}
\tag{E.5.1}
$$

$$
\begin{aligned}
g_1^{B_3}(z) = {} & z\,a\log(a) + \Big[(z-1)\left(2z^2+2z+1\right)\,\log(1-z) - 2z^3\,\log(z) - z\Big]a \\
& + \mathcal{O}\Big(a^{\frac{3}{2}}\log(a)\Big)
\end{aligned}
\tag{E.5.2}
$$

$$
g_2^{B_3}(z) = (1-z)\,z^2\big[2+\log(z)\big]a + \mathcal{O}\Big(a^{\frac{3}{2}}\log(a)\Big) \tag{E.5.3}
$$

$$
\mathcal{J}_{23}^{B_3} = -\frac{1}{2}\,\mathcal{L}\,a\log^2(a) - \mathcal{L}\,a\log(a) + \left[\left(\frac{\pi^2}{6}+\frac{1}{4}\right)\mathcal{L} - \frac{5}{9}\,\mathcal{L}'\right]a + \mathcal{O}\Big(a^{\frac{3}{2}}\log(a)\Big) \tag{E.5.4}
$$

E.6 C_1^{qg}: C_{A} coefficient

$$
\begin{aligned}
{}^{C_{\mathrm{A}}}g_0^{C_1}(z) = {} & -\frac{1}{6}\,p_{qg}(z)\log^3(a) + p_{qg}(z)\log(1-z)\log^2(a) \\
& - p_{qg}(z)\left[\frac{\pi^2}{6} + 2\log^2(1-z)\right]\log(a) \\
& + \frac{1}{3}\,p_{qg}(z)\left(4\log^3(1-z) + \pi^2\log\frac{1-z}{z} - \frac{1}{2}\,\log^3(z)\right) \\
& + \left(-\frac{3}{4}\,z^2 + \frac{1}{2}\,z + \frac{1}{4}\right)\log^2(z) + \left(-\frac{1}{2}\,z^2 + z - \frac{1}{2}\right)\log(z) \\
& + \frac{\pi^2}{6}\left(1 + 2z - 3z^2\right) - \left[\frac{3}{2}\,z + \frac{3}{2} + z\log(z)\right]a\log(a) \\
& + \left[2z\log(1-z)\log(z) - z\log^2(z) - \left(z+\frac{3}{2}\right)\log(z)\right]a + \mathcal{O}\Big(a^{\frac{3}{2}}\log(a)\Big)
\end{aligned}
\tag{E.6.1}
$$

$$
\begin{aligned}
{}^{C_{\rm A}}g_1^{C_1}(z) = &-\frac{z}{2}\,(3z+1)\,a\log^2(a)\\
&+\left[z\,(3z+1)\left(\log\frac{(1-z)^2}{z}+\frac{1}{2}\right)+\frac{3}{2}\right]a\log(a)\\
&+\left[2z\,(3z+1)\left(\log(1-z)\log(z)-\log^2(1-z)-\frac{1}{2}\log^2(z)\right)\right.\\
&\quad\left.-3z\left(2z+\frac{1}{2}\right)\log(1-z)+\left(\frac{3}{2}\,z^2+z+\frac{3}{2}\right)\log(z)-\frac{\pi^2}{6}z\,(3z+1)\right]a\\
&+\mathcal{O}\Big(a^{\frac{3}{2}}\log(a)\Big)
\end{aligned}
\tag{E.6.2}
$$

$$
\begin{aligned}
{}^{C_{\rm A}}g_2^{C_1}(z) = &-z\,p_{qg}(z)\,a\log^2(a)\\
&+\left[2z\log\frac{(1-z)^2}{z}\,p_{qg}(z)+\frac{z}{2}(1-z)\right]a\log(a)\\
&+\left[4z\left(\log(1-z)\log(z)-\log^2(1-z)-\frac{1}{2}\log^2(z)\right)p_{qg}(z)\right.\\
&\quad-\frac{z}{2}(1-z)\log(1-z)+\frac{1}{2}z\left(9z^2-10z+5\right)\log(z)\\
&\quad\left.-\frac{\pi^2}{3}z\,p_{qg}(z)+z\left(3z^2-2z-1\right)\right]a+\mathcal{O}\Big(a^{\frac{3}{2}}\log(a)\Big)
\end{aligned}
\tag{E.6.3}
$$

$$
\begin{aligned}
{}^{C_{\rm A}}\mathcal{J}_{23}^{C_1} = &-\frac{1}{6}\left[\mathcal{L}+\mathcal{L}^{'}\right]a\log^3(a)-\left[\frac{3}{4}\,\mathcal{L}+\frac{5}{3}\,\mathcal{L}^{'}\right]a\log^2(a)\\
&-\left[\left(\frac{\pi^2}{2}+\frac{7}{2}\right)\mathcal{L}+\left(\frac{\pi^2}{2}+\frac{241}{36}\right)\mathcal{L}^{'}\right]a\log(a)\\
&-\left[\left(\frac{\pi^2}{12}+12\right)\mathcal{L}+\left(\frac{4}{3}\,\pi^2+\frac{1391}{108}\right)\mathcal{L}^{'}\right]a+\mathcal{O}\Big(a^{\frac{3}{2}}\log(a)\Big)
\end{aligned}
\tag{E.6.4}
$$

E.7 C_1^{qg}: C_F coefficient

$$
\begin{aligned}
{}^{C_F}g_0^{C_1}(z) = &-\frac{1}{3}\,p_{qg}(z)\log^3(a) + p_{qg}(z)\left[\log(1-z)+\frac{3}{4}\right]\log^2(a)\\
&- p_{qg}(z)\left[\log^2(1-z)+\frac{3}{2}\log(1-z)+\frac{7}{2}\right]\log(a)\\
&+ p_{qg}(z)\left(\frac{2}{3}\log^3(1-z) - \log(1-z)\log(z)\log\frac{1-z}{z} - \frac{1}{3}\log^3(z)\right)\\
&+ \left(-\frac{3}{2}\,z^2+z+\frac{1}{2}\right)\log^2(1-z) + \left(-3z^2+\frac{5}{2}\,z-\frac{1}{4}\right)\log^2(z)\\
&+ \left(6z^2-5z+\frac{1}{2}\right)\log(1-z)\log(z) + \left(-\frac{51}{4}\,z^2+\frac{23}{2}\,z-\frac{9}{4}\right)\log(z)\\
&+ \left(\frac{79}{4}\,z^2-\frac{37}{2}\,z+\frac{23}{4}\right)\log(1-z) - \frac{93}{8}\,z^2+\frac{37}{4}\,z+\frac{19}{8}\\
&+ \frac{1}{2}\,z\,a\log^2(a) + \left[-z\log(1-z)-\frac{93}{16}\,z-\frac{19}{8}\right]a\log(a)\\
&+ \left[-\frac{1}{2}\,z\log^2(z) - z\left(\frac{23}{16}\,z^2+\frac{37}{8}\,z+\frac{31}{16}\right)\log(z) + z\log(1-z)\log(z)\right.\\
&\quad\left. + \left(\frac{23}{16}\,z^3+\frac{37}{8}\,z^2+\frac{81}{8}\,z+\frac{51}{8}\right)\log(1-z) + \frac{23}{16}\,z^2+\frac{19}{8}\,z\right]a\\
&+ \mathcal{O}\Big(a^{\frac{3}{2}}\log(a)\Big)
\end{aligned}
\tag{E.7.1}
$$

$$
\begin{aligned}
{}^{C_F}g_1^{C_1}(z) = &-\frac{z}{2}\,(3z+1)\,a\log^2(a)\\
&+ \left[z\,(3z+1)\log(1-z) + \frac{47}{16}\,z^2+\frac{59}{16}\,z+\frac{19}{8}\right]a\log(a)\\
&+ \left[-z\,(3z+1)\left(\log(1-z)\log\frac{1-z}{z}+\frac{1}{2}\log^2(z)\right)\right.\\
&\quad + \left(\frac{23}{16}\,z^4+\frac{51}{16}\,z^3-\frac{9}{4}\,z-\frac{51}{8}\right)\log(1-z)\\
&\quad \left. - \left(\frac{23}{16}\,z^4+\frac{51}{16}\,z^3+\frac{9}{16}\,z^2-\frac{3}{16}\,z\right)\log(z) + \frac{139}{32}\,z^3-\frac{877}{32}\,z^2-\frac{105}{32}\,z\right]a\\
&+ \mathcal{O}\Big(a^{\frac{3}{2}}\log(a)\Big)
\end{aligned}
\tag{E.7.2}
$$

$$
\begin{aligned}
{}^{C_{\mathrm{F}}} g_2^{C_1}(z) = & -z\, p_{qg}(z)\, a \log^2(a) \\
& + \left[2z\, p_{qg}(z) \log(1-z) + \frac{1}{4} z \left(19z^2 - 18z + 5 \right) \right] a \log(a) \\
& + \Bigg[z \left(2\log(z)\log(1-z) - 2\log^2(1-z) - \log^2(z) \right) p_{qg}(z) \\
& \quad - \frac{1}{4} z \left(19z^2 - 18z + 5 \right) \log(z) \\
& \quad + \frac{1}{32} z \left(93z^3 - 888z^2 + 878z - 307 \right) \Bigg] a + \mathcal{O}\Big(a^{\frac{3}{2}} \log(a) \Big)
\end{aligned}
\tag{E.7.3}
$$

$$
\begin{aligned}
{}^{C_{\mathrm{F}}} \mathcal{J}_{23}^{C_1} = & -\frac{1}{3} \left[\mathcal{L} + \mathcal{L}' \right] a \log^3(a) - \frac{1}{2} \left[\mathcal{L} + \frac{11}{6}\, \mathcal{L}' \right] a \log^2(a) \\
& - \left[\frac{47}{32}\, \mathcal{L} + \frac{341}{72}\, \mathcal{L}' \right] a \log(a) \\
& + \left[\left(-\frac{\pi^2}{3} + \frac{1013}{128} \right) \mathcal{L} - \frac{1}{36} \left(29\,\pi^2 + \frac{58691}{96} \right) \mathcal{L}' \right] a + \mathcal{O}\Big(a^{\frac{3}{2}} \log(a) \Big)
\end{aligned}
\tag{E.7.4}
$$

E.8 C_2^{qg}

$$
g_i^{C_2}(z) = \frac{1}{3} \log \frac{\mu_{\mathrm{F}}^2}{Q^2}\, g_i^A(z) \qquad\qquad i = 0, 1, 2 \tag{E.8.1}
$$

$$
\mathcal{J}_{23}^{C_2} = \frac{1}{3} \log \frac{\mu_{\mathrm{F}}^2}{Q^2}\, \mathcal{J}_{23}^A \tag{E.8.2}
$$

Appendix F

Altarelli–Parisi splitting functions

The zero-order Altarelli–Parisi splitting functions are defined as

$$\begin{aligned} P_{qq}(z) &= P_{\bar{q}\bar{q}}(z) = C_{\mathrm{F}}\left[\frac{1+z^2}{(1-z)_+} + \frac{3}{2}\delta(1-z)\right] = C_{\mathrm{F}}\left[\frac{1+z^2}{1-z}\right]_+ \\ &\equiv C_{\mathrm{F}}\, p_{qq}(z) + \frac{3}{2}C_{\mathrm{F}}\,\delta(1-z)\,, \end{aligned} \tag{F.1}$$

$$P_{qg}(z) = P_{\bar{q}g}(z) = T_{\mathrm{R}}\left[z^2+(1-z)^2\right] = T_{\mathrm{R}}\left[2z^2-2z+1\right] \equiv T_{\mathrm{R}}\, p_{qg}(z)\,, \tag{F.2}$$

$$P_{gq}(z) = P_{g\bar{q}}(z) = C_{\mathrm{F}}\left[\frac{1+(1-z)^2}{z}\right] = C_{\mathrm{F}}\left[\frac{z^2-2z+2}{z}\right] \equiv C_{\mathrm{F}}\, p_{gq}(z)\,, \tag{F.3}$$

$$\begin{aligned} P_{gg}(z) &= 2C_{\mathrm{A}}\left[\frac{z}{(1-z)_+} + \frac{1-z}{z} + z(1-z)\right] + \frac{1}{6}\left[11C_{\mathrm{A}} - 4n_{\mathrm{f}}T_{\mathrm{R}}\right]\delta(1-z) \\ &\equiv C_{\mathrm{A}}\, p_{gg}(z) + \frac{1}{6}\left[11C_{\mathrm{A}} - 4n_{\mathrm{f}}T_{\mathrm{R}}\right]\delta(1-z)\,. \end{aligned} \tag{F.4}$$

The unregularised Altarelli–Parisi splitting functions are given by

$$\hat{P}_{qq}(z) = \hat{P}_{\bar{q}\bar{q}}(z) = C_{\mathrm{F}}\frac{1+z^2}{1-z} \equiv C_{\mathrm{F}}\,\hat{p}_{qq}(z)\,, \tag{F.5}$$

$$\hat{P}_{gg}(z) = 2\,C_{\mathrm{A}}\left[\frac{z}{1-z} + \frac{1-z}{z} + z(1-z)\right] = C_{\mathrm{A}}\frac{2\left(z^2-z+1\right)^2}{z(1-z)} \equiv C_{\mathrm{A}}\,\hat{p}_{gg}(z)\,. \tag{F.6}$$

Appendix G

Plus distributions

We define a plus distribution of order n as

$$\int_0^1 \mathrm{d}z\, l(z)\, [g(z)]_{n+} \equiv \int_0^1 \mathrm{d}z \left\{ l(z) - \sum_{i=0}^{n-1} \frac{1}{i!}\, l^{(i)}(1)\, (z-1)^i \right\} g(z)\,, \tag{G.1}$$

where $g(z)$ has a pole of order n for $z = 1$, and $l(z)$ is a continuous function around $z = 1$, together with all its derivatives up to order $(n-1)$. For example, the first three plus distributions read

$$\int_0^1 \mathrm{d}z\, l(z)\, [g(z)]_{+} \equiv \int_0^1 \mathrm{d}z \left\{ l(z) - l(1) \right\} g(z)\,, \tag{G.2}$$

$$\int_0^1 \mathrm{d}z\, l(z)\, [g(z)]_{2+} \equiv \int_0^1 \mathrm{d}z \left\{ l(z) - l(1) - l^{(1)}(1)\, (z-1) \right\} g(z)\,, \tag{G.3}$$

$$\int_0^1 \mathrm{d}z\, l(z)\, [g(z)]_{3+} \equiv \int_0^1 \mathrm{d}z \left\{ l(z) - l(1) - l^{(1)}(1)\, (z-1) - \frac{1}{2!}\, l^{(2)}(1)\, (z-1)^2 \right\} g(z)\,. \tag{G.4}$$

With simple manipulations, some useful identities follow

$$\int_0^1 \mathrm{d}z\, l(z) \left[\frac{n(z)}{d(z)} \right]_{+} = \int_0^1 \mathrm{d}z \left\{ l(z)\, n(z) \left[\frac{1}{d(z)} \right]_{+} - l(1)\, n(z) \left[\frac{1}{d(z)} \right]_{+} \right\}, \tag{G.5}$$

$$\begin{aligned} \int_0^1 \mathrm{d}z\, l(z) \left[\frac{n(z)}{d(z)} \right]_{2+} = \int_0^1 \mathrm{d}z \Bigg\{ & l(z)\, n(z) \left[\frac{1}{d(z)} \right]_{2+} - l(1)\, n(z) \left[\frac{1}{d(z)} \right]_{2+} \\ & - l^{(1)}(1)\, n(z) \left[\frac{z-1}{d(z)} \right]_{+} \Bigg\}, \end{aligned} \tag{G.6}$$

$$\begin{aligned} \int_0^1 \mathrm{d}z\, l(z) \left[\frac{n(z)}{d(z)} \right]_{3+} = \int_0^1 \mathrm{d}z \Bigg\{ & l(z)\, n(z) \left[\frac{1}{d(z)} \right]_{3+} - l(1)\, n(z) \left[\frac{1}{d(z)} \right]_{3+} \\ & - l^{(1)}(1)\, n(z) \left[\frac{z-1}{d(z)} \right]_{2+} - \frac{1}{2!}\, l^{(2)}(1)\, n(z) \left[\frac{(z-1)^2}{d(z)} \right]_{+} \Bigg\}, \end{aligned} \tag{G.7}$$

and, in general,

$$\int_0^1 \mathrm{d}z\, l(z) \left[\frac{n(z)}{d(z)}\right]_{p+} = \int_0^1 \mathrm{d}z \left\{ l(z)\, n(z) \left[\frac{1}{d(z)}\right]_{p+} - \sum_{i=0}^{p-1} \frac{1}{i!}\, l^{(i)}(1)\, n(z) \left[\frac{(z-1)^i}{d(z)}\right]_{(p-i)+} \right\}. \tag{G.8}$$

Appendix H

Čebyšëv polynomials

The Čebyšëv polynomial of degree n is referred to as[1]

$$T_n(x) \tag{H.1}$$

and is given by the explicit formula

$$T_n(x) = \cos(n \arccos x) \tag{H.2}$$

that reduces to explicit polynomial expressions by using trigonometric identities, namely

$$T_0(x) = 1 \tag{H.3}$$
$$T_1(x) = x \tag{H.4}$$
$$T_{n+1}(x) = 2x\, T_n(x) - T_{n-1}(x) \qquad n \geqslant 1\,. \tag{H.5}$$

These polynomials have a number of useful properties that allow us to use them in order to fit functions whose analytic form is unknown, such as in the case of parton distribution functions and their derivatives. To begin with, they are orthogonal in the interval $[-1, 1]$

$$\int_{-1}^{1} \mathrm{d}x \frac{T_i(x)\, T_j(x)}{\sqrt{1-x^2}} = \begin{cases} 0 & i \neq j \\ \dfrac{\pi}{2} & i = j \neq 0 \\ \pi & i = j = 0\,. \end{cases} \tag{H.6}$$

In addition, the polynomial $T_n(x)$ has n zeros in the interval $[-1, 1]$, located at points

$$x = \cos \frac{\pi\left(k - \frac{1}{2}\right)}{n}\,, \qquad k = 1, 2, \ldots, n\,. \tag{H.7}$$

[1]The following paragraphs are inspired by ref. [157]. The FORTRAN subroutines used to deal with Čebyšëv polynomials were obtained therein.

and such that the polynomial satisfies a discrete orthogonality relation along with the continuous one of eq. (H.6). In fact, if x_k, $k = 1, \ldots, m$, are the m zeros of $T_m(x)$ given by eq. (H.7), and if $i, j < m$ then

$$\sum_{k=1}^{m} T_i(x_k)\, T_j(x_k) = \begin{cases} 0 & i \neq j \\ \dfrac{m}{2} & i = j \neq 0 \\ m & i = j = 0\,. \end{cases} \tag{H.8}$$

With the help of eqs. (H.2), (H.7), (H.8), one can prove that, if $f(x)$ is an arbitrary function in the interval $[-1, 1]$, and if N coefficients c_j, $j = 1, \ldots, N$, are defined by

$$\begin{aligned} c_j &= \frac{2}{N} \sum_{k=1}^{N} f(x_k)\, T_{j-1}(x_k) \\ &= \frac{2}{N} \sum_{k=1}^{N} f\left(\cos \frac{\pi \left(k - \frac{1}{2}\right)}{N} \right) \cos \frac{\pi\,(j-1)\left(k - \frac{1}{2}\right)}{N}\,, \end{aligned} \tag{H.9}$$

then the approximation formula

$$f(x) \simeq \left[\sum_{k=1}^{N} c_k\, T_k(x) \right] - \frac{c_1}{2} \tag{H.10}$$

is exact for x equal to all of the N zeros of $T_N(x)$. The reader interested in the magic properties of the Čebyšëv polynomials, and in particular on the reasons why one should prefer this approximation over others, is referred to Section 5.8 of ref. [157]. Here, we only recall that the subroutines that were used in our code implemented the change of variable

$$y = \frac{x - \frac{1}{2}\,(b + a)}{\frac{1}{2}\,(b - a)} \tag{H.11}$$

in order to approximate a function $f(x)$ in the interval $[a, b]$, $a < b$, via a Čebyšëv polynomial in y. Moreover, the approximation is evaluated by using the recurrence relation of eq. (H.3) to generate values for $T_k(x)$ from $T_0 = 1$, $T_1 = x$, while also accumulating the sum of eq. (H.10).

Once the Čebyšëv coefficients that approximate a function in a certain range are obtained, it is straightforward to transform them into Čebyšëv coefficients corresponding to the derivative of the function and then to evaluate them. In detail, if c_i, $i = 1, \ldots, m$, are the coefficients that approximate a function f as in eq. (H.10), the coefficients that approximate the derivative of f, c'_i, are such that satisfy the recurrence relation

$$c'_{i-1} = c'_{i+1} + 2\,(i-1)\, c_i\,, \qquad i = m-1, m-2, \ldots, 2\,, \tag{H.12}$$

starting with $c'_m = c'_{m+1} = 0$. These relations can be used as well in order to compute higher-order derivatives.

Appendix I

More reweighted plots

In the following we present all the results obtained with the POWHEG BOX V2 reweighting feature, as explained in Section 3.3.5, except the ones already discussed therein. In particular, the figures display the normalised differential cross section as a function of the transverse momentum and the pseudorapidity of the X_0 boson, $p_{\mathrm{T}}^{X_0}$ and η^{X_0}, with a cut on the dijet mass of 250 GeV on the left panels and of 500 GeV on the right ones. The color code is the same on the two panels, while the distributions are specified by the caption of each couple of figures.

In general, blue and its shades are associated to the scalar CP scenario, red and its shades to the pseudoscalar CP scenario, black and its shades to the mixed CP scenario. The dotted lines represent the distributions that have been taken as references within the reweighting procedure, the full colors represent the original distributions, i.e. obtained without any reweighting, while the lighter colors represent the corresponding distributions obtained by reweighting (rw). On the lower panels, the ratios between the distributions obtained by reweighting and the original ones are also shown.

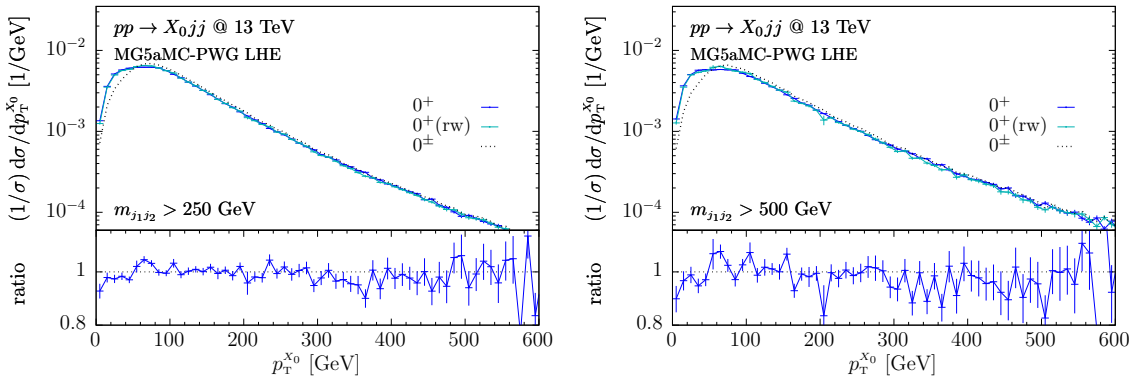

Figure I.1. Normalised differential cross section as a function of $p_\mathrm{T}^{X_0}$. The scalar original distribution in blue, the scalar as obtained by reweighting (rw) in light blue, and the mixed one in dotted black. Refer to the text above for further details.

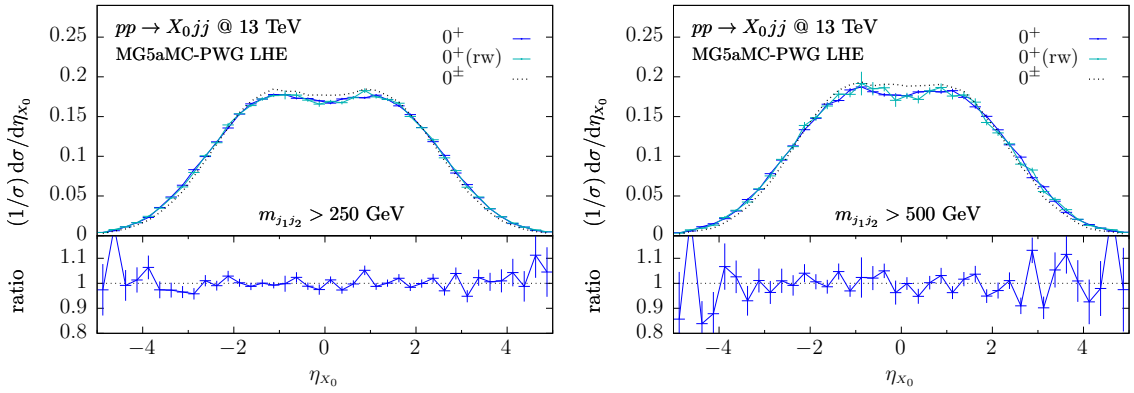

Figure I.2. Normalised differential cross section as a function of η_{X_0}. The scalar original distribution in blue, the scalar as obtained by reweighting (rw) in light blue, and the mixed one in dotted black. Refer to the text above for further details.

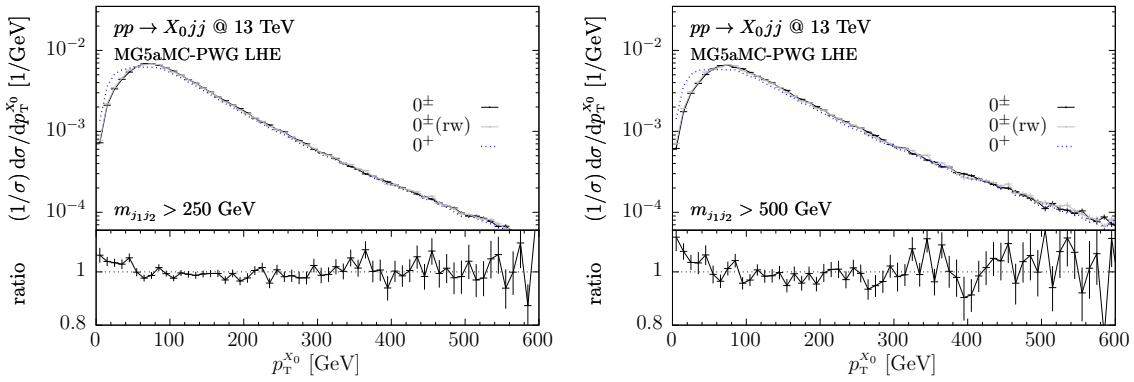

Figure I.3. Normalised differential cross section as a function of $p_{\mathrm{T}}^{X_0}$. The mixed original distribution in black, the mixed as obtained by reweighting (rw) in grey, and the scalar one in dotted blue. Refer to the text above for further details.

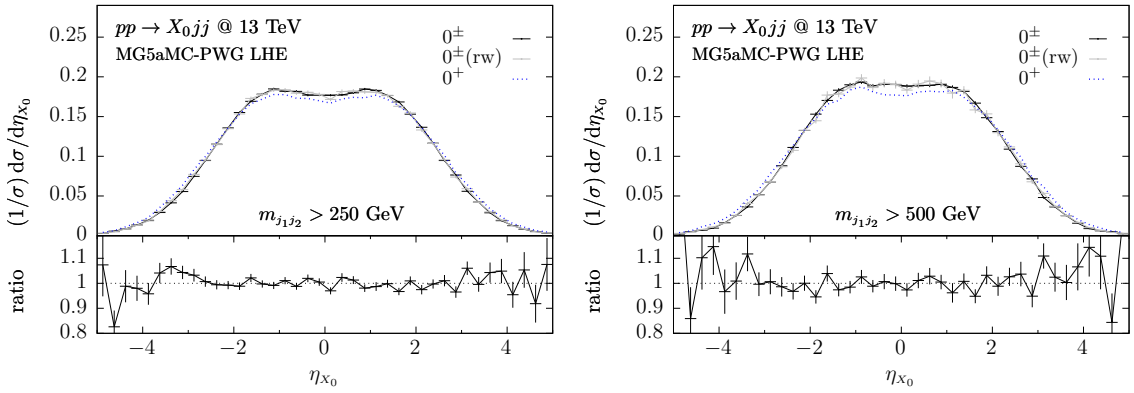

Figure I.4. Normalised differential cross section as a function of η^{X_0}. The mixed original distribution in black, the mixed as obtained by reweighting (rw) in grey, and the scalar one in dotted blue. Refer to the text above for further details.

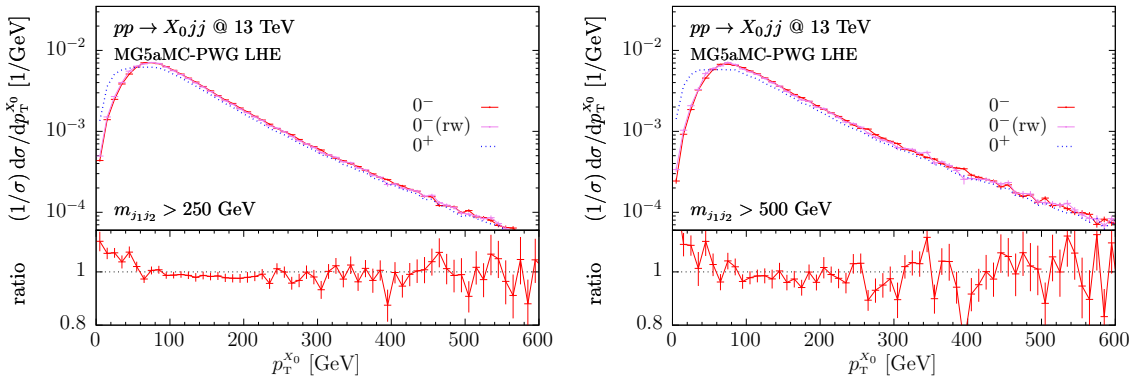

Figure I.5. Normalised differential cross section as a function of $p_\mathrm{T}^{X_0}$. The mixed pseudoscalar distribution in red, the pseudoscalar as obtained by reweighting (rw) in pink, and the scalar one in dotted blue. Refer to the text above for further details.

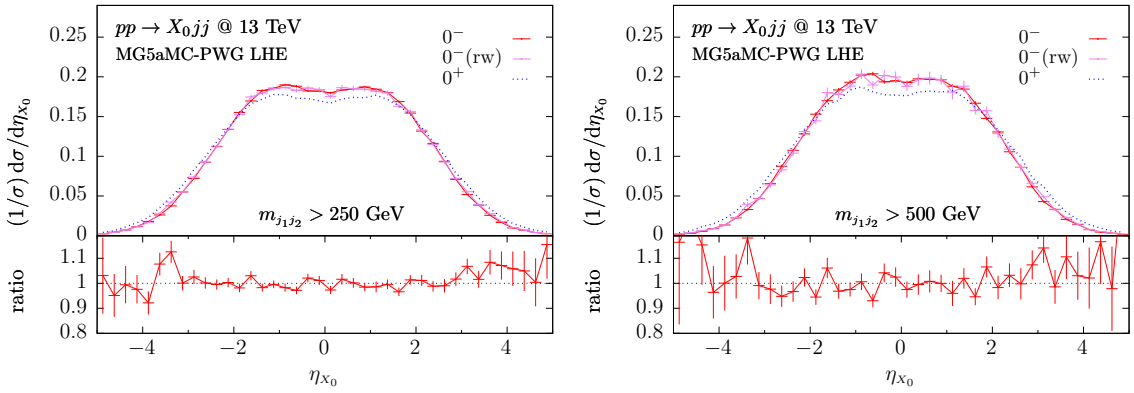

Figure I.6. Normalised differential cross section as a function of η^{X_0}. The mixed pseudoscalar distribution in red, the pseudoscalar as obtained by reweighting (rw) in pink, and the scalar one in dotted blue. Refer to the text above for further details.

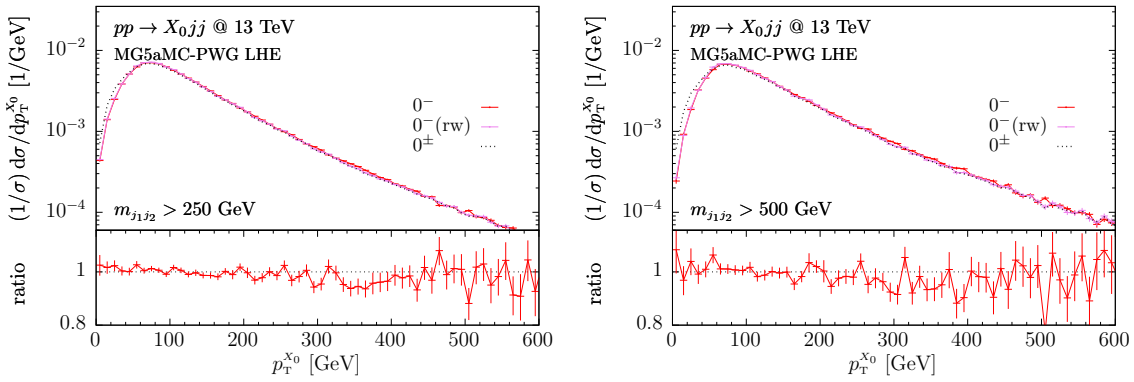

Figure I.7. Normalised differential cross section as a function of $p_\mathrm{T}^{X_0}$. The mixed pseudoscalar distribution in red, the pseudoscalar as obtained by reweighting (rw) in pink, and the mixed one in dotted black. Refer to the text above for further details.

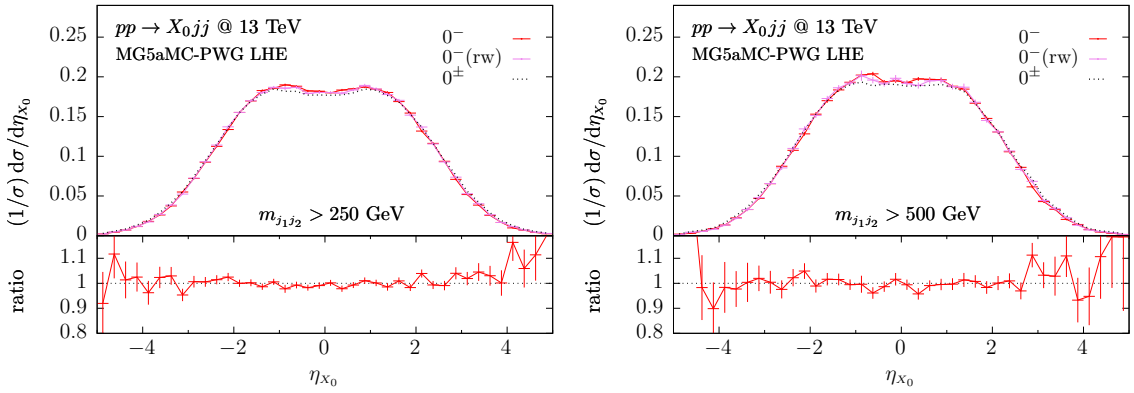

Figure I.8. Normalised differential cross section as a function of η^{X_0}. The mixed pseudoscalar distribution in red, the pseudoscalar as obtained by reweighting (rw) in pink, and the mixed one in dotted black. Refer to the text above for further details.

Bibliography

[1] C. Buttar et al., *Les Houches Physics at TeV Colliders 2005, Standard Model and Higgs Working group: Summary Report*, in *4th Les Houches Workshop on Physics at TeV Colliders*, 4, 2006, hep-ph/0604120.

[2] S. Frixione, Z. Kunszt and A. Signer, *Three jet cross-sections to next-to-leading order*, *Nucl. Phys.* **B467** (1996) 399 [hep-ph/9512328].

[3] S. Catani and M. H. Seymour, *A General algorithm for calculating jet cross-sections in NLO QCD*, *Nucl. Phys.* **B485** (1997) 291 [hep-ph/9605323].

[4] S. Catani and M. Grazzini, *An NNLO subtraction formalism in hadron collisions and its application to Higgs boson production at the LHC*, *Phys. Rev. Lett.* **98** (2007) 222002 [hep-ph/0703012].

[5] G. Bozzi, S. Catani, D. de Florian and M. Grazzini, *Transverse-momentum resummation and the spectrum of the Higgs boson at the LHC*, *Nucl. Phys.* **B737** (2006) 73 [hep-ph/0508068].

[6] R. Bonciani, S. Catani, M. Grazzini, H. Sargsyan and A. Torre, *The q_T subtraction method for top quark production at hadron colliders*, *Eur. Phys. J.* **C75** (2015) 581 [1508.03585].

[7] S. Catani, S. Devoto, M. Grazzini, S. Kallweit, J. Mazzitelli and H. Sargsyan, *Top-quark pair hadroproduction at next-to-next-to-leading order in QCD*, *Phys. Rev.* **D99** (2019) 051501 [1901.04005].

[8] R. Boughezal, X. Liu and F. Petriello, *N-jettiness soft function at next-to-next-to-leading order*, *Phys. Rev.* **D91** (2015) 094035 [1504.02540].

[9] J. Gaunt, M. Stahlhofen, F. J. Tackmann and J. R. Walsh, *N-jettiness Subtractions for NNLO QCD Calculations*, *JHEP* **09** (2015) 058 [1505.04794].

[10] S. Frixione and B. R. Webber, *Matching NLO QCD computations and parton shower simulations*, *JHEP* **06** (2002) 029 [hep-ph/0204244].

[11] P. Nason, *A New method for combining NLO QCD with shower Monte Carlo algorithms*, *JHEP* **11** (2004) 040 [hep-ph/0409146].

[12] S. Frixione, P. Nason and C. Oleari, *Matching NLO QCD computations with Parton Shower simulations: the POWHEG method*, *JHEP* **11** (2007) 070 [0709.2092].

[13] T. Sjöstrand, S. Ask, J. R. Christiansen, R. Corke, N. Desai, P. Ilten et al., *An*

introduction to PYTHIA 8.2, *Comput. Phys. Commun.* **191** (2015) 159 [1410.3012].

[14] M. Bahr et al., *Herwig++ Physics and Manual*, *Eur. Phys. J. C* **58** (2008) 639 [0803.0883].

[15] S. Alioli, P. Nason, C. Oleari and E. Re, *A general framework for implementing NLO calculations in shower Monte Carlo programs: the POWHEG BOX*, *JHEP* **06** (2010) 043 [1002.2581].

[16] J. M. Campbell, R. Ellis, R. Frederix, P. Nason, C. Oleari and C. Williams, *NLO Higgs Boson Production Plus One and Two Jets Using the POWHEG BOX, MadGraph4 and MCFM*, *JHEP* **07** (2012) 092 [1202.5475].

[17] G. Luisoni, P. Nason, C. Oleari and F. Tramontano, *$HW^{\pm}/HZ$ + 0 and 1 jet at NLO with the POWHEG BOX interfaced to GoSam and their merging within MiNLO*, *JHEP* **10** (2013) 083 [1306.2542].

[18] G. Luisoni, C. Oleari and F. Tramontano, *$Wb\bar{b}j$ production at NLO with POWHEG+MiNLO*, *JHEP* **04** (2015) 161 [1502.01213].

[19] T. Ježo, J. M. Lindert, P. Nason, C. Oleari and S. Pozzorini, *An NLO+PS generator for $t\bar{t}$ and Wt production and decay including non-resonant and interference effects*, *Eur. Phys. J. C* **76** (2016) 691 [1607.04538].

[20] J. Alwall, R. Frederix, S. Frixione, V. Hirschi, F. Maltoni, O. Mattelaer et al., *The automated computation of tree-level and next-to-leading order differential cross sections, and their matching to parton shower simulations*, *JHEP* **07** (2014) 079 [1405.0301].

[21] S. Dawson, *Radiative corrections to Higgs boson production*, *Nucl. Phys.* **B359** (1991) 283.

[22] D. de Florian and M. Grazzini, *The Structure of large logarithmic corrections at small transverse momentum in hadronic collisions*, *Nucl. Phys.* **B616** (2001) 247 [hep-ph/0108273].

[23] L. Cieri, X. Chen, T. Gehrmann, E. W. N. Glover and A. Huss, *Higgs boson production at the LHC using the q_T subtraction formalism at N^3LO QCD*, *JHEP* **02** (2019) 096 [1807.11501].

[24] F. Dulat, B. Mistlberger and A. Pelloni, *Precision predictions at N^3LO for the Higgs boson rapidity distribution at the LHC*, *Phys. Rev.* **D99** (2019) 034004 [1810.09462].

[25] F. A. Dreyer and A. Karlberg, *Vector-Boson Fusion Higgs Production at Three Loops in QCD*, *Phys. Rev. Lett.* **117** (2016) 072001 [1606.00840].

[26] F. A. Dreyer and A. Karlberg, *Vector-Boson Fusion Higgs Pair Production at N^3LO*, *Phys. Rev. D* **98** (2018) 114016 [1811.07906].

[27] L.-B. Chen, H. T. Li, H.-S. Shao and J. Wang, *Higgs boson pair production via gluon fusion at N^3LO in QCD*, *Phys. Lett. B* **803** (2020) 135292 [1909.06808].

[28] L.-B. Chen, H. T. Li, H.-S. Shao and J. Wang, *The gluon-fusion production of Higgs boson pair: N^3LO QCD corrections and top-quark mass effects*, *JHEP* **03** (2020) 072 [1912.13001].

[29] J. Currie, T. Gehrmann, E. Glover, A. Huss, J. Niehues and A. Vogt, *N^3LO corrections to jet production in deep inelastic scattering using the Projection-to-Born method*, *JHEP* **05** (2018) 209 [1803.09973].

[30] T. Gehrmann, A. Huss, J. Niehues, A. Vogt and D. Walker, *Jet production in charged-current deep-inelastic scattering to third order in QCD*, *Phys. Lett. B* **792** (2019) 182 [1812.06104].

[31] M. Cacciari, F. A. Dreyer, A. Karlberg, G. P. Salam and G. Zanderighi, *Fully Differential Vector-Boson-Fusion Higgs Production at Next-to-Next-to-Leading Order*, *Phys. Rev. Lett.* **115** (2015) 082002 [1506.02660].

[32] M. Czakon, *Double-real radiation in hadronic top quark pair production as a proof of a certain concept*, *Nucl. Phys.* **B849** (2011) 250 [1101.0642].

[33] R. Boughezal, K. Melnikov and F. Petriello, *A subtraction scheme for NNLO computations*, *Phys. Rev.* **D85** (2012) 034025 [1111.7041].

[34] A. Gehrmann-De Ridder, T. Gehrmann and E. W. N. Glover, *Antenna subtraction at NNLO*, *JHEP* **09** (2005) 056 [hep-ph/0505111].

[35] A. Daleo, T. Gehrmann and D. Maitre, *Antenna subtraction with hadronic initial states*, *JHEP* **04** (2007) 016 [hep-ph/0612257].

[36] J. Currie, E. W. N. Glover and S. Wells, *Infrared Structure at NNLO Using Antenna Subtraction*, *JHEP* **04** (2013) 066 [1301.4693].

[37] Y. L. Dokshitzer, D. Diakonov and S. I. Troian, *On the Transverse Momentum Distribution of Massive Lepton Pairs*, *Phys. Lett.* **79B** (1978) 269.

[38] Y. L. Dokshitzer, D. Diakonov and S. I. Troian, *Hard Processes in Quantum Chromodynamics*, *Phys. Rept.* **58** (1980) 269.

[39] G. Parisi and R. Petronzio, *Small Transverse Momentum Distributions in Hard Processes*, *Nucl. Phys.* **B154** (1979) 427.

[40] G. Curci, M. Greco and Y. Srivastava, *QCD Jets From Coherent States*, *Nucl. Phys.* **B159** (1979) 451.

[41] J. C. Collins and D. E. Soper, *Back-To-Back Jets in QCD*, *Nucl. Phys.* **B193** (1981) 381.

[42] J. Kodaira and L. Trentadue, *Summing Soft Emission in QCD*, *Phys. Lett.* **112B** (1982) 66.

[43] J. Kodaira and L. Trentadue, *Single Logarithm Effects in Electron-Positron Annihilation*, *Phys. Lett.* **123B** (1983) 335.

[44] J. C. Collins, D. E. Soper and G. F. Sterman, *Transverse Momentum Distribution in Drell-Yan Pair and W and Z Boson Production*, *Nucl. Phys.* **B250** (1985) 199.

[45] S. Catani, E. D'Emilio and L. Trentadue, *The Gluon Form-factor to Higher Orders: Gluon Gluon Annihilation at Small Q_t*, *Phys. Lett.* **B211** (1988) 335.

[46] D. de Florian and M. Grazzini, *Next-to-next-to-leading logarithmic corrections at small transverse momentum in hadronic collisions*, *Phys. Rev. Lett.* **85** (2000) 4678 [hep-ph/0008152].

[47] S. Alioli, C. W. Bauer, C. Berggren, F. J. Tackmann and J. R. Walsh, *Drell-Yan production at NNLL'+NNLO matched to parton showers*, *Phys. Rev.* **D92** (2015) 094020 [1508.01475].

[48] S. Catani, L. Cieri, D. de Florian, G. Ferrera and M. Grazzini, *Diphoton production at hadron colliders: a fully-differential QCD calculation at NNLO*, *Phys. Rev. Lett.* **108** (2012) 072001 [1110.2375].

[49] S. Catani, L. Cieri, D. de Florian, G. Ferrera and M. Grazzini, *Diphoton production at the LHC: a QCD study up to NNLO*, *JHEP* **04** (2018) 142 [1802.02095].

[50] M. Grazzini, S. Kallweit and M. Wiesemann, *Fully differential NNLO computations with MATRIX*, *Eur. Phys. J.* **C78** (2018) 537 [1711.06631].

[51] R. Boughezal, J. M. Campbell, R. K. Ellis, C. Focke, W. Giele, X. Liu et al., *Color singlet production at NNLO in MCFM*, *Eur. Phys. J.* **C77** (2017) 7 [1605.08011].

[52] Z. Bern, S. Davies and J. Nohle, *On Loop Corrections to Subleading Soft Behavior of Gluons and Gravitons*, *Phys. Rev.* **D90** (2014) 085015 [1405.1015].

[53] A. J. Larkoski, D. Neill and I. W. Stewart, *Soft Theorems from Effective Field Theory*, *JHEP* **06** (2015) 077 [1412.3108].

[54] H. Luo, P. Mastrolia and W. J. Torres Bobadilla, *Subleading soft behavior of QCD amplitudes*, *Phys. Rev.* **D91** (2015) 065018 [1411.1669].

[55] M. van Beekveld, W. Beenakker, R. Basu, E. Laenen, A. Misra and P. Motylinski, *Next-to-leading power threshold effects for resummed prompt photon production*, *Phys. Rev. D* **100** (2019) 056009 [1905.11771].

[56] M. van Beekveld, W. Beenakker, E. Laenen and C. D. White, *Next-to-leading power threshold effects for inclusive and exclusive processes with final state jets*, *JHEP* **03** (2020) 106 [1905.08741].

[57] V. Del Duca, E. Laenen, L. Magnea, L. Vernazza and C. D. White, *Universality of next-to-leading power threshold effects for colourless final states in hadronic collisions*, *JHEP* **11** (2017) 057 [1706.04018].

[58] D. Bonocore, E. Laenen, L. Magnea, S. Melville, L. Vernazza and C. D. White, *A factorization approach to next-to-leading-power threshold logarithms*, *JHEP* **06** (2015) 008 [1503.05156].

[59] D. Bonocore, E. Laenen, L. Magnea, L. Vernazza and C. D. White, *The method of regions and next-to-soft corrections in Drell-Yan production*, *Phys. Lett.* **B742** (2015) 375 [1410.6406].

[60] E. Laenen, L. Magnea, G. Stavenga and C. D. White, *Next-to-eikonal corrections to soft gluon radiation: a diagrammatic approach*, *JHEP* **01** (2011) 141 [1010.1860].

[61] E. Laenen, L. Magnea and G. Stavenga, *On next-to-eikonal corrections to threshold resummation for the Drell-Yan and DIS cross sections*, *Phys. Lett.* **B669** (2008) 173 [0807.4412].

[62] M. Beneke, A. Broggio, M. Garny, S. Jaskiewicz, R. Szafron, L. Vernazza et al., *Leading-logarithmic threshold resummation of the Drell-Yan process at next-to-leading power*, *JHEP* **03** (2019) 043 [1809.10631].

[63] M. Beneke, A. Broggio, S. Jaskiewicz and L. Vernazza, *Threshold factorization of the Drell-Yan process at next-to-leading power*, *JHEP* **07** (2020) 078 [1912.01585].

[64] I. Moult, L. Rothen, I. W. Stewart, F. J. Tackmann and H. X. Zhu, *Subleading Power Corrections for N-Jettiness Subtractions*, *Phys. Rev.* **D95** (2017) 074023 [1612.00450].

[65] R. Boughezal, X. Liu and F. Petriello, *Power Corrections in the N-jettiness Subtraction Scheme*, *JHEP* **03** (2017) 160 [1612.02911].

[66] R. Boughezal, A. Isgrò and F. Petriello, *Next-to-leading-logarithmic power corrections for N-jettiness subtraction in color-singlet production*, *Phys. Rev.* **D97** (2018) 076006 [1802.00456].

[67] I. Moult, L. Rothen, I. W. Stewart, F. J. Tackmann and H. X. Zhu, *N-jettiness subtractions for $gg \to H$ at subleading power*, *Phys. Rev.* **D97** (2018) 014013 [1710.03227].

[68] M. A. Ebert, I. Moult, I. W. Stewart, F. J. Tackmann, G. Vita and H. X. Zhu, *Power Corrections for N-Jettiness Subtractions at $\mathcal{O}(\alpha_s)$*, *JHEP* **12** (2018) 084 [1807.10764].

[69] A. Bhattacharya, I. Moult, I. W. Stewart and G. Vita, *Helicity Methods for High Multiplicity Subleading Soft and Collinear Limits*, *JHEP* **05** (2019) 192 [1812.06950].

[70] J. M. Campbell, R. K. Ellis and S. Seth, *H + 1 jet production revisited*, *JHEP* **10** (2019) 136 [1906.01020].

[71] I. Moult, I. W. Stewart, G. Vita and H. X. Zhu, *First Subleading Power Resummation for Event Shapes*, *JHEP* **08** (2018) 013 [1804.04665].

[72] R. Boughezal, A. Isgrò and F. Petriello, *Next-to-leading power corrections to $V + 1$ jet production in N-jettiness subtraction*, *Phys. Rev. D* **101** (2020) 016005 [1907.12213].

[73] M. A. Ebert and F. J. Tackmann, *Impact of isolation and fiducial cuts on q_T and N-jettiness subtractions*, *JHEP* **03** (2020) 158 [1911.08486].

[74] M. A. Ebert, J. K. Michel, I. W. Stewart and F. J. Tackmann, *Drell-Yan q_T Resummation of Fiducial Power Corrections at N^3LL*, 2006.11382.

[75] C. W. Bauer, S. Fleming and M. E. Luke, *Summing Sudakov logarithms in $B \to X_s\gamma$ in effective field theory*, *Phys. Rev.* **D63** (2000) 014006 [hep-ph/0005275].

[76] C. W. Bauer, S. Fleming, D. Pirjol and I. W. Stewart, *An Effective field theory for collinear and soft gluons: Heavy to light decays*, *Phys. Rev.* **D63** (2001) 114020 [hep-ph/0011336].

[77] C. W. Bauer and I. W. Stewart, *Invariant operators in collinear effective theory*, *Phys. Lett.* **B516** (2001) 134 [hep-ph/0107001].

[78] C. W. Bauer, D. Pirjol and I. W. Stewart, *Soft collinear factorization in effective field theory*, *Phys. Rev.* **D65** (2002) 054022 [hep-ph/0109045].

[79] C. W. Bauer, D. Pirjol and I. W. Stewart, *Factorization and endpoint singularities in heavy to light decays*, *Phys. Rev.* **D67** (2003) 071502 [hep-ph/0211069].

[80] I. Moult, I. W. Stewart and G. Vita, *Subleading Power Factorization with Radiative Functions*, *JHEP* **11** (2019) 153 [1905.07411].

[81] M. A. Ebert, I. Moult, I. W. Stewart, F. J. Tackmann, G. Vita and H. X. Zhu, *Subleading power rapidity divergences and power corrections for q_T*, *JHEP* **04** (2019) 123 [1812.08189].

[82] L. Cieri, C. Oleari and M. Rocco, *Higher-order power corrections in a transverse-momentum cut for colour-singlet production at NLO*, *Eur. Phys. J. C* **79** (2019) 852 [1906.09044].

[83] L. Buonocore, M. Grazzini and F. Tramontano, *The q_T subtraction method: electroweak corrections and power suppressed contributions*, *Eur. Phys. J. C* **80** (2020) 254 [1911.10166].

[84] C. Oleari and M. Rocco, *Power corrections in a transverse-momentum cut for vector-boson production at NNLO: the qg-initiated real-virtual contribution*, 2012.10538.

[85] S. Catani and M. Grazzini, *Higgs Boson Production at Hadron Colliders: Hard-Collinear Coefficients at the NNLO*, *Eur. Phys. J.* **C72** (2012) 2013 [1106.4652].

[86] S. Catani, L. Cieri, D. de Florian, G. Ferrera and M. Grazzini, *Vector boson production at hadron colliders: hard-collinear coefficients at the NNLO*, *Eur. Phys. J.* **C72** (2012) 2195 [1209.0158].

[87] S. Catani, D. de Florian and M. Grazzini, *Direct Higgs production and jet veto at the Tevatron and the LHC in NNLO QCD*, *JHEP* **01** (2002) 015 [hep-ph/0111164].

[88] S. Catani and M. Grazzini, *QCD transverse-momentum resummation in gluon fusion processes*, *Nucl. Phys.* **B845** (2011) 297 [1011.3918].

[89] S. Catani, L. Cieri, D. de Florian, G. Ferrera and M. Grazzini, *Universality of transverse-momentum resummation and hard factors at the NNLO*, *Nucl. Phys.* **B881** (2014) 414 [1311.1654].

[90] S. Catani, D. de Florian and M. Grazzini, *Universality of nonleading logarithmic contributions in transverse momentum distributions*, *Nucl. Phys.* **B596** (2001) 299 [hep-ph/0008184].

[91] A. D. Martin, W. J. Stirling, R. S. Thorne and G. Watt, *Parton distributions for the LHC*, *Eur. Phys. J.* **C63** (2009) 189 [0901.0002].

[92] G. Bozzi, S. Catani, G. Ferrera, D. de Florian and M. Grazzini, *Transverse-momentum resummation: A Perturbative study of Z production at the Tevatron*, *Nucl. Phys.* **B815** (2009) 174 [0812.2862].

[93] G. Bozzi, S. Catani, G. Ferrera, D. de Florian and M. Grazzini, *Production of Drell-Yan lepton pairs in hadron collisions: Transverse-momentum resummation at next-to-next-to-leading logarithmic accuracy*, *Phys. Lett.* **B696** (2011) 207 [1007.2351].

[94] D. de Florian, G. Ferrera, M. Grazzini and D. Tommasini, *Transverse-momentum resummation: Higgs boson production at the Tevatron and the LHC*, *JHEP* **11** (2011) 064 [1109.2109].

[95] R. J. Gonsalves, J. Pawlowski and C.-F. Wai, *QCD Radiative Corrections to Electroweak Boson Production at Large Transverse Momentum in Hadron Collisions*, *Phys. Rev.* **D40** (1989) 2245.

[96] S. Jadach, W. Placzek, S. Sapeta, A. Siódmok and M. Skrzypek, *Matching NLO QCD with parton shower in Monte Carlo scheme — the KrkNLO method*, *JHEP* **10** (2015) 052 [1503.06849].

[97] S. Alioli, C. W. Bauer, C. J. Berggren, A. Hornig, F. J. Tackmann, C. K. Vermilion et al., *Combining Higher-Order Resummation with Multiple NLO Calculations and Parton Showers in GENEVA*, *JHEP* **09** (2013) 120 [1211.7049].

[98] L. Lönnblad and S. Prestel, *Merging Multi-leg NLO Matrix Elements with Parton Showers*, *JHEP* **03** (2013) 166 [1211.7278].

[99] F. Cascioli, P. Maierhofer and S. Pozzorini, *Scattering Amplitudes with Open Loops*, *Phys. Rev. Lett.* **108** (2012) 111601 [1111.5206].

[100] G. Cullen, N. Greiner, G. Heinrich, G. Luisoni, P. Mastrolia, G. Ossola et al., *Automated One-Loop Calculations with GoSam*, *Eur. Phys. J. C* **72** (2012) 1889 [1111.2034].

[101] S. Actis, A. Denner, L. Hofer, J.-N. Lang, A. Scharf and S. Uccirati, *RECOLA: REcursive Computation of One-Loop Amplitudes*, *Comput. Phys. Commun.* **214** (2017) 140 [1605.01090].

[102] C. Berger, Z. Bern, L. Dixon, F. Febres Cordero, D. Forde, H. Ita et al., *An Automated Implementation of On-Shell Methods for One-Loop Amplitudes*, *Phys. Rev. D* **78** (2008) 036003 [0803.4180].

[103] T. Gleisberg, S. Hoeche, F. Krauss, A. Schalicke, S. Schumann and J.-C. Winter,

SHERPA 1. alpha: A Proof of concept version, *JHEP* **02** (2004) 056 [hep-ph/0311263].

[104] C. Degrande, C. Duhr, B. Fuks, D. Grellscheid, O. Mattelaer and T. Reiter, *UFO - The Universal FeynRules Output*, *Comput. Phys. Commun.* **183** (2012) 1201 [1108.2040].

[105] N. D. Christensen and C. Duhr, *FeynRules - Feynman rules made easy*, *Comput. Phys. Commun.* **180** (2009) 1614 [0806.4194].

[106] A. Alloul, N. D. Christensen, C. Degrande, C. Duhr and B. Fuks, *FeynRules 2.0 - A complete toolbox for tree-level phenomenology*, *Comput. Phys. Commun.* **185** (2014) 2250 [1310.1921].

[107] C. Degrande, *Automatic evaluation of UV and R2 terms for beyond the Standard Model Lagrangians: a proof-of-principle*, *Comput. Phys. Commun.* **197** (2015) 239 [1406.3030].

[108] S. Frixione, B. Fuks, V. Hirschi, K. Mawatari, H.-S. Shao, P. Sunder et al., *Automated simulations beyond the Standard Model: supersymmetry*, *JHEP* **12** (2019) 008 [1907.04898].

[109] R. Frederix, S. Frixione, S. Prestel and P. Torrielli, *On the reduction of negative weights in MC@NLO-type matching procedures*, 2002.12716.

[110] K. Hamilton, P. Nason and G. Zanderighi, *MINLO: Multi-Scale Improved NLO*, *JHEP* **10** (2012) 155 [1206.3572].

[111] K. Hamilton, P. Nason, C. Oleari and G. Zanderighi, *Merging H/W/Z + 0 and 1 jet at NLO with no merging scale: a path to parton shower + NNLO matching*, *JHEP* **05** (2013) 082 [1212.4504].

[112] K. Hamilton, P. Nason, E. Re and G. Zanderighi, *NNLOPS simulation of Higgs boson production*, *JHEP* **10** (2013) 222 [1309.0017].

[113] P. F. Monni, P. Nason, E. Re, M. Wiesemann and G. Zanderighi, *MiNNLO$_{PS}$: a new method to match NNLO QCD to parton showers*, *JHEP* **05** (2020) 143 [1908.06987].

[114] P. F. Monni, E. Re and M. Wiesemann, *MiNNLO$_{\rm PS}$: Optimizing $2 \to 1$ hadronic processes*, 2006.04133.

[115] R. Frederix and S. Frixione, *Merging meets matching in MC@NLO*, *JHEP* **12** (2012) 061 [1209.6215].

[116] S. Alioli, C. W. Bauer, C. Berggren, F. J. Tackmann, J. R. Walsh and S. Zuberi, *Matching Fully Differential NNLO Calculations and Parton Showers*, *JHEP* **06** (2014) 089 [1311.0286].

[117] S. Höche, Y. Li and S. Prestel, *Drell-Yan lepton pair production at NNLO QCD with parton showers*, *Phys. Rev.* **D91** (2015) 074015 [1405.3607].

[118] T. Ježo and P. Nason, *On the Treatment of Resonances in Next-to-Leading Order Calculations Matched to a Parton Shower*, *JHEP* **12** (2015) 065 [1509.09071].

[119] R. Frederix, S. Frixione, A. S. Papanastasiou, S. Prestel and P. Torrielli, *Off-shell single-top production at NLO matched to parton showers*, *JHEP* **06** (2016) 027 [1603.01178].

[120] R. Frederix, S. Frixione, V. Hirschi, D. Pagani, H.-S. Shao and M. Zaro, *The automation of next-to-leading order electroweak calculations*, *JHEP* **07** (2018) 185 [1804.10017].

[121] V. Hirschi, R. Frederix, S. Frixione, M. V. Garzelli, F. Maltoni and R. Pittau, *Automation of one-loop QCD corrections*, *JHEP* **05** (2011) 044 [1103.0621].

[122] G. Ossola, C. G. Papadopoulos and R. Pittau, *Reducing full one-loop amplitudes to scalar integrals at the integrand level*, *Nucl. Phys. B* **763** (2007) 147 [hep-ph/0609007].

[123] P. Mastrolia, E. Mirabella and T. Peraro, *Integrand reduction of one-loop scattering amplitudes through Laurent series expansion*, *JHEP* **06** (2012) 095 [1203.0291].

[124] G. Passarino and M. Veltman, *One Loop Corrections for e^+e^- Annihilation Into $\mu^+\mu^-$ in the Weinberg Model*, *Nucl. Phys. B* **160** (1979) 151.

[125] A. I. Davydychev, *A Simple formula for reducing Feynman diagrams to scalar integrals*, *Phys. Lett. B* **263** (1991) 107.

[126] A. Denner and S. Dittmaier, *Reduction schemes for one-loop tensor integrals*, *Nucl. Phys. B* **734** (2006) 62 [hep-ph/0509141].

[127] G. Ossola, C. G. Papadopoulos and R. Pittau, *CutTools: A Program implementing the OPP reduction method to compute one-loop amplitudes*, *JHEP* **03** (2008) 042 [0711.3596].

[128] T. Peraro, *Ninja: Automated Integrand Reduction via Laurent Expansion for One-Loop Amplitudes*, *Comput. Phys. Commun.* **185** (2014) 2771 [1403.1229].

[129] V. Hirschi and T. Peraro, *Tensor integrand reduction via Laurent expansion*, *JHEP* **06** (2016) 060 [1604.01363].

[130] A. Denner, S. Dittmaier and L. Hofer, *Collier: a fortran-based Complex One-Loop LIbrary in Extended Regularizations*, *Comput. Phys. Commun.* **212** (2017) 220 [1604.06792].

[131] P. de Aquino, W. Link, F. Maltoni, O. Mattelaer and T. Stelzer, *ALOHA: Automatic Libraries Of Helicity Amplitudes for Feynman Diagram Computations*, *Comput. Phys. Commun.* **183** (2012) 2254 [1108.2041].

[132] S. Alioli, P. Nason, C. Oleari and E. Re, *NLO Higgs boson production via gluon fusion matched with shower in POWHEG*, *JHEP* **04** (2009) 002 [0812.0578].

[133] F. Demartin, F. Maltoni, K. Mawatari, B. Page and M. Zaro, *Higgs*

characterisation at NLO in QCD: CP properties of the top-quark Yukawa interaction, *Eur. Phys. J. C* **74** (2014) 3065 [1407.5089].

[134] P. Artoisenet et al., *A framework for Higgs characterisation*, *JHEP* **11** (2013) 043 [1306.6464].

[135] F. Maltoni, K. Mawatari and M. Zaro, *Higgs characterisation via vector-boson fusion and associated production: NLO and parton-shower effects*, *Eur. Phys. J. C* **74** (2014) 2710 [1311.1829].

[136] F. Demartin, F. Maltoni, K. Mawatari and M. Zaro, *Higgs production in association with a single top quark at the LHC*, *Eur. Phys. J.* **C75** (2015) 267 [1504.00611].

[137] F. Demartin, B. Maier, F. Maltoni, K. Mawatari and M. Zaro, *tWH associated production at the LHC*, *Eur. Phys. J.* **C77** (2017) 34 [1607.05862].

[138] R. D. Ball et al., *Parton distributions with LHC data*, *Nucl. Phys. B* **867** (2013) 244 [1207.1303].

[139] M. Whalley, D. Bourilkov and R. Group, *The Les Houches accord PDFs (LHAPDF) and LHAGLUE*, in *HERA and the LHC: A Workshop on the Implications of HERA and LHC Physics (Startup Meeting, CERN, 26-27 March 2004; Midterm Meeting, CERN, 11-13 October 2004)*, pp. 575–581, 8, 2005, hep-ph/0508110.

[140] A. Buckley, J. Ferrando, S. Lloyd, K. Nordström, B. Page, M. Rüfenacht et al., *LHAPDF6: parton density access in the LHC precision era*, *Eur. Phys. J. C* **75** (2015) 132 [1412.7420].

[141] M. Cacciari, G. P. Salam and G. Soyez, *The anti-k_t jet clustering algorithm*, *JHEP* **04** (2008) 063 [0802.1189].

[142] M. Cacciari, G. P. Salam and G. Soyez, *FastJet User Manual*, *Eur. Phys. J. C* **72** (2012) 1896 [1111.6097].

[143] K. Hagiwara, Q. Li and K. Mawatari, *Jet angular correlation in vector-boson fusion processes at hadron colliders*, *JHEP* **07** (2009) 101 [0905.4314].

[144] V. Del Duca, W. Kilgore, C. Oleari, C. Schmidt and D. Zeppenfeld, *Gluon fusion contributions to H + 2 jet production*, *Nucl. Phys. B* **616** (2001) 367 [hep-ph/0108030].

[145] V. Del Duca, W. Kilgore, C. Oleari, C. Schmidt and D. Zeppenfeld, *Higgs + 2 jets via gluon fusion*, *Phys. Rev. Lett.* **87** (2001) 122001 [hep-ph/0105129].

[146] T. Plehn, D. L. Rainwater and D. Zeppenfeld, *Determining the Structure of Higgs Couplings at the LHC*, *Phys. Rev. Lett.* **88** (2002) 051801 [hep-ph/0105325].

[147] G. Klamke and D. Zeppenfeld, *Higgs plus two jet production via gluon fusion as a signal at the CERN LHC*, *JHEP* **04** (2007) 052 [hep-ph/0703202].

[148] J. R. Andersen, K. Arnold and D. Zeppenfeld, *Azimuthal Angle Correlations for Higgs Boson plus Multi-Jet Events*, *JHEP* **06** (2010) 091 [1001.3822].

[149] F. Campanario, M. Kubocz and D. Zeppenfeld, *Gluon-fusion contributions to Φ + 2 Jet production*, *Phys. Rev. D* **84** (2011) 095025 [1011.3819].

[150] C. Englert, M. Spannowsky and M. Takeuchi, *Measuring Higgs CP and couplings with hadronic event shapes*, *JHEP* **06** (2012) 108 [1203.5788].

[151] C. Englert, D. Goncalves-Netto, K. Mawatari and T. Plehn, *Higgs Quantum Numbers in Weak Boson Fusion*, *JHEP* **01** (2013) 148 [1212.0843].

[152] M. J. Dolan, P. Harris, M. Jankowiak and M. Spannowsky, *Constraining CP-violating Higgs Sectors at the LHC using gluon fusion*, *Phys. Rev. D* **90** (2014) 073008 [1406.3322].

[153] V. Hankele, G. Klamke, D. Zeppenfeld and T. Figy, *Anomalous Higgs boson couplings in vector boson fusion at the CERN LHC*, *Phys. Rev. D* **74** (2006) 095001 [hep-ph/0609075].

[154] A. V. Gritsan, J. Roskes, U. Sarica, M. Schulze, M. Xiao and Y. Zhou, *New features in the JHU generator framework: constraining Higgs boson properties from on-shell and off-shell production*, *Phys. Rev. D* **102** (2020) 056022 [2002.09888].

[155] R. Frederix and K. Hamilton, *Extending the MINLO method*, *JHEP* **05** (2016) 042 [1512.02663].

[156] M. Becchetti and R. Bonciani, *Two-Loop Master Integrals for the Planar QCD Massive Corrections to Di-photon and Di-jet Hadro-production*, *JHEP* **01** (2018) 048 [1712.02537].

[157] W. H. Press, S. A. Teukolsky, W. T. Vetterling and B. P. Flannery, *Numerical Recipes in Fortran 77. The Art of Scientific Computing*. Cambridge University Press, Cambridge, United Kingdom, 2nd ed., 1992.